Quality control of visual gamma oscillation frequency in studies of pharmacology, cognitive neuroscience and large-scale multi-site collaborations

Lorenzo Magazzini

Supervisor: Krish D. Singh

A thesis submitted to Cardiff University for the degree of Doctor of Philosophy

September 2016

Summary

In visual cortex, high-contrast grating stimuli induce neurons to oscillate synchronously with a centre frequency in the gamma range (~30–80 Hz). The peak frequency of visual gamma oscillations is modulated by numerous factors, including stimulus properties, cortical architecture and genetics, however, it can be measured reliably over time. As demonstrated by both animal models and human pharmacological studies, the gamma peak frequency is determined by the excitation/inhibition balance and the time constants of GABAergic processes. This oscillatory parameter could thus reflect inter-individual differences in cortical function/physiology, representing a possible biomarker for pharmacological treatment in conditions such as epilepsy, autism and schizophrenia.

This thesis demonstrates the importance of measuring the gamma peak frequency accurately and reliably in magnetoencephalographic (MEG) recordings. In Chapter 2, a novel quality-control (QC) approach was validated for peak frequency estimation and identification of poor-quality data. In Chapter 3, QC of a previous pharmacological MEG study of visual gamma with tiagabine revealed a marked drug-induced reduction of peak frequency. Although contrasting with the null finding originally reported (Muthukumaraswamy et al., 2013), the result is supported by both animal models and recent human studies, demonstrating the potentialities of appropriate QC routines. In Chapter 4, testing for the effect of spatial attention on the gamma peak frequency in primary visual cortex resulted in no evidence of a change. However, the modulation of gamma amplitude by attention was consistent with a role in feed-forward signal propagation across the visual hierarchy. In Chapter 5, the QC approach was used to compare visual gamma data recorded at different sites of the UK MEG Partnership, demonstrating the feasibility of combining data from different MEG systems.

These results have implications particularly for pharmacological and large-scale multi-site studies, both of which are emerging as promising approaches for the study of brain function with MEG.

Declaration and statements

DECLARATION

This work has not been submitted in substance for any other degree or award at this or any other university or place of learning, nor is being submitted concurrently in candidature for any degree or other award.

Signed …… (candidate) Date ……..……

STATEMENT 1

This thesis is being submitted in partial fulfillment of the requirements for the degree of PhD

Signed …… (candidate) Date ……..……

STATEMENT 2

This thesis is the result of my own independent work/investigation, except where otherwise stated, and the thesis has not been edited by a third party beyond what is permitted by Cardiff University's Policy on the Use of Third Party Editors by Research Degree Students. Other sources are acknowledged by explicit references. The views expressed are my own.

Signed …… (candidate) Date ……..……

STATEMENT 3

I hereby give consent for my thesis, if accepted, to be available online in the University's Open Access repository and for inter-library loan, and for the title and summary to be made available to outside organisations.

Signed …… (candidate) Date ……..……

Acknowledgments

A number of people have made this thesis possible. First of all, I would like to thank my supervisor, Krish Singh, for his constant support throughout the three years of my PhD. His approach to problem solving and critical look at data has made me grow considerably as a scientist during this time.

As part of my PhD, I had the fortune to collaborate with other PhD Students of the UK MEG Partnership. I would like to thank Beth Routley, who shared with me the burden of data collection and whose organisation made things work out smoothly. Thanks also to Ben Hunt, Mike Hall, Kevin Prinsloo and Sofie Meyer for contributing their data, co-developing the FieldTrip analysis scripts and helping to figure things out. Sharing training courses, conferences and associated social events with all the Partnership guys has been a lot of fun.

My analysis of the 100 Brains data would not have been possible without the work of Jennifer Brealy and other researchers at Cubric. In particular, I would like to thank Kali Barawi, without whom participant recruitment would have been a nightmare, and Sonya Foley, for help with MRI data acquisition. Thanks also to Suresh Muthukumaraswamy and Annie Campbell, who had no hesitation in letting me use their pharmacological data for this thesis.

The work of a number of people in Cubric has helped me to get through my projects as smoothly as possible. Among these, thanks to Dr Cyril Charron, uncommon IT guy who is always there to help, and Spiro Stathakis, for the work behind the scenes. I thank all the MEG people for their support in the lab and at our meetings, in particular Gavin Perry, for technical assistance and help with data that did not make it into this thesis.

A number of people have contributed to making life in Cardiff enjoyable. Philipp Ruhnau, mentor and friend from the Trento days, gave me confidence and a wind jacket, both of which helped me survive a PhD in the UK (later, I realised that a *rain* jacket was necessary, too). Nick Clifton kick-started my social life in Cardiff and has since been trying to explain to me the obscure rules of the English language. In the office, Alex Shaw fostered my passion for Matlab coding, music rhythms and rock climbing. With Kacper Wieczorek and Alberto Merola I enjoyed both sporadic intense debates and daily chilled coffee times.

I thank my parents, who are always close despite being far in distance. I could not have made it without the numerous visits to family and friends back home over the last three years. Finally, a special thank goes to Martina, for brightening the cloudy days with exciting prospects for the future. Thanks for being always present and for all the amazing meals you cooked while I was busy writing. Now that I have finished this thesis, I can say it was fun, too.

Impact of this thesis

Parts of Chapter 2 and Chapter 3 have been published in the form of a peer-reviewed journal article:

Magazzini, L., Muthukumaraswamy, S. D., Campbell, A. E., Hamandi, K., Lingford-Hughes, A., Myers, J. F., ... & Singh, K. D. (2016). Significant reductions in human visual gamma frequency by the GABA reuptake inhibitor tiagabine revealed by robust peak frequency estimation. *Human Brain Mapping*. doi:10.1002/hbm.23283

Chapter 4 is in the final stages of preparation for submission for publication:

Magazzini, L., & Singh, K. D. (in preparation). Spatial attention modulates visual gamma oscillations across the human ventral stream.

Data Collection

All analyses presented in this thesis were performed by me.

The MEG Partnership data from Cardiff University, which was included in full in Chapter 2 and partially in Chapter 5, was collected by me, together with PhD Student Bethany Routley.

The multi-site comparison MEG Partnership data included in Chapter 5 was collected by PhD Students Benjamin Hunt (University of Nottingham), Michael Hall (Aston University) and Kevin Prinsloo (University of Glasgow).

The MEG data for the attention study presented in Chapter 4 was collected by me.

The 100 Brains MEG data included in Chapter 2 was collected by Dr Jennifer Brealy.

The tiagabine and alcohol pharmacological MEG data included in Chapter 3 was collected by Dr Suresh Muthukumaraswamy and Dr Anne Campbell, respectively.

List of Contents

Abbreviations

AAL (automated anatomical labeling)

ABC (Aston Brain Centre)

AMPA (α-amino-3-hydroxy-5-methyl-4-isoxazolepropionic acid)

BA (Brodmann area)

BOLD (blood oxygenation level-dependent)

CBF (cerebral blood flow)

CBU (Cognition and Brain Sciences Unit)

CCNi (Centre for Cognitive Neuroimaging)

CSD (cross-spectral density)

CUBRIC (Cardiff University Brain Research Imaging Centre)

DICS (dynamic imaging of coherent sources)

EEG (electroencephalography)

fMRI (functional magnetic resonance imaging)

FMRIB (Oxford Centre for Functional MRI of the Brain)

FSL (FMRIB Software Library)

GABA (γ-aminobutyric acid)

GAT (GABA transporter)

ICA (independent component analysis)

ICC (intra-class correlation coefficient)

ICP (iterative closest point)

IPSC (inhibitory post-synaptic currents)

IPSP (inhibitory post-synaptic potential)

ITI (inter-trial interval)

LCMV (linearly constrained minimum variance)

LFP (local field potential)

MEG (magnetoencephalography)

MNE (minimum-norm estimates)

MNI (Montreal Neurological Institute)

MRC (Medical Research Council)

MRI (magnetic resonance imaging)

MRS (magnetic resonance spectroscopy)

MSR (magnetically-shielded room)

MUA (multi-unit activity)

NMDA (N-methyl-D-aspartate)

OHBA (Oxford Centre for Human Brain Activity)

OPM (optically-pumped magnetometer)

PCA (principal component analysis)

PET (positron emission tomography)

QC (quality control)

RT (response time)

SAM (synthetic aperture magnetometry)

SD (standard deviation)

SEM (standard error of the mean)

SNR (signal-to-noise ratio)

SPMIC (Sir Peter Mansfield Imaging Centre)

SQUID (superconducting quantum interference device)

SSS (Signal Space Separation)

SVD (singular value decomposition)

UCL (University College London)

UK (United Kingdom)

WTCN (Wellcome Trust Centre for Neuroimaging)

YNiC (York Neuroimaging Centre)

Chapter 1.

General introduction

1.1 A brief history of gamma oscillations

The study of neuronal oscillations in humans began with the observation of large-amplitude voltage fluctuations in the electroencephalographic (EEG) signal, at a frequency of ~10 Hz (Berger, 1929). The 'alpha rhythm' was observed predominantly over occipital areas, during periods of rest with eyes closed. Sixty years later, pioneering work by Singer and colleagues (Gray and Singer, 1989; Gray et al., 1989) demonstrated synchronous oscillatory activity in cat primary visual cortex, at frequencies of ~40 Hz, in response to visual stimulation. In the study by Gray et al. (1989), drifting square-wave gratings elicited synchronous rhythmic responses in groups of neurons that were recorded from separate locations within the visual cortex. Crucially, synchronisation was dependent on the configuration of the visual stimulus, with distinct neuronal groups establishing oscillatory synchrony in response to simultaneous and coherent stimulation of their receptive fields. Synchrony was thus hypothesised to serve as a neuronal principle relating spatially separated neuronal groups based on simple characteristics of the visual input (for a review, see Singer, 2007).

Oscillatory activity at high frequencies (20–80 Hz) had already been reported previously in the olfactory bulb of the hedgehog (Adrian, 1942) and rabbit (Freeman, 1975; Gray and Skinner, 1988; Viana Di Prisco and Freeman, 1985), as well as in neocortical sensory areas of other animals, such as cats (Bouyer et al., 1981, 1987), dogs (Lopes da Silva et al., 1970) and monkeys (Freeman and van Dijk, 1987; Rougeul et al., 1979), and even in the human visual cortex (Chatrian et al., 1960). However, the studies by Singer and colleagues were remarkable because they provided, for the first time, experimental evidence in support of the so-called 'binding by synchrony' hypothesis (Milner, 1974; Singer, 1999). In particular, their results fostered research on the potential role of gamma oscillations (30–100 Hz) in organising spike timing and

defining neuronal coding schemes, which, at least in theory, could represent a fundamental computational principle in the brain (Singer, 1999; Singer and Gray, 1995). Subsequently, one popular theoretical proposal, the 'communication through coherence' hypothesis (Fries, 2005, 2009), suggested that since synchronised pre-synaptic neurons have greatest downstream impact when their spikes arrive during periods of high post-synaptic excitability, neuronal communication could be flexibly modulated by establishing different phase relations among groups of coherently oscillating neurons (for a review and recent formulation of this hypothesis, see Bastos et al., 2015b).

The supposed role of oscillatory synchrony as a neuronal processing mechanism (Fries, 2005, 2009; Singer, 1993; Singer and Gray, 1995), together with the discovery of gamma oscillations in other areas of the brain, such as the hippocampus (Bragin et al., 1995), led researchers to hypothesise a possible role of gamma-band synchronisation in human cognition (Engel et al., 2001; Varela et al., 2001; Wang, 2010). To date, human gamma oscillations have been implicated in a wide range of sensory and cognitive tasks, e.g., perception (Tallon-Baudry and Bertrand, 1999), memory (Herrmann et al., 2004) and attention (Jensen et al., 2007). Unfortunately, however, most of the initial human studies on gamma oscillations were based on EEG measurements, a technique which has now been demonstrated vulnerable to different forms of artefactual activity in the gamma frequency range (Hipp and Siegel, 2013; Muthukumaraswamy, 2013; Nunez and Srinivasan, 2010). As such, the work presented within this thesis builds primarily on more recent evidence gathered using magnetoencephalographic (MEG) recordings, which, as discussed below, offer a number of advantages over EEG to study gamma oscillations in humans.

1.2 Overview of the technical basis of MEG

The use of MEG as a technique to record the electro-physiological activity produced by the brain was first demonstrated on the alpha rhythm (Cohen, 1968, 1972) and this was later extended to measuring auditory signals in the gamma frequency range (e.g., Mäkelä and Hari, 1987; Ribary et al., 1991). While the first measurements were performed with a single sensor, which was repositioned multiple times to record from different locations of the head, MEG gradually developed from single- to multi-channel systems, which implemented whole-head coverage as well as various strategies for noise reduction (Hari and Salmelin, 2012).

1.2.1 The biophysical basis of MEG

From a physiological point of view, MEG measures the magnetic fields produced by intracellular currents flowing within the apical dendrites of pyramidal neurons, which are oriented in parallel with respect to each other and perpendicularly with respect to the cortical surface (Baillet et al., 2001). One of the main reasons why post-synaptic potentials provide the major contribution to the measured magnetic fields is that they occur on relatively slow time scales, lasting up to several tens or hundreds of milliseconds (Del Gratta et al., 2001; Williamson and Kaufman, 1990). This, in combination with the spatial superposition produced by the structural arrangement of the dendrites, allows the generated magnetic fields to sum in time and space, becoming of measurable intensity. On the contrary, the axonal currents produced by the firing of action potentials are thought to provide minimal or no contribution to the measured fields (Lopes da Silva, 2010). In fact, action potentials are much faster compared to post-synaptic potentials and thus less likely to synchronise over a sufficiently large number of neurons (see below). In addition, while post-synaptic potentials can be modelled as dipoles with fields falling with the square of the distance, the magnetic

fields produced by the axonal currents decay much more rapidly, falling with the cube of the distance.

This type of cell population, i.e. pyramidal neurons, can be found primarily in the external and internal granular layers, i.e. layer II and layer V of the neocortex, respectively (Bear et al., 2007). In theory, those neurons that have a tangential component with respect to the scalp produce magnetic fields that are measurable with MEG, whereas those that are radially-oriented do not. This latter scenario is realised at the sulci and crests of cortical gyri, which however constitute only ~5% of the cortex (Hillebrand and Barnes, 2002). The presence of non-tangentially oriented pyramidal neurons in a limited portion of the cortex would thus not represent a major limitation for MEG.

Importantly, rather, synchronisation among relatively large numbers of pyramidal neurons is required, for the resulting magnetic fields to be of measurable intensity, i.e. at least 50–500 fT (Hämäläinen et al., 1993). It has been estimated that between 10,000–50,000 pyramidal cells need to be synchronously active for the signal to be detected (Murakami and Okada, 2006), for areas of the cortex between 0.1–4 cm^2, depending on the type of neuronal activity and cortical region being recorded (cf. Barth, 1991; Chapman et al., 1984; Lü and Williamson, 1991). Also for this reason, and in support of the argument mentioned above, it is unlikely for a cortical source to be fully radial and hence silent (Hillebrand and Barnes, 2002).

One important limiting factor of MEG, instead, is the relatively low sensitivity to deep sources. The magnetic field decays with the square of the distance (as stated by the Biot-Savart law) and thus sources deep in the brain need to be of large intensity in order to be detected with MEG (Hillebrand and Barnes, 2002). Despite this, both empirical evidence and computational models suggest that some subcortical structures, such as the

hippocampus, might be measurable with MEG (Attal et al., 2007; Dalal et al., 2009; Kaplan et al., 2012).

1.2.2 MEG instrumentation

The challenge of measuring from deep sources is partly related also to the difficulty of reducing the distance between the MEG pick-up coils and the scalp, which represents the main disadvantage of MEG compared, for example, to EEG (Muthukumaraswamy, 2014). In modern MEG systems, the magnetic fields produced by the brain are coupled to superconducting quantum interference devices (SQUIDs; Zimmerman, 1970) via flux transformers, which consist of a pick-up coil and a coupling coil (Vrba and Robinson, 2001). SQUIDs and flux transformers need to be cooled to superconductive temperatures (4°K, i.e. -269°C) and for this reason are kept inside a cryogenic dewar, immersed in liquid helium. Together, the dewar and the skull/scalp create a minimum distance of ~4 cm between the cortex and the pick-up coil.

The configuration of the pick-up coils, illustrated in Figure 1.1, represents one of the major differences among the various MEG systems commercially available. There are three main types of pick-up coils: magnetometers, axial gradiometers and planar gradiometers (Hämäläinen et al., 1993; Muthukumaraswamy, 2014; Vrba and Robinson, 2001). A magnetometer consists of a single coil connected to a SQUID and is relatively sensitive to large and distant sources of noise. Magnetometers produce field maps with a positive and a negative peak on either side of the measured dipole; the larger the distance between minimum and maximum, the deeper the dipole. An axial gradiometer consists of two magnetometers looped in the opposite direction and oriented parallel to the dipole source, i.e. on top of each other. Axial gradiometers measure the change in magnetic field between the two coils and are thus less sensitive to large and distant sources of noise, which are picked up by both coils and cancelled out. The resulting

field maps are similar to those produced by magnetometers, but have a more focal pattern. Planar gradiometers exploit the same principles of axial gradiometers, but consist of two coils looped in a figure of eight, perpendicular to the dipole. Differently to both axial gradiometers and magnetometers, their field maps show a single peak directly above the dipole. The fields measured by an axial gradiometer system can be transformed into a planar gradiometer configuration, by calculating the second spatial derivative of the recorded field (Oostenveld et al., 2011).

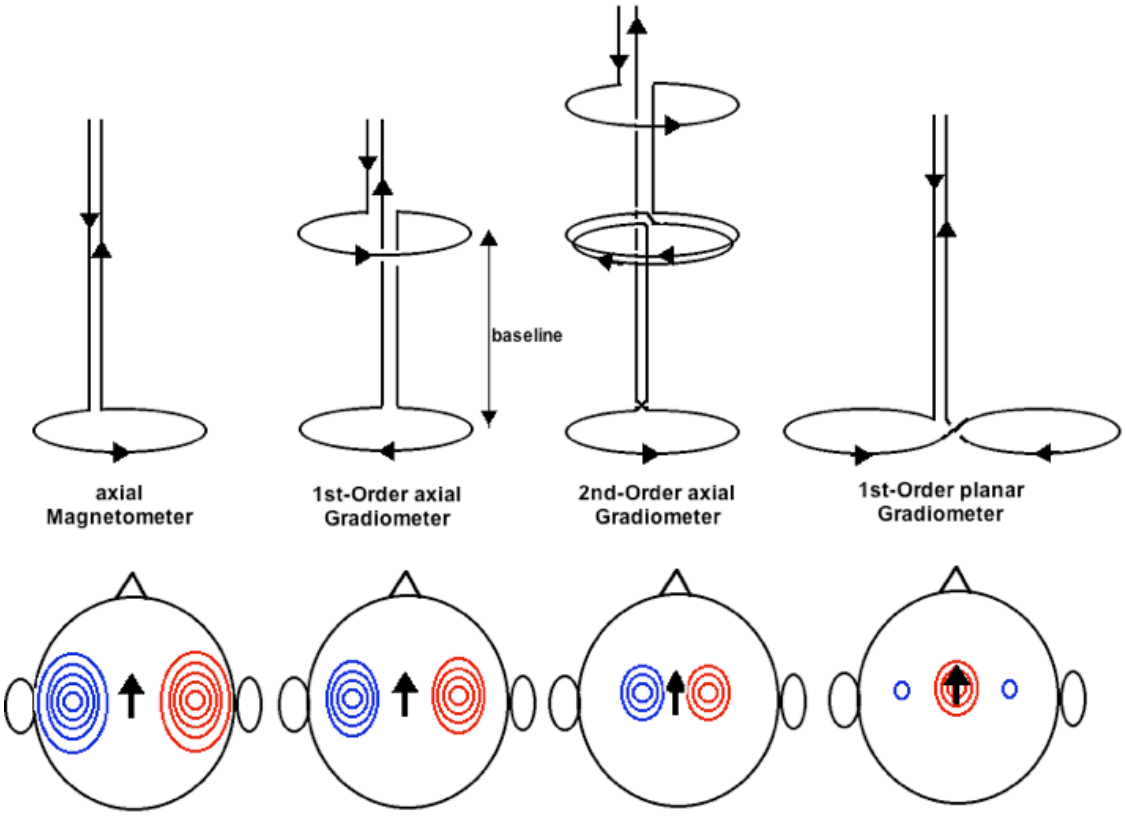

Figure 1.1. Configuration and field pattern of four different pick-up coils.

Schematic illustration of the coil configuration for axial magnetometers, axial gradiometers and planar gradiometers (top), with the typical field patterns generated in each of them (bottom). The black arrow in each plot represents a single tangential dipolar current source at the vertex. The red and blue circles indicate magnetic field lines entering and exiting the head, respectively. Note the spatially tighter field maps of higher-order gradiometers and the different field map produced by the planar gradiometers. Reproduced from Singh (2006).

In addition to the widely adopted magnetically-shielded rooms (MSRs), advanced approaches to noise reduction are implemented in a manufacturer-specific manner, in part depending on the type of pick-up coils in use. The CTF-MEG system, for example, is equipped with a set of reference magnetometers, which allow the conversion from first- to synthetic third-order gradiometers to further attenuate environmental noise, reduce vibrational noise and even eliminate head motion artefacts (Vrba and Robinson, 2001). For the Elekta Neuromag MEG system, instead, spatio-temporal signal space separation (SSS) algorithms are typically used to separate and remove the magnetic fields originating outside a volume of interest (e.g., the brain) from those arising from inside the volume of interest itself, without distorting the measured MEG signal (Taulu and Simola, 2006; Vrba et al., 2010). A summary of the main technical features of three major MEG systems, which will be analysed in Chapter 5, is illustrated in Table 1.1.

Table 1.1. Technical characteristics of three different MEG systems.

MEG system	**primary sensors**	**noise cancellation (system-specific)**
CTF-MEG	275 first-order axial gradiometers	synthetic third-order gradiometers (generated using a linear combination of a set of weighted reference sensors)
Elekta Neuromag (VectorView, Triux)	102 magnetometers 102 orthogonal pairs of planar gradiometers	signal-space separation (SSS) (MaxFilter and MaxShield)
4-D Neuroimaging (Magnes 3600 WH)	248 magnetometers	principal component analysis (PCA) (the principal components of a set of reference sensors are regressed out of the primary sensors)

1.2.3 Analysis of MEG data

Irrespective of the type of system, the MEG signal-to-noise ratio (SNR) can be improved by adopting common source analysis approaches. For example, compared to data analysed directly at the sensor level, beamformer source reconstruction of visually induced gamma oscillations can result in spectral modulations of greater amplitude and, for some parameters, higher test-retest repeatability values (Tan et al., 2016). Although spatial filtering should not be considered an explicit noise-reduction technique, this approach often results in various forms of signal artefacts either being projected outside the area of space occupied by the brain, or becoming easily detectable within the brain source image (Muthukumaraswamy, 2013).

As also discussed below, the MEG signal can be considered insensitive to the different tissue compartments of the head, which means that relatively simple forward models can be used. The MEG forward model, or leadfield, consists of a definition of the magnetic fields that would be measured at every sensor location if a dipole source was active at a given location in the brain (Mosher et al., 1999). Adequate forward models can be as simple as a single sphere (Hämäläinen and Sarvas, 1989), although more complex ones are often used, such as multi-sphere models (Huang et al., 1999) or models in which a spherical volume conductor is corrected using realistic information about the head shape (Nolte, 2003). The accuracy of the forward model contributes to the accuracy of the solution to the MEG inverse problem, which consists of determining the location of the dipole sources, given the magnetic fields measured at every sensor location.

One common solution to the inverse problem is the beamformer approach (Hillebrand et al., 2005). Beamforming is a spatial filtering technique originally developed for radar applications (Van Veen and Buckley, 1988), which allows a given three-dimensional

area of space to be 'scanned' systematically in order to estimate the signal from each location independently. In simple terms, the algorithm weights the measurement of each sensor so as to increase the sensitivity to signals coming from a location of interest, while suppressing the interfering signals from other locations (Hillebrand et al., 2005). This is achieved by minimising the projected power at the source location, subject to a unit-gain constraint (Barnes and Hillebrand, 2003). The beamformer solution is thus determined by two key ingredients. The first is the leadfield, as the unit-gain constraint implies that power at a given source location, projected to the sensors through the leadfield, should be recovered in full when weighting the sensors to reconstruct the activity at that location (Brookes et al., 2008). The second ingredient is the data covariance matrix, for time-domain beamformers such as LCMV (Van Veen et al., 1997) and SAM (Robinson and Vrba, 1999), or the cross-spectral density (CSD) matrix, for frequency-domain beamformers such as DICS (Gross et al., 2001), which contribute to the calculation of the beamformer weights (Brookes et al., 2008). Ultimately, the weights minimise the power projected at a given source location by reducing the contribution from other sources (Hillebrand et al., 2005), under the assumption that the sources are not correlated (Van Veen et al., 1997).

Various beamformer algorithms have been proposed (Gross et al., 2001; Robinson and Vrba, 1999; Van Veen et al., 1997), which are actually mathematically very similar (Hillebrand et al., 2005). In the original linearly constrained minimum variance (LCMV) beamformer formulation by Van Veen et al. (1997), a vectorial solution is computed for each source location. In fact, the leadfield consists of a 3-by-N matrix, mapping three orthogonal dipole orientations to N sensors. With this approach, a different set of weights is calculated for each of the three possible dipole orientations (or two, if the radial orientation is ignored), resulting in three separate source reconstructions, one for each orientation. In the experimental chapters of this thesis,

however, singular value decomposition (SVD) will be used to reduce the leadfield matrix to a single dipole orientation (i.e. a 1-by-N matrix for each scanned source location). By SVD, the beamformer solution is computed for the dipole orientation that should theoretically explain most of the measured data. Importantly, although this procedure can potentially lead to loss of information, it reduces the dimensionality of the data, thereby avoiding additional multiple comparison problems and facilitating every subsequent analysis step (e.g., time-frequency or spectral analysis of the source-reconstructed time-series). Throughout this thesis, this scalar beamformer approach will be referred to simply as LCMV.

As mentioned above, dynamic imaging of coherent sources (DICS; Gross et al., 2001) corresponds to a frequency-domain LCMV, as the covariance matrix is simply replaced with the CSD matrix in the weights calculation. As for LCMV, a scalar DICS beamformer will be used in the experimental part of this thesis, by SVD of the leadfield matrix. Finally, synthetic aperture magnetometry (SAM; Robinson and Vrba, 1999) is the third type of beamformer that will be referred to in this thesis, which differs from a scalar LCMV simply by the method used to derive the dipole orientation. In SAM, the dipole orientation at each source location is calculated by 'spinning' the dipole in several different orientations, until the algorithm achieves the maximal ratio between total and noise power. It is entirely possible that the optimal dipole orientation obtained with SAM will often correspond to the orientation obtained by SVD of the leadfield with LCMV.

In contrast to beamforming, in other approaches, such as minimum-norm estimates (MNE), the data are modelled simultaneously for a large number of potential sources. The measured data are then explained by the source configuration with the least energy that also minimises the difference between measured and estimated fields (Hämäläinen

and Ilmoniemi, 1994). Typically, however, this requires the specification of an arbitrarily-defined depth bias (Hillebrand et al., 2005). Several other inverse solutions for source localisation exist, beyond beamforming and MNE (for an overview, see Ramìrez, 2008). Since only beamforming will be used in the experimental chapters of this thesis, the alternative approaches will not be discussed further here.

1.2.4 The history of three MEG systems

In the last experimental chapter (Chapter 5), the results of a comparative analysis will be presented for MEG data pooled across four research centres in the UK and recorded using three different MEG systems. As such, what follows hereafter is an attempt to provide a brief historical perspective on three common MEG systems currently used in MEG research. In everyday language, these are known as CTF, Elekta and 4-D, though some confusion appears to exists around the use of their commercial names. The information reported hereafter was gathered by combining the literature (Brahme, 2014; Hämäläinen et al., 1993; Mason et al., 2013) with descriptions available on the companies' websites and may therefore be partly inaccurate or incomplete.

According to a recent estimate, at present there are about 160 MEG laboratories worldwide (Hari and Salmelin, 2012). The first whole-head MEG in the UK was installed at Aston University, in Birmingham, and was a 151-channel CTF system, which is now no longer in use at Aston. Founded in 1970, Canadian Thin Films (CTF) Systems Inc. was one of the first MEG manufacturers. From a commercial perspective, instead, the first multi-channel magnetometer system was introduced in 1985, by the American company Biomagnetic Technologies Inc. (BTi). In later years, the Finnish company Neuromag, merged with BTi and founded 4-D Neuroimaging. Neuromag then split from 4-D and in 2003 merged with Elekta Inc., becoming Elekta Neuromag. In the meantime, in 2001, CTF were acquired by VSM MedTech Ltd., a company who then

sold it to MEG International Services Ltd. (MISL) in 2007. In 2009, MISL acquired also 4-D, becoming service providers for both 4-D and CTF-MEG systems.

The latest product by CTF, the 275-gradiometer CTF-MEG system, is currently in use at three MEG laboratories in the UK (Cardiff, Nottingham and UCL). The latest 4-D Neuroimaging MEG product, the 248-magnetometer system Magnes 3600 WH, is currently installed both in Glasgow and in York. Two of the most recent Elekta Neuromag MEG systems, VectorView and Triux, which combine 102 magnetometers with 102 pairs of orthogonal planar gradiometers, are in use in Birmingham (Aston), Cambridge and Oxford. At present, apart from Elekta and CTF, other operative MEG manufacturers are the Japanese company Yokogawa Inc. and the American company Tristan Technologies Inc. (Brahme, 2014), although no MEG system from these companies has ever been installed in the UK.

1.3 Studying visual gamma oscillations in humans with MEG

1.3.1 The advantages of MEG over EEG

The robustness of EEG as a technique to study induced oscillatory phenomena in the higher portion of the frequency spectrum has been questioned since the early days of research on human gamma oscillations (Juergens et al., 1999). In particular, several observations on the susceptibility of EEG to electro-myogenic artefacts (Hipp and Siegel, 2013; Muthukumaraswamy, 2013; Nunez and Srinivasan, 2010) cast doubt on the robustness of the early reports of gamma-band activity in the human EEG (e.g., Gruber et al., 1999; Müller et al., 2000; Tallon-Baudry et al., 1996). At frequencies above ~30 Hz, the EEG spectrum is strongly contaminated by artefacts produced by the electro-myogenic activity from face and neck muscles (Goncharova et al., 2003; O'Donnell et al., 1974; Whitham et al., 2008). The contraction of these muscles can even be modulated by task-related factors and, therefore, can potentially add further uncertainty to the quantification and interpretation of gamma activity measured with EEG (see Hipp and Siegel, 2013). In addition, micro-saccadic eye movements have been shown to contaminate the high-frequency EEG signals (Yuval-Greenberg et al., 2008) in a task-dependent manner.

Magnetoencephalography offers a number of advantages over EEG for the study of high-frequency neuronal activity. First, unlike EEG, MEG is virtually insensitive to the smearing of electrical potentials across different types of conductive tissues (Buzsáki et al., 2012), meaning that less complex forward models are adequate for source localisation (Muthukumaraswamy, 2014). Second, the superior SNR of MEG over EEG and increased robustness of a number of MEG-derived parameters of gamma activity have been demonstrated empirically (Muthukumaraswamy and Singh, 2013). Third, and partly related to the first point, the increased accuracy of MEG source reconstruction

can result in more focal localisation of physiological artefacts (Muthukumaraswamy, 2014), leading to relatively simple identification of artefacts such as those created by saccadic eye movements (Carl et al., 2012). Fourth, preliminary evidence suggests that the sustained component of visual gamma oscillations is unaffected by the micro-saccadic artefacts (Wieczorek, 2015).

1.3.2 The study of visual gamma oscillations in humans

Other than the visual system (Gray et al., 1989) and the hippocampus (Bragin et al., 1995), gamma oscillations have been studied in several parts of the brain, such as in parietal (Pesaran et al., 2002) and frontal cortex (Gregoriou et al., 2009), as well as in subcortical regions (Popescu et al., 2009). The literature described hereafter, however, will refer primarily to *visual* gamma oscillations, which have been the focus of most of the experimental work in this thesis (see Chapters 2, 3, 4 and 5). The term 'visual gamma' refers to neuronal gamma-band activity generated in visual cortex in response to simple contrast pattern stimuli and sustained throughout the presentation of a stimulus (Singh, 2012). As already mentioned above, this type of oscillatory activity was first reported using local field potential (LFP) recordings in the cat primary visual cortex (Gray et al., 1989; Kayser et al., 2003).

The first demonstration of visual gamma oscillations in humans, with MEG, can be traced back to a study in 2004 (Adjamian et al., 2004b). In this study, Adjamian and colleagues managed for the first time to successfully apply a beamformer source reconstruction technique, synthetic aperture magnetometry (SAM; Vrba and Robinson, 2001), to reconstruct gamma oscillations from the human primary visual cortex (Adjamian et al., 2004b). The authors also demonstrated the dependency of visual gamma on the parameters of visual stimulation, e.g., spatial frequency in their study. These results were replicated and extended soon after by another study (Hall et al.,

2005), while, over time, the development of improved data analysis techniques, together with the optimisation of experimental protocols, allowed the same and other research groups to precisely illustrate the spectral and temporal evolution of this response (e.g., Hoogenboom et al., 2006; Swettenham et al., 2009).

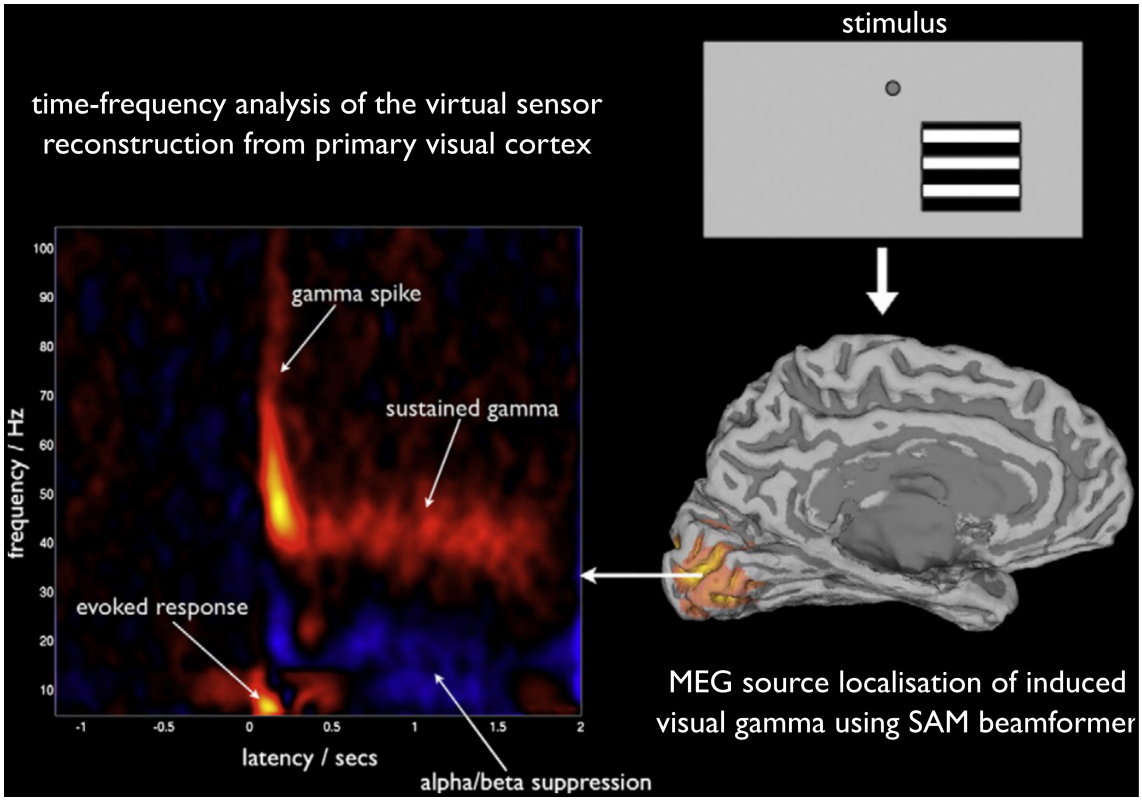

Figure 1.2. Source localisation and time-frequency representation of the visual gamma response. The epochs of interest in a typical visual gamma paradigm are analysed using a beamformer, which reveals a peak response in the primary visual cortex. A virtual sensor is generated and the time-course of activity reconstructed at this peak location is analysed in the time-frequency domain. This reveals the classic visual gamma response (section 1.3.2), as well as other features of the neuronal response to visual stimulation outside the gamma frequency range (30–100 Hz), i.e. an initial low-frequency evoked response, followed by the suppression of induced oscillatory power in the alpha/beta range (5–30 Hz). Adapted without permission from Singh (2012).

As shown in Figure 1.2, the classic time-frequency spectrogram for visual gamma is characterised by a transient and broadband 'spike', spanning frequencies between ~30–100 Hz (or even higher) and terminating ~250–300 ms after stimulus onset. This initial evoked response, which is thought to be coupled to oscillatory potentials both in the retina and in the lateral geniculate nucleus (Castelo-Branco et al., 1998; Neuenschwander and Singer, 1996), is then followed by narrow-band gamma oscillations, typically sustained for the duration of the visual stimulus. This latter response is often referred to as the induced response, being time-locked but not phase-locked to stimulus onset (Galambos, 1992; Tallon-Baudry and Bertrand, 1999). Importantly, these features can all be recorded with high consistency across non-human primates, with LFPs, and humans, using MEG or EEG (Fries et al., 2008a; Hall et al., 2005).

Over the course of the last 10 years, the oscillatory parameters of human visual gamma responses have been studied with respect to a number of factors. In particular, the amplitude, frequency, or bandwidth of gamma oscillations have been shown to depend strongly on the parameters of visual stimulation, in both humans and animals. This is the case for stimulus properties such as contrast (Hall et al., 2005; Henrie and Shapley, 2005; Perry et al., 2015; Ray and Maunsell, 2010), size (Gieselmann and Thiele, 2008; Ray and Maunsell, 2011; van Pelt and Fries, 2013), orientation (Berens et al., 2008; Frien et al., 2000; Jia et al., 2011), spatial frequency (Adjamian et al., 2004b; Hadjipapas et al., 2007), motion (Gray et al., 1990; Muthukumaraswamy and Singh, 2013; Swettenham et al., 2009) and motion velocity (Friedman-Hill et al., 2000; Gray and Viana Di Prisco, 1997). In general, both the gamma peak amplitude and peak frequency are modulated by the structural properties of the visual stimulus (Lima et al., 2010; Perry, 2015). Interestingly, however, some dissociations have been observed between these two oscillatory parameters, which do not always co-vary with changes in

the stimulus properties (Jia et al., 2013). This led Jia and colleagues to conclude that the gamma peak amplitude and peak frequency are determined by different mechanisms and cannot be explained by models in which both amplitude and frequency increase with increasing input strength (see Whittington et al., 2011). An overview of the mechanisms that have been proposed to underpin the generation of gamma oscillations is presented in a later paragraph (section 1.4.1).

1.3.3 Visual gamma and pharmaco-MEG

In one of the experimental chapters of this thesis (Chapter 3), I will briefly review the pharmacological MEG (pharmaco-MEG) literature (for reviews, see Kähkönen, 2006; Muthukumaraswamy, 2014). In agreement with modelling work (e.g., Brunel and Wang, 2003), several recent pharmaco-MEG studies have consistently linked the properties of gamma oscillations to the balance between excitatory and inhibitory processes in the brain. As reported by Singh (2012), the possibility that specific oscillatory parameters could index inter-individual differences in cortical inhibition was initially suggested by two studies combining magnetic resonance spectroscopy (MRS) and MEG, which found a positive correlation between the individual gamma peak frequency and the γ-aminobutyric acid (GABA) concentration in occipital cortex (Edden et al., 2009; Muthukumaraswamy et al., 2009). However, a later study on a larger sample failed to replicate the result (Cousijn et al., 2014). MRS is in fact severely limited by the impossibility of distinguishing between intracellular and synaptic GABA concentrations (Muthukumaraswamy, 2014). In contrast, pharmaco-MEG can be used with drugs that have well-understood and well-defined mechanisms of action in order to probe the neurophysiological generative mechanism of neuronal responses that are measured consistently both invasively in animals and in humans with MEG (Muthukumaraswamy, 2014). Since this is the case for visual gamma oscillations (Fries

et al., 2008a; Hall et al., 2005), pharmaco-MEG represents a highly promising approach for the translation of animal models to humans.

1.4 Mechanisms and functions of gamma oscillations

1.4.1 The role of GABAergic interneurons and glutamatergic pyramidal cells

The two main types of neurons in the cerebral cortex are excitatory pyramidal cells and inhibitory interneurons, both of which have been implicated in the generation of gamma oscillations (Buzsáki and Wang, 2012). The two principal neurotransmitters in the brain are glutamate and GABA, with excitatory and inhibitory effect, respectively (Kandel et al., 2000). The excitatory action of glutamatergic pyramidal neurons occurs primarily via activation of ionotropic receptors that allow the influx of positively charged ions in the post-synaptic neurons and bring them to a depolarised state with respect to their resting membrane potential. The primary receptors for glutamatergic transmission are AMPA (alpha-amino-3-hydroxy-5-methyl-4-isoxazolepropionic acid) and NMDA (N-methyl-D-aspartate), which allow the inward flow of Na^+ and Ca^{++} and mediate fast and slow excitation processes, respectively (Buzsáki et al., 2012). Conversely, the inhibitory action of GABAergic interneurons mediated by $GABA_A$ receptors generates an influx of negatively charged Cl^- ions in the post-synaptic neurons. The time constants of both $GABA_A$ and AMPA receptors contribute to determining the time window of the gamma cycle (Buzsáki and Wang, 2012).

The role of fast-spiking, parvalbumin-expressing interneurons in the generation of gamma oscillations is generally acknowledged (Bartos et al., 2007; Gonzalez-Burgos and Lewis, 2012; Tiesinga and Sejnowski, 2009). An individual GABAergic interneuron can form peri-somatic synapses with a large number of pyramidal neurons (Figure 1.3A) – about 15 in the neocortex (Markram et al., 2004) and up to 1500 in the hippocampus (Sik et al., 1995). The interneurons can thus modulate the excitability of relatively large populations of pyramidal cells, thereby shaping their firing activity. Crucially, the inhibitory post-synaptic potentials (IPSPs) reduce the firing probability

simultaneously in all post-synaptic pyramidal neurons with which the interneuron forms synaptic contacts (Gonzalez-Burgos and Lewis, 2008). Therefore, soon after the IPSPs terminate, the level of excitability recovers simultaneously across the whole cell population, resulting in the pyramidal neurons firing synchronously (Figure 1.3B). The rhythmic generation of IPSPs in the population of pyramidal cells translates to oscillations in the LFP, which can be observed also in the MEG signal. The exact mechanisms generating gamma oscillation, however, are not yet fully understood and the role of pyramidal cell firing, in particular, is still debated. As illustrated in Figure 1.3C, two main circuit mechanisms have been proposed: the Interneuron Network Gamma (ING) and the Pyramidal Interneuron Network Gamma (PING) models (for reviews, see Gonzalez-Burgos and Lewis, 2012; Tiesinga and Sejnowski, 2009).

According to the ING model, synchronisation in the gamma frequency range would arise simply from networks of interconnected and mutually inhibiting interneurons (Whittington et al., 2000). In this model, synchronous input from the pyramidal neurons is not required; the timing of pyramidal cells firing is determined by the decay time of GABAergic inhibition, but does not contribute to generating the gamma rhythm itself. In support to this model, *in vitro* pharmacological studies have shown that synchronous gamma oscillations in the hippocampus can be induced by tonic excitatory drive to the interneurons via metabotropic glutamate receptor activation (Whittington et al., 1995). The gamma oscillations observed following phasic excitation of the interneurons via a cholinergic agonist (Fisahn et al., 1998), instead, are more consistent with the PING model (Bartos et al., 2007; Tiesinga and Sejnowski, 2009). In the PING model, the interneurons are driven by the pyramidal cells, which become synchronised following feedback inhibition (Gonzalez-Burgos and Lewis, 2012). The generation of gamma oscillations would thus depend on the presence of recurrent connections between the pyramidal cells and the GABAergic interneurons (Whittington et al., 2000).

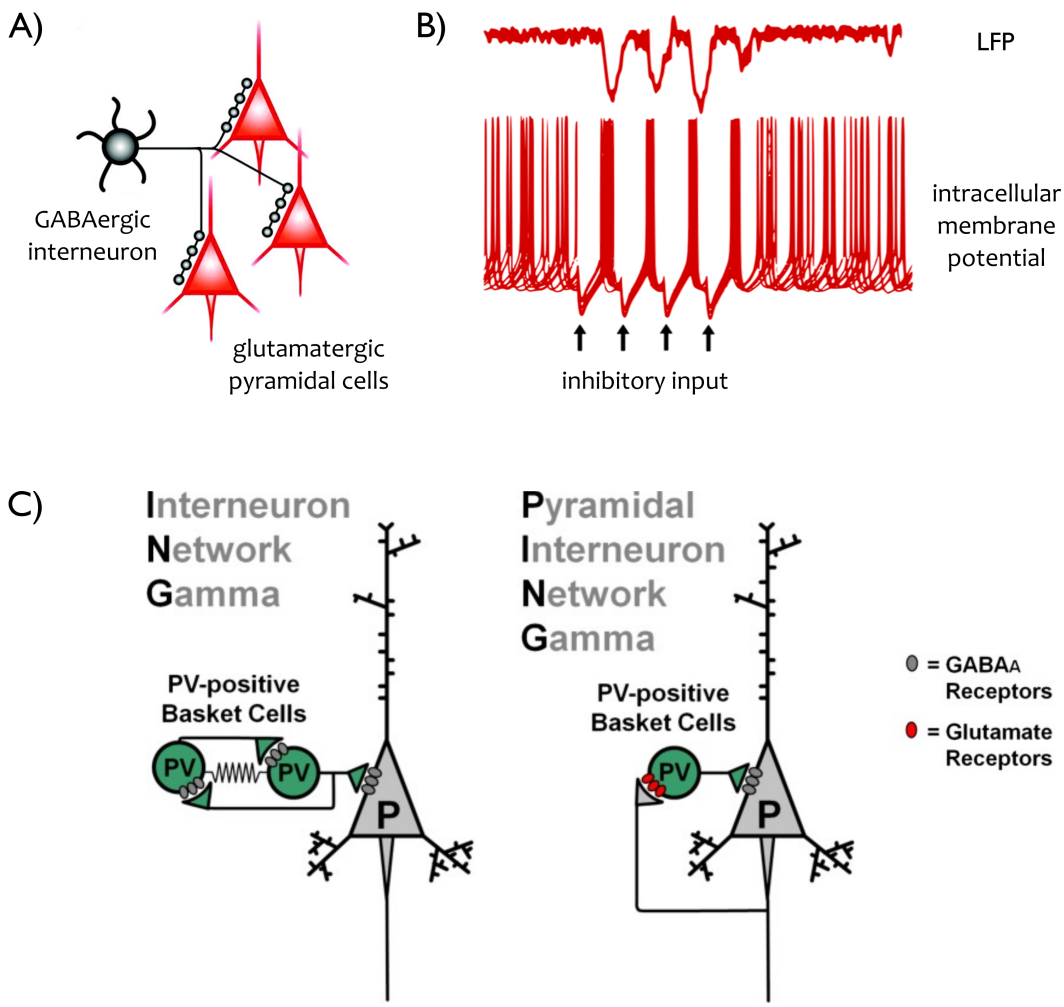

Figure 1.3. Mechanisms of gamma oscillations.

A) Schematic illustration of an individual GABAergic interneuron making multiple synaptic contacts onto multiple post-synaptic pyramidal cells. **B)** Top, LFP recorded with an extracellular electrode in proximity of the pyramidal neurons. Bottom, superimposed traces of intracellular membrane potential recording, illustrating the synchronous firing of pyramidal neurons following phasic inhibitory input (black arrows). The IPSPs transiently inhibit spike firing, resulting in synchronous spikes soon after the IPSPs terminate. The negative components of the LFP reflect the synchronisation of pyramidal cell firing. **C)** In the ING model (left panel), gamma oscillations are generated by reciprocal inhibition between fast-spiking, parvalbumin-expressing interneurons, which are activated by some form of tonic excitatory input. The pyramidal cells are synchronised by the interneurons, but do not contribute to the rhythmogenesis. In the PING model (right panel), gamma oscillations are generated by the interplay between interneurons and pyramidal cells, which contribute directly to the rhythmogenesis. The interneurons are driven by the phasic excitatory input from the glutamatergic pyramidal neurons, which are synchronised by feedback inhibition. Adapted without permission from Gonzalez-Burgos and Lewis (2008, 2012).

In recent years, *in vivo* optogenetic studies in mice have provided further evidence in support of the crucial role played by fast-spiking, parvalbumin-expressing interneurons in the generation of gamma oscillations (Cardin et al., 2009; Sohal et al., 2009). In these studies, gamma oscillations were amplified by light-driven activation of the interneurons (Cardin et al., 2009) and suppressed by their inhibition (Sohal et al., 2009). Furthermore, gamma oscillations were abolished by AMPA and NMDA receptor blockade, despite the presence of tonic excitatory drive to the interneurons, suggesting that phasic excitatory input to the interneurons is necessary for the generation of these oscillations (Cardin et al., 2009). Optogenetic manipulation appears thus a highly promising approach to study gamma oscillations *in vivo*. In particular, the possibility of precisely controlling the activity of different types of neurons, such as interneurons and pyramidal cells, will likely shed light on the circuit-level mechanisms implicated in the rhythmogenesis of gamma oscillations.

1.4.2 The functional role of oscillatory rhythms in different frequency bands

Our understanding of the neuronal networks generating gamma oscillations has recently been advanced by another line of research, which has revealed how superficial and deep layers of the cortex contribute differently to the generation of oscillations at different frequencies. This observation comes primarily from invasive studies in animals, in which LFP recordings were performed with multi-contact laminar electrodes (e.g., Spaak et al., 2012). In humans, similar results may be achieved also with MEG (Troebinger et al., 2014) and have already been demonstrated by a recent combined EEG-fMRI study (Scheeringa et al., 2016). In early visual cortex, gamma activity predominates in the more superficial layers, i.e. layer II, the external granular or supragranular layer (Buffalo et al., 2011; Maier et al., 2010; Scheeringa et al., 2016; Xing et al., 2012b). At lower frequencies, instead, both alpha (8–12 Hz; Buffalo et al., 2011; Spaak et al., 2012) and beta oscillations (15–30 Hz; Maier et al., 2011) appear to

be generated in the deeper layers, i.e. layer V, the internal granular or infragranular layer (although, see also Haegens et al., 2015; Scheeringa et al., 2016).

These studies corroborate the hypothesis that different oscillation frequencies may fulfil different cortical functions, such as establishing local representations at gamma frequencies and enabling long-range integration processes at lower frequencies (Donner and Siegel, 2011; Kopell et al., 2000). The afferent and efferent projections to and from each cortical layer differ between the different laminae and can be formed either within the same or across different brain regions (Douglas and Martin, 2004). Therefore, oscillations generated in different layers may reflect different mechanisms of information processing within a given cortical area and information transmission across different brain regions. In support of this view, recent evidence suggests that gamma and alpha/beta oscillations propagate in opposite directions between different areas of the visual system, with gamma reflecting feed-forward signal propagation and alpha/beta indexing feedback effects (Bastos et al., 2015a; Michalareas et al., 2016; van Kerkoerle et al., 2014).

To date, the gamma rhythm has been implicated in a range of cognitive functions (Fries, 2015; Jensen et al., 2007) as well as in pathological conditions (Lewis et al., 2005; Uhlhaas and Singer, 2006). Although not without some controversies (see Ray and Maunsell, 2015), visual gamma, in cooperation with alpha oscillations (Jensen et al., 2014), have been proposed as a mechanism for selective routing of information across the visual cortical hierarchy (see Fries, 2015). The visual system represents a particularly well-suited scenario for the achievement of these functions, as the input from upstream neurons progressively converges to downstream regions with bigger receptive fields, where invariant stimulus representations can be formed (Desimone and Duncan, 1995; Reynolds and Chelazzi, 2004). In particular, a recent LFP study in

monkeys (Bosman et al., 2012) reported gamma-band synchronisation between low- and high-level visual regions, suggesting that inter-areal communication could be partly regulated by the oscillation frequency in primary visual cortex (Fries, 2015). In one of the experimental chapters of this thesis (Chapter 4), I will investigate the modulation of visual gamma oscillations in a spatial attention cueing task, testing specifically for the effect of attention on the gamma peak frequency.

1.5 Aims of this thesis

One of the major problems in modern neuroscience concerns the quality of the data obtained with the techniques currently available. In part, this depends on the ability of the experimenter in designing appropriate experimental paradigms and adopting adequate strategies to mitigate the effects of undesired confounding variables, in order to collect the best possible quality data. Noise, however, is an intrinsic feature of any recording of brain activity and is particularly challenging in the case of MEG, where the signals of interest are thousands of times weaker than the Earth's magnetic field. Furthermore, one of the most popular approaches to noise reduction, i.e. averaging over an 'infinite' number of trials, cannot always be exploited in full with human participants, whose noise-determining level of compliance largely depends on their comfort inside the MEG system and on the duration of the experimental session.

In this thesis, I will focus on a specific parameter of sustained visual gamma oscillations, i.e. their peak frequency, which is often neglected in human MEG research. I will introduce a recently developed method for the quantitative estimation of the robustness of this parameter, which will be used as a proxy for data quality. In Chapter 2, this quality-control (QC) approach, which is based on bootstrapping across trials, will first be tested on simulated data and then applied to a large-sample dataset, the '100 Brains', to illustrate the reliability of the gamma peak frequency in real MEG data, as well as the distribution of other QC and gamma oscillatory parameters. In Chapter 3, the potential applications of the QC approach will be tested on pharmaco-MEG data from two previous studies, which offered the advantageous opportunity of relating any observed modulations of peak frequency to relatively well-established animal models. Some of the results presented in Chapters 2 and 3 have recently been published in the form of a peer-reviewed journal article (Magazzini et al., 2016). In Chapter 3, I will use the QC method for peak frequency estimation to test a recently formulated hypothesis

on the role of the gamma peak frequency in attentional selection processes within primary visual cortex. The results of this study will soon be submitted for publication. In Chapter 4, I will use the QC approach to compare data quality across four visual gamma datasets, combining data collected with three different MEG systems, from four research centres of the UK MEG Partnership. The preliminary results of this study will lay the foundations for collaborative work aimed at establishing a shared database of MEG data and defining common analytical and QC procedures for future MEG research.

Chapter 2.

A novel method for optimal peak frequency estimation and quality control

Parts of this Chapter have been published in the form of a peer-reviewed journal article:

Magazzini, L., Muthukumaraswamy, S. D., Campbell, A. E., Hamandi, K., Lingford-Hughes, A., Myers, J. F., ... & Singh, K. D. (2016). Significant reductions in human visual gamma frequency by the GABA reuptake inhibitor tiagabine revealed by robust peak frequency estimation. *Human Brain Mapping*. doi:10.1002/hbm.23283

2.1 Abstract

Increasing evidence suggests that the peak frequency of visual gamma oscillations could reflect individual parameters of synaptic function and physiology. This oscillatory parameter has been linked to inter-individual differences in sensory processing, cognitive function, cortical structure and appears to have a genetic contribution. To disentangle the intricate relationship among these factors, accurate and reliable estimates of peak frequency are required. Here, we developed a bootstrapping approach that fulfilled two purposes, providing both optimal measures of peak frequency and estimates of peak frequency reliability. In the first part of this study, we tested the validity of this method by generating synthetic time-series and simulating electrophysiological data as they would be obtained from MEG recordings. We compared the gamma peak frequency measured with our novel approach with the estimates obtained with an alternative method used in our lab before. The bootstrap approach resulted in increased estimation accuracy, with the bootstrap peak frequency showing reduced estimation error particularly in conditions of poor signal-to-noise ratio. In the second part of this work, we used the distribution of bootstrapped peak frequencies as a tool for data quality control (QC) with real MEG data. In a large sample of 97 participants, we found that the gamma peak frequency was estimated with high reliability in almost 90% of the sample. Three measures of visual gamma oscillations, namely peak amplitude, peak frequency and peak frequency reliability, were estimated with the bootstrap approach. We illustrate the distribution of these parameters across the sample and compare these measures among themselves as well as between different approaches to peak frequency estimation. The present work represents a first step towards establishing normative distributions of these oscillatory parameters in a large sample of healthy individuals.

2.2 Introduction

The frequency at which neurons in visual cortex oscillate in response to visual stimulation, i.e. the gamma peak frequency, is modulated by a number of factors, both extrinsic and intrinsic to the individuals from whom recordings are taken. Among the extrinsic factors, several physical properties of the visual stimulus modulate the gamma peak frequency. For example, the gamma peak frequency increases monotonically with increasing stimulus contrast (Jia et al., 2013; Ray and Maunsell, 2010; Roberts et al., 2013), is higher for moving stimuli compared to static ones (Friedman-Hill et al., 2000), for fast-moving compared to slow-moving stimuli (Gray et al., 1990; Gray and Viana Di Prisco, 1997), and for plaid stimuli compared to gratings (Lima et al., 2010). In turn, the gamma peak frequency decreases with increasing stimulus size (Gieselmann and Thiele, 2008; Jia et al., 2013; Ray and Maunsell, 2011), increasing stimulus eccentricity (Lima et al., 2010) and increasing levels of noise-masking (Jia et al., 2013).

Several of these findings were first reported in monkeys but have now been replicated in humans, including studies of stimulus contrast (Hadjipapas et al., 2015; Perry et al., 2014, 2015), size (van Pelt and Fries, 2013), motion (Muthukumaraswamy and Singh, 2013; Swettenham et al., 2009), motion velocity (Orekhova et al., 2015), eccentricity (van Pelt and Fries, 2013) and cross-orientation masking (Perry, 2015). However, the methodological differences between invasive LFP recordings and MEG can sometimes complicate the translation of animal models to humans. For example, in one MEG study by Perry et al. (2013), the decrease in peak frequency for large stimuli, previously reported in several monkey studies (Gieselmann and Thiele, 2008; Jia et al., 2013; Ray and Maunsell, 2011), was not observed consistently across human individuals (Perry et al., 2013). Since another MEG study on a smaller sample did replicate the relationship between these two parameters (van Pelt and Fries, 2013), the possible contribution of measurement noise to the high inter-individual variability reported by Perry et al. (2013)

cannot be completely ruled out. For example, the presence of multiple peaks in the gamma spectrum, which is sometimes observed in MEG recordings (Muthukumaraswamy and Singh, 2013), can introduce uncertainties in the interpretation of the MEG data and impact on the process of statistical inference.

Complicating this scenario, the gamma peak frequency appears to be modulated also by a number of intrinsic factors. Across individuals, the gamma peak frequency was shown to correlate positively with the surface area of V1 and V2 (Schwarzkopf et al., 2012) and with the thickness of the pericalcarine cortex (Muthukumaraswamy et al., 2010), although later studies failed to replicate either of these findings (Robson et al., 2015). The gamma peak frequency also correlates with psychophysical performance in visual discrimination tasks (Dickinson et al., 2015; Edden et al., 2009) and appears to co-vary with cognitive traits of possible clinical relevance (Dickinson et al., 2015; Kahlbrock et al., 2012a; Stroganova et al., 2015). The inter-individual differences in peak frequency are large and likely under genetic influences (van Pelt et al., 2012) and although the individual gamma peak frequency decreases with age (Gaetz et al., 2012; Muthukumaraswamy et al., 2010; Robson et al., 2015), this measure is highly repeatable over shorter time scales (Muthukumaraswamy et al., 2010; Tan et al., 2016).

Our ability to disentangle the relationship between gamma oscillation frequency and other parameters depends partly on the accurate and reliable estimation of peak frequency. The inclusion of weakly estimated parameters in inferential statistics can lead to enhanced risk of both spurious findings and false negative results. For these reasons, we developed a novel approach to identify poor-quality data by means of objective procedures that identify confidence intervals on the parameter estimates via bootstrapping. In the first part of this study, we tested this method on simulated data, demonstrating its validity as well as its increased accuracy in peak frequency

estimation. In the second part, we used the method to analyse real MEG data, providing descriptive metrics of visual gamma oscillatory parameter estimates in a large-sample cohort of healthy individuals.

2.3 Part I – Quality-control method validation with simulated data

2.3.1 Simulated data

We used Matlab (The MathWorks) to simulate electrophysiological data, as they would be recorded in visual gamma paradigms with MEG. The data resembled the time course of source-reconstructed cortical activity in the occipital lobe (for an example with real data, see Muthukumaraswamy et al., 2010) and were generated on a trial-by-trial basis (100 trials per dataset). Each trial was 2 seconds long, sampled at 1200 Hz, and was initially constructed with randomly generated noise that had a $1/f$ frequency scaling of the power spectrum. To reproduce the sustained component of visual gamma responses, the second half of each trial (i.e. 1 s) was embedded with a sinusoidal signal that had a different frequency in each trial. The frequency of the oscillation was normally distributed across trials, with both a mean and mode of 60 Hz, and a standard deviation (SD) increasing exponentially from 2.5 to 20 Hz across six different conditions (Figure 2.1). The six conditions were used to represent the inter-individual variability in gamma quality that is observed in real participants (e.g., Muthukumaraswamy et al., 2010). The amplitude of the oscillation was also normally distributed across trials (mean = 10%, SD = 1%, relative to noise amplitude). The phase of the oscillation was generated at random, to avoid phase consistency across trials and reproduce the induced component of visual gamma responses (i.e. time-locked but not phase-locked across trials). Thirty datasets were generated in each SD condition. The distribution of frequencies across trials differed slightly between datasets, although it always conformed in mean, mode, and SD, to the appropriate condition. Therefore, by manipulating the consistency of gamma frequency, while precisely controlling for other parameters, we created an ideal scenario for testing the performance of our method with data of progressively degraded quality. The spectra derived with the envelope and bootstrap methods (par. 2.3.2) are shown in Figure 2.1C and Figure 2.1D, respectively.

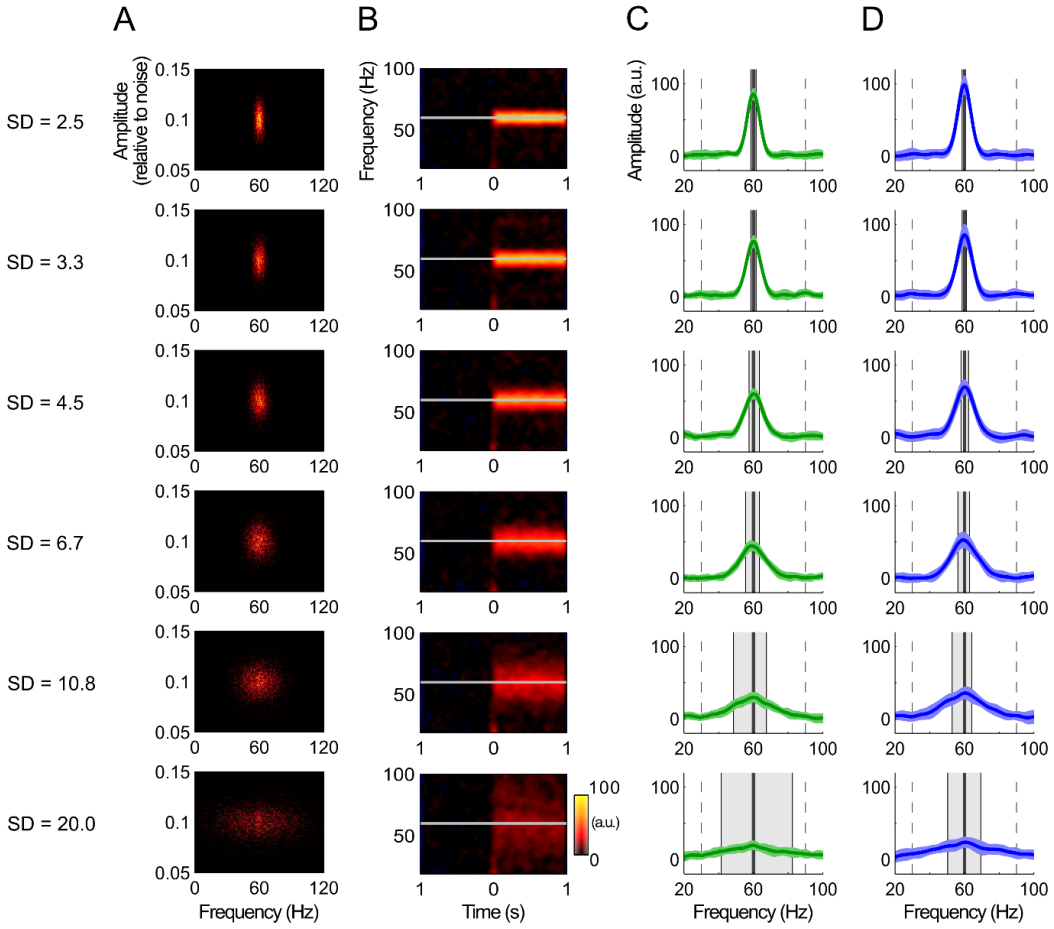

Figure 2.1. Simulated data.

A) Distribution of simulated frequencies and amplitudes pooled across all trials and all datasets, with decreasing frequency consistency across conditions. **B)** Time-frequency spectrograms derived using the envelope method, averaged across trials and across datasets. The warm colours index the percentage change from baseline, with the same scale in all conditions. The horizontal white line represents the real peak frequency in the data, defined by mean and mode frequency across trials. **C)** Spectra of percentage signal change from baseline derived using the envelope method, by averaging across the time dimension (0–1 s) of the time-frequency spectrograms. The coloured shadings represent ± 1 SD across datasets, the thick vertical black lines indicate the gamma peak frequency, the vertical dashed lines mark the frequency range in which peaks were searched, and the grey background areas define the range of observed peaks across datasets. **D)** The same as in C), but with spectra derived using the bootstrap method, by averaging the bootstrapped spectra calculated with the smoothed periodogram.

2.3.2 Bootstrap peak frequency estimation and quality control

An overview of our approach to peak frequency estimation and QC is illustrated schematically in Figure 2.2. To estimate the gamma peak frequency, we performed spectral analysis using a Fourier method, the smoothed periodogram (Bloomfield, 2000). In each trial, the time-series of baseline and stimulus (1 s each) were demeaned and tapered with a Hanning window. The raw periodogram was computed individually for each trial, separately for baseline and stimulus epochs, and smoothed with a Gaussian kernel (SD = 2 Hz). The single-trial spectra were averaged across trials, separately for baseline and stimulus, and the amplitude spectrum was calculated as percentage signal change from baseline.

At this point, our method departed from the typical approach to peak frequency estimation. The bootstrap procedure consisted of 10,000 iterations, in each of which trials were resampled, with replacement. Assuming an original sample composed of N trials, in each iteration, the sample resulting from the resampling procedure consisted always of N trials. However, by resampling with replacement, some trials would be included in the resampled pool of trials more than once, while others would be excluded. The resampling was at random in each iteration. In other words, in the extreme case that the same trial was included N times, the new sample would consist of N times the same trial. In the opposite extreme case, if each trial was included only once, the resampling would return the original sample. Note, though, that these extreme scenarios were highly unlikely to be realised over 10,000 iterations only (see below).

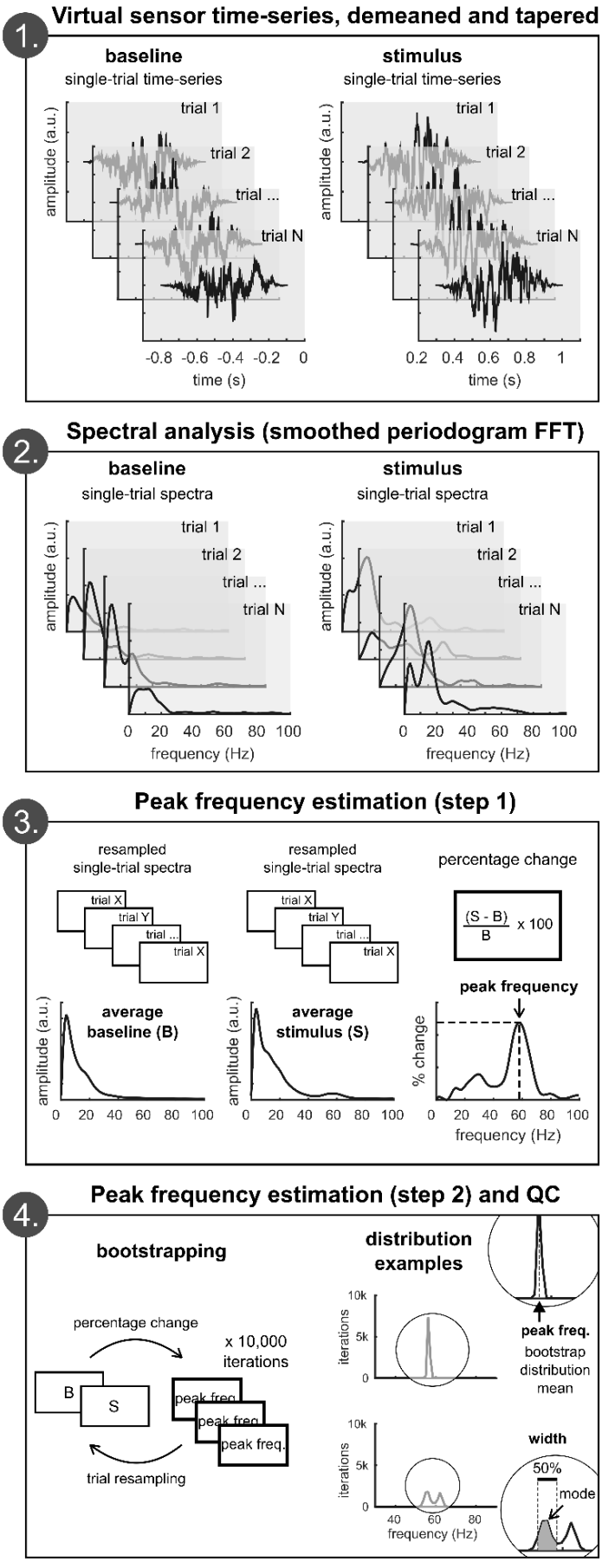

Figure 2.2. Schematic illustration of the approach to peak frequency estimation and QC.

The baseline and stimulus spectra of the same trial were always selected in pairs, i.e. there was no shuffling between trial epochs. In each bootstrap iteration, the resampled single-trial spectra were averaged, separately for baseline and stimulus spectra, and peak frequency was measured from the resulting spectrum of percentage change, as the peak of greatest increase in power in the 30–90 Hz range. The distribution of peak frequencies, across 10,000 bootstrap iterations, was then used in a QC procedure, which evaluated the reliability of the estimated peak frequencies, by calculating the width in frequency that was necessary to accommodate at least 50% of the bootstrapped frequencies around the distribution mode.

To test the properties of the bootstrap resampling approach, we simulated the resampling of 100 trials over 10,000 iterations. The procedure was repeated 10 times, in order to test the consistency of the results across repetitions. As illustrated in Figure 2.3A, on average 64 unique trials were included in each iteration. The distribution showed a Gaussian shape, ranging between 52 and 76 unique trials per iteration. The mean and mode of the distribution, as well as its shape, were highly repeatable across the 10 repetitions. Next, for each of the 10,000 iterations, we calculated how many times each trial (indexed from 1 to 100) was included in the resampling. As illustrated in Figure 2.3B, each trial was included on average once per iteration (average across iterations). Overall, these results indicate that the bootstrap approach is a valid method for obtaining estimates of central tendency and dispersion across trials, which does not introduce systematic biases in the resampled trials.

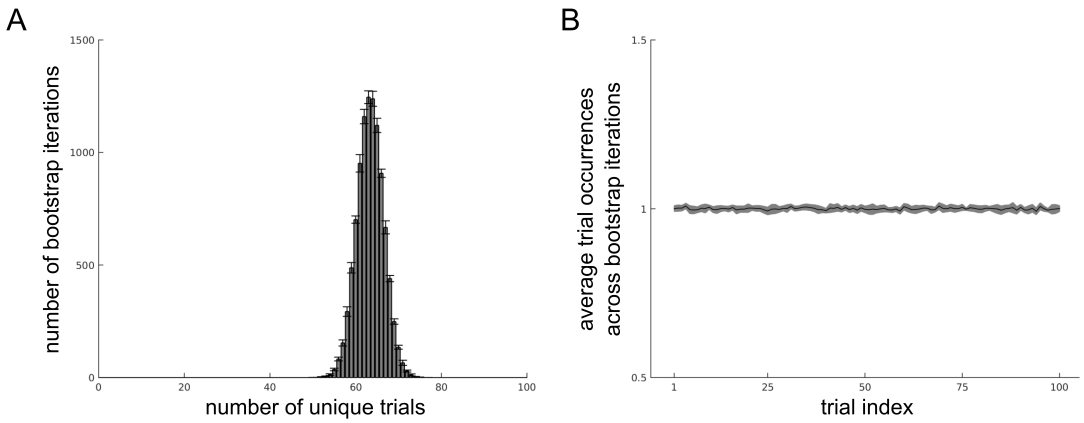

Figure 2.3. Properties of the bootstrap resampling approach.

A) The histogram illustrates the number of iterations (y axis) in which a given number of unique trials (x axis) was included in the resampled pool of trials. The distribution was averaged over 10 repetitions of the simulation, with error bars indicating ± 1 SD across repetitions. B) The thick line indicates how many times (y axis) each of the 100 trials (x axis) was included in the resampling of each iteration. This was calculated by averaging first across 10,000 iterations and then across 10 repetitions of the simulation. The grey shaded area indicates ± 1 SD across repetitions.

The gamma peak frequency was calculated by averaging over the distribution of bootstrapped peak frequencies. To test the validity of this measure as an improved estimate of peak frequency, hereafter also referred to as the 'bootstrap peak frequency', we compared its accuracy to a standard measure used in our lab, the 'envelope peak frequency'. The envelope peak frequency was calculated by bandpass-filtering the individual frequencies between 30–90 Hz in steps of 0.5 Hz, then calculating the magnitude of the analytic signal (Matlab function: *hilbert),* to yield the amplitude envelope for this frequency range. The envelopes were baselined, in order to express the response as a percentage change from baseline, and then 'stacked' to form a time-frequency spectrogram (Figure 2.1B). From this spectrogram, the amplitude values were averaged over the stimulus time-range, within each frequency, yielding the average amplitude spectrum. This spectrum can be used to estimate the gamma peak frequency induced by visual stimulation (for an example, see Muthukumaraswamy et al., 2010).

2.4 Part I - Results

2.4.1 Simulation results

The QC analysis of the simulated data showed that the width of the bootstrap peak frequency distribution necessary to accommodate at least 50% of the iterations increased monotonically across the six conditions of exponentially decreasing frequency consistency (Figure 2.4A). Similarly, we observed a monotonic decrease in the percentage of bootstrap iterations falling within ± 1.2 Hz of the bootstrap distribution mode (Figure 2.4B). This indicated the validity of the QC as a method to obtain reliability estimates of peak frequency.

Next, we compared the accuracy in peak frequency estimation between the bootstrap peak frequency and the envelope peak frequency. As shown in Figure 2.4C, the bootstrap method performed better than the envelope method, with higher estimation accuracy particularly at the lowest levels of gamma quality. This is also illustrated in Figure 2.1, where, as the SD of the response frequency increased, the range of estimated peak frequencies across datasets also increased (grey background areas in Figure 2.1C and Figure 2.1D). Overall, the range of peaks estimated with the bootstrap method was smaller and closer to the real peak frequency of the data.

These results provided the first indications for the choice of a QC cut-off threshold. In the two conditions of lowest frequency consistency (i.e. 10.8 and 20.0 SD), the frequency window accommodating 50% iterations around the bootstrap mode increased to widths markedly higher than 2.4 Hz (Figure 2.4A) and the percentage of iterations within ± 1.2 Hz fell below 50%. At these two levels of data quality, additionally, the estimation error of the bootstrap peak frequency was higher than ~1 Hz. These observations contributed to the choice of QC criterion adopted in the second part of this study (par. 2.5.6).

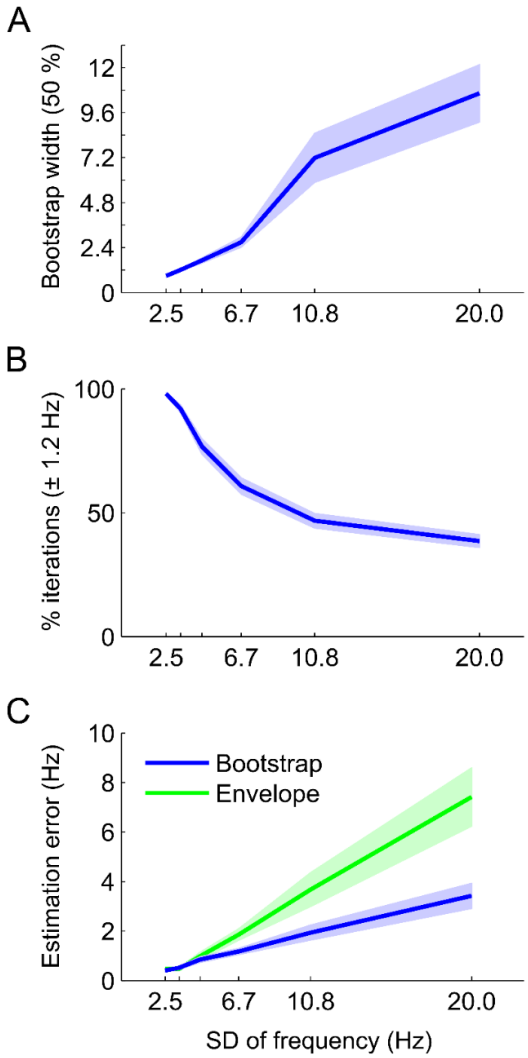

Figure 2.4. Results of the method validation with simulated data.

A) Width of the frequency range accommodating 50% or more of the bootstrapped peaks around the bootstrap distribution mode. **B)** Percentage of bootstrapped peaks within ± 1.2 Hz of the distribution mode. **C)** Absolute difference between the real and the estimated peak frequencies, averaged across datasets and plotted separately for the bootstrap (blue) and envelope (green) estimation methods. In all plots, shaded areas represent ± 1 SEM across datasets.

2.5 Part II – Quality control in the 100 Brains MEG cohort

2.5.1 Participants of the 100 Brains study

The '100 Brains' is a large genetic and multi-modal imaging project conducted at Cardiff University (Brealy, 2015). The participants of this study consisted of 100 healthy individuals, with normal or corrected vision, who were relatively homogenous in age, ethnicity, education and handedness. Participants were right-handed (as determined by the Edinburgh Inventory; Oldfield, 1971), of Caucasian ethnicity and had all completed or were completing a degree at the time they took part to the study. Their mental health was screened using the 12-Item General Health Questionnaire (Goldberg and Williams, 1988), with additional questions on history of excessive drug or alcohol use and any regular medications. The MEG data were available in 97 out of 100 participants (for more detailed information, see Brealy, 2015).

2.5.2 Visual gamma paradigm

The MEG data that we analysed here were collected while participants performed a visual paradigm known to induce strong gamma responses in occipital cortex (Muthukumaraswamy and Singh, 2009). The paradigm is illustrated schematically in Figure 2.5A. The visual stimulus consisted of a vertical, stationary, maximum contrast, square-wave grating with a spatial frequency of three cycles per degree, covering 8° × 8° of visual angle. The grating was presented centrally, on a mean luminance background, for a jittered duration between 1.5–2 s and was followed by an ITI of 2 s. Participants were instructed to fixate a red dot positioned at the centre of the grating and to press a button once the grating disappeared. A warning would be presented if no response was detected within 750 ms. The paradigm consisted of 100 trials, for a total duration of ~10 min. The stimulus presentations were programmed in Matlab (The Mathworks) using the Psychophysics Toolbox (Kleiner et al., 2007). Stimuli were

displayed on a Mitsubishi Diamond Pro 2070 monitor operating at a refresh rate of 100 Hz.

2.5.3 MEG data acquisition

The MEG recordings were performed using a 275-channel CTF axial gradiometer system (VSM MedTech), located inside a magnetically shielded room. An additional 29 reference channels were recorded for noise cancellation purposes and the primary sensors were analysed as synthetic third-order gradiometers (Vrba and Robinson, 2001). The sampling rate was 1200 Hz. Three electromagnetic coils were placed on three fiduciary locations (nasion, left and right pre-auricular) and their position relative to the MEG sensors was localised before and after the session.

2.5.4 MEG data pre-processing and MEG/MRI co-registration

The pre-processed MEG datasets and co-registered MRIs were courtesy of Dr Jennifer Brealy (Brealy, 2015). For each dataset, the individual trial epochs (-2–2 s) were visually inspected and trials containing large artefacts (e.g., head movements, muscle clenching and eye blinks) were excluded (~10% of the trials on average; range, 0–51%). For source-localization purposes, the MEG data were co-registered to the individual anatomical MRI of each participant by marking the MRI voxels corresponding to the position of the three fiducial coils. The individual anatomical MRIs (1-mm isotropic, T1-weighted FSPGR) were acquired as part of the 100 Brains study protocol, using a 3.0 T MRI scanner (General Electric).

2.5.5 Source localization analysis

The source localization analysis was performed in Matlab using the FieldTrip toolbox (Oostenveld et al., 2011). In order to reconstruct oscillatory activity at brain locations directly comparable across participants, 1) the MNI template brain was divided into a

grid with 5 mm isotropic voxel resolution, 2) the individual anatomical MRI was warped to the template MRI and 3) the inverse transformation matrix was used to warp the template grid onto an individual grid for each participant. The leadfield was calculated using a semi-realistic volume conduction model based on the individual anatomy (Nolte, 2003). The optimal dipole orientation at each voxel was calculated by SVD and power was estimated using the LCMV beamformer algorithm (Van Veen et al., 1997).

The beamformer weights were computed using a covariance matrix calculated from -1.5 to 1.5 s around stimulus onset, after bandpass-filtering the data between 35–75 Hz. The peak voxel was identified by selecting the voxel of greatest increase in gamma power (35–75 Hz) in the occipital lobe, measured as percentage change between stimulus (0.3–1.5 s) and baseline (-1.2–0 s). The individual peak voxel location of each participant was used to reconstruct the virtual sensor time-series in visual cortex, by multiplying the sensor-level data by the beamformer weights.

2.5.6 Quality control (100 Brains)

For descriptive purposes, the peak frequency reliability estimates were defined both 1) as the width, in Hz, of the frequency window that was necessary to accommodate 50% or more of the iterations around the bootstrap distribution mode and 2) as the percentage of iterations falling within a frequency window of pre-defined width, around the bootstrap distribution mode. With a baseline and stimulus analysis time-range of 1.2 s duration each, the frequency resolution of the periodogram, was ~0.6 Hz (see Discussion). The cut-off threshold used to determine whether the peak frequency was estimated with sufficient reliability was defined based on the percentage of iterations falling within ± 1.2 Hz around the distribution mode. In other words, if the frequency window necessary to accommodate 50% or more of the iterations had a width larger

than 2.4 Hz, the dataset was considered of poor quality. This width criterion was chosen based on the results of both the validation study (par. 2.4.1) and the QC analysis of the 100 Brains (par. 2.6.2). Furthermore, this cut-off width of 2.4 Hz was chosen to avoid excessively conservative thresholds, such as that of 1.2 Hz width, and to allow comparability with datasets in which a shorter analysis time-range can result in lower frequency resolution (see Discussion).

2.5.7 Quality control (UK MEG Partnership)

To test the reproducibility of the QC results of the 100 Brains cohort, the analysis was repeated on another large-sample dataset, from the UK MEG Partnership study at Cardiff University. A detailed description of this study is provided in the last experimental chapter of this thesis (Chapter 5). In brief, the data were recorded from 84 participants as part of a visual gamma paradigm similar to the one used in the 100 Brains study. The visual stimulus represented the major difference between the two protocols, as the grating used in the Partnership study subtended 4° of visual angle (both vertically and horizontally), compared to 8°, and was presented in the lower left visual field, rather than centrally. The processing parameters were the same as for the 100 Brains, for both source (par. 2.5.5) and QC analyses (par. 2.5.6). In contrast to the 100 Brains data, however, and in contrast to the analysis described for the twenty participants included in Chapter 5, the Partnership data were not visually inspected to remove gross artefacts.

2.6 Part II - Results

2.6.1 Visual gamma responses

The results of the source localization analysis are illustrated in Figure 2.5C. The percentage change in gamma power (35–75 Hz) between stimulus (0.3–1.5 s; sustained gamma) and baseline (-1.2–0 s) at each voxel location was calculated separately for each participant and then averaged. The average visual gamma response peaked in the left calcarine fissure (~80% power increase; MNI coordinates: [-8 -92 14] mm) and extended to the surrounding occipital cortex bilaterally. After visual inspection of the individual source topographies, three out of the initial 97 participants were excluded from further analysis, as they did not show a clear gamma peak in the occipital lobe.

The time-frequency analysis was performed individually for each of the remaining 94 participants by bandpass-filtering the virtual sensor time-series from -1.5 to 1.5 s at each frequency between 4–100 Hz in steps of 0.5 Hz (8 Hz bandpass, 3rd order Butterworth filter). The amplitude envelope of the analytic signal (Matlab function: *hilbert*) was then averaged across trials (e.g., Muthukumaraswamy et al., 2010) and expressed as percentage change from baseline (-1.5–0 s). The grand-average across participants (Figure 2.5B) illustrates the typical spectral and temporal evolution of visual gamma responses, characterised by a transient broadband power increase (~0–0.3 s; ~30–100 Hz) followed by a sustained narrowband oscillatory response (~0.3–1.5 s). The spectral properties of the latter component were the focus of the present investigation (see par. 2.6.2).

Overall, these observations are in line with the results reported by Brealy (2015), whose analysis differed mainly by the use of an alternative approach to source localization, namely SAM (Robinson and Vrba, 1999) as opposed to the LCMV beamformer algorithm used here (Van Veen et al., 1997). The following paragraphs focus on the

inter-individual variability in two parameters that are classically derived from the visual gamma spectral response, i.e. the gamma peak amplitude and peak frequency (par. 2.6.3), as well as on the reliability of the individual peak frequency estimates (par. 2.6.2).

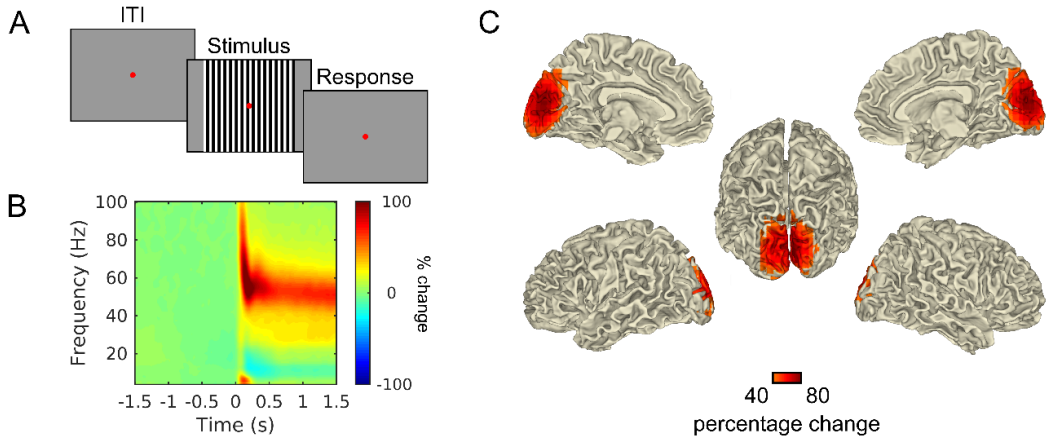

Figure 2.5. Visual gamma in the 100 Brains.

A) Schematic illustration of the visual gamma paradigm. Note that the motor response (button press) was provided within the first 750 ms of the 2 s ITI. **B)** Time-frequency representation of the virtual sensors reconstructed in visual cortex, calculated as percentage change from baseline (-1.5–0 s) and averaged over 94 participants. **C)** Beamformer source localization, averaged over 97 participants and projected onto the surface of an MNI template brain. For illustration purposes, values lower than a 40% increase from baseline were masked.

2.6.2 Data quality in the 100 Brains

The QC approach was used to illustrate, across participants, the percentage of iterations falling around the bootstrap distribution mode, for frequency windows of width increasing between 0–4.8 Hz in steps of 1.2 Hz. The height of the histogram bars in Figure 2.6 indicates the number of participants showing a given percentage of iterations, within a given frequency window width. As expected, as the width criterion gets looser (i.e. the frequency window gets wider around the mode), the distribution of participants shifts towards higher values of percentage iterations. In the majority of participants, only 15–25% iterations coincided with the bootstrap distribution mode (i.e. width = 0

Hz; Figure 2.6, top panel). Most participants showed 65–75% iterations within ± 0.6 Hz, i.e. within a frequency window of 1.2 Hz width (Figure 2.6, second panel from the top). At a width of 2.4 Hz, the distribution of participants started to peak at 95–100% iterations, with only a few participants showing less than 45–55% iterations falling within ± 1.2 Hz (Figure 2.6, middle panel). Similar patterns were observed at the least conservative width criteria of 3.6 and 4.8 Hz (Figure 2.6, bottom two panels).

The power spectra calculated with the QC method are illustrated in Figure 2.7, individually for each participant. The individual bootstrap peak frequency distributions are illustrated in Figure 2.8. The QC reliability criterion, i.e. at least 50% iterations falling within ± 1.2 Hz around the mode (par. 2.5.6), was not met in ~12% of the participants (11 out of 94).

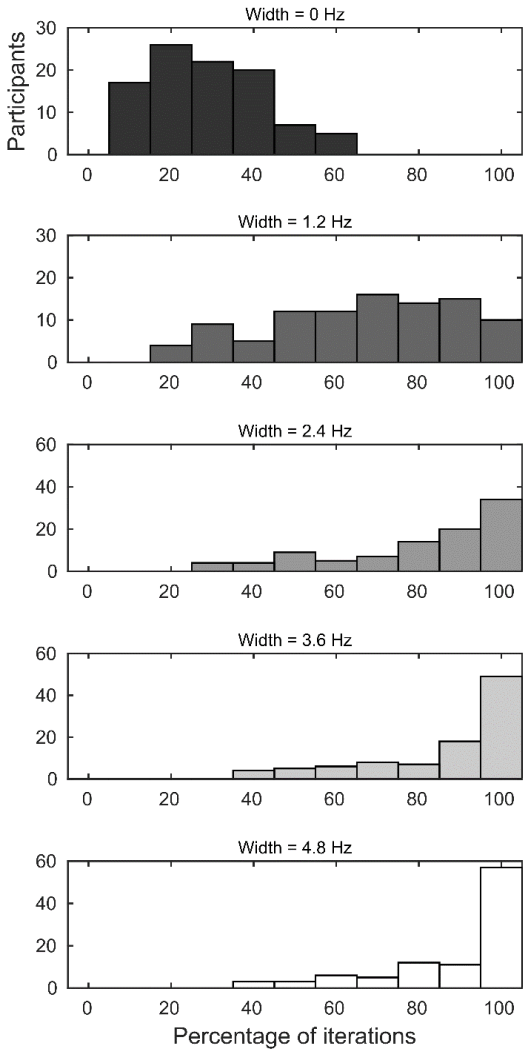

Figure 2.6. Distribution of the percentage of bootstrap iterations across participants.

In each plot, the histogram bars illustrate the distribution, across participants, of bootstrap iterations falling within a given width criterion. From top to bottom, the width criterion is increased in steps of 1.2 Hz (i.e. 0.6 Hz on each side of the distribution mode). As expected, as the width criterion gets less conservative, the number of participants showing high percentage values increases. Note the different y-axis scale between the top two and the bottom three histogram panels.

Figure 2.7. Individual visual gamma spectra (100 Brains).

Individual spectra of percentage change from baseline in the gamma frequency range (35–75 Hz). The shaded areas represent the 95% CI across bootstrapped trials. The vertical line in each panel indicates the mode of the bootstrap distribution. Poor-quality data (i.e. less than 50% of iterations within ± 1.2 Hz around the distribution mode) are shown in red. The empty panels correspond to participants without a peak voxel in visual cortex. Arbitrary participant labels are shown at the top of each plot.

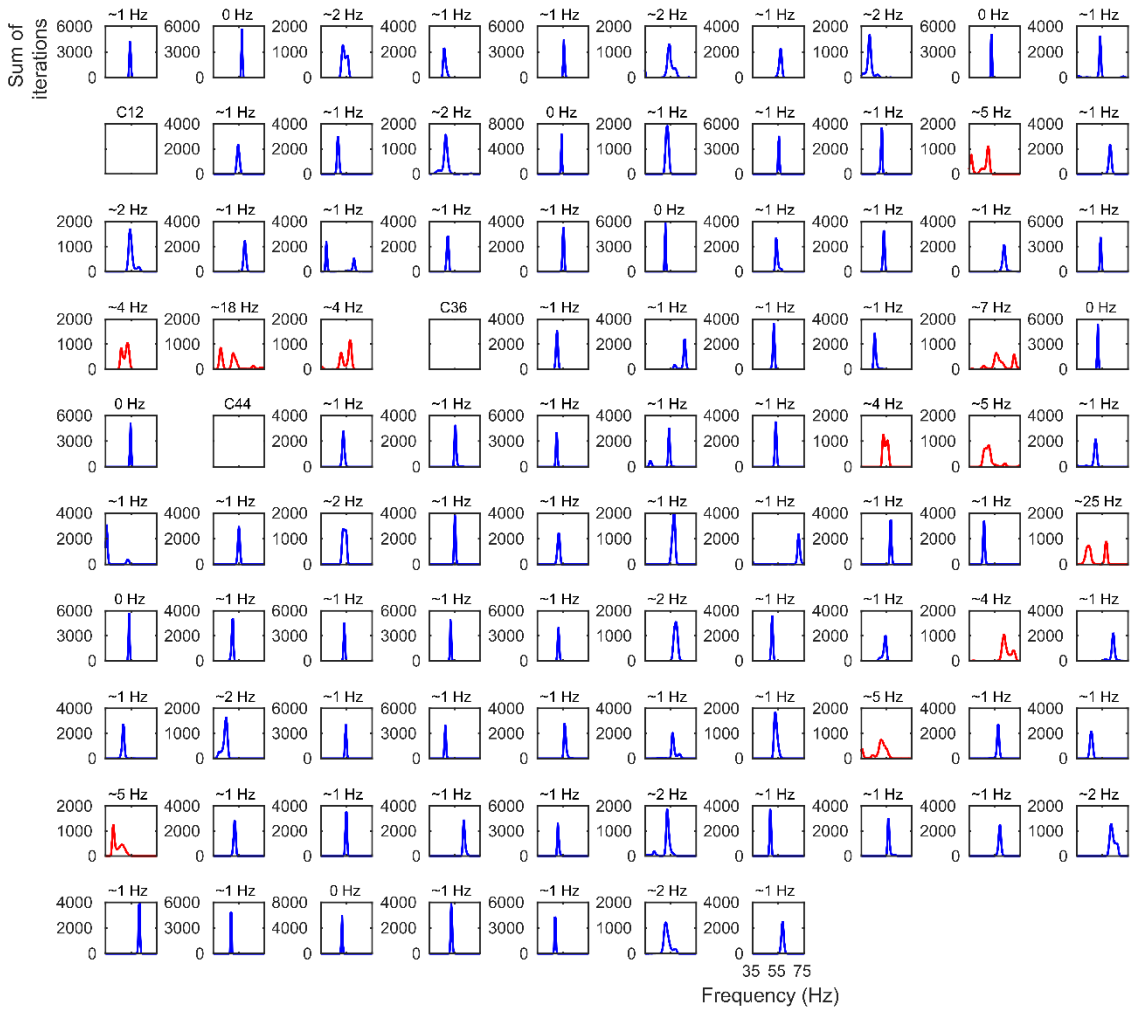

Figure 2.8. Individual bootstrap distributions of the gamma peak frequency.

The distributions were calculated over 10,000 bootstrap iterations. Poor-quality data (i.e. less than 50% of iterations within ± 1.2 Hz around the distribution mode) are shown in red. The width in frequency necessary to accommodate 50% or more of the bootstrap iterations is shown at the top of each panel. The empty panels correspond to participants without a peak voxel in visual cortex.

2.6.3 Distributions and correlations of parameter estimates

The distribution of the gamma peak amplitude and peak frequency parameters across the sample is illustrated in Figure 2.9A and Figure 2.9B, respectively. The gamma peak amplitude, measured by averaging over the bootstrap iterations within each participant, showed a skewed distribution, right-tailed towards high amplitude values, with an average gamma amplitude of 230% increase from baseline (SD = 180%; range, 18–1,060%). The gamma peak frequency, measured as the mode of the bootstrapped peak frequencies, was distributed symmetrically around a mean of 53.1 Hz (SD = 5.6 Hz; range, 35.7–70.9 Hz). The relationship between the gamma peak amplitude and peak frequency was tested using Pearson's *r*. We found no evidence for a linear relationship between these two parameters (Figure 2.9D), either when all participants (r = -0.06, p = 0.58) or only good-quality data were included in the analysis (r = -0.08, p = 0.47).

The distribution of peak frequency reliability across the sample (as indexed by the width in Hz necessary to accommodate at least 50% iterations around the bootstrap mode) is illustrated in Figure 2.9C. The frequency window width was 0 Hz in ~8%, 1.2 Hz in ~68%, 2.4 Hz in ~12%, 3.6 Hz in ~4% and 4.8 Hz or higher in the remaining ~8% of the participants. To test the relationship between data quality and gamma amplitude, the reliability of peak frequency was estimated using the percentage of iterations falling within a frequency window of 1.2 Hz width (i.e. ± 0.6 Hz), as this was the criterion showing the largest inter-individual variability across the sample (Figure 2.6, second panel from the top). The amplitude and reliability estimates were positively correlated (Figure 2.9E), with both all participants (r = 0.57, $p < 10^{-9}$) and only good-quality data included (r = 0.55, $p < 10^{-8}$). This indicated that the gamma peak frequency tended to be estimated more reliably in participants showing gamma responses of higher amplitude. No significant correlation was found between the gamma peak frequency and the estimates of peak frequency reliability (r = -0.01, p = 0.89; data not shown).

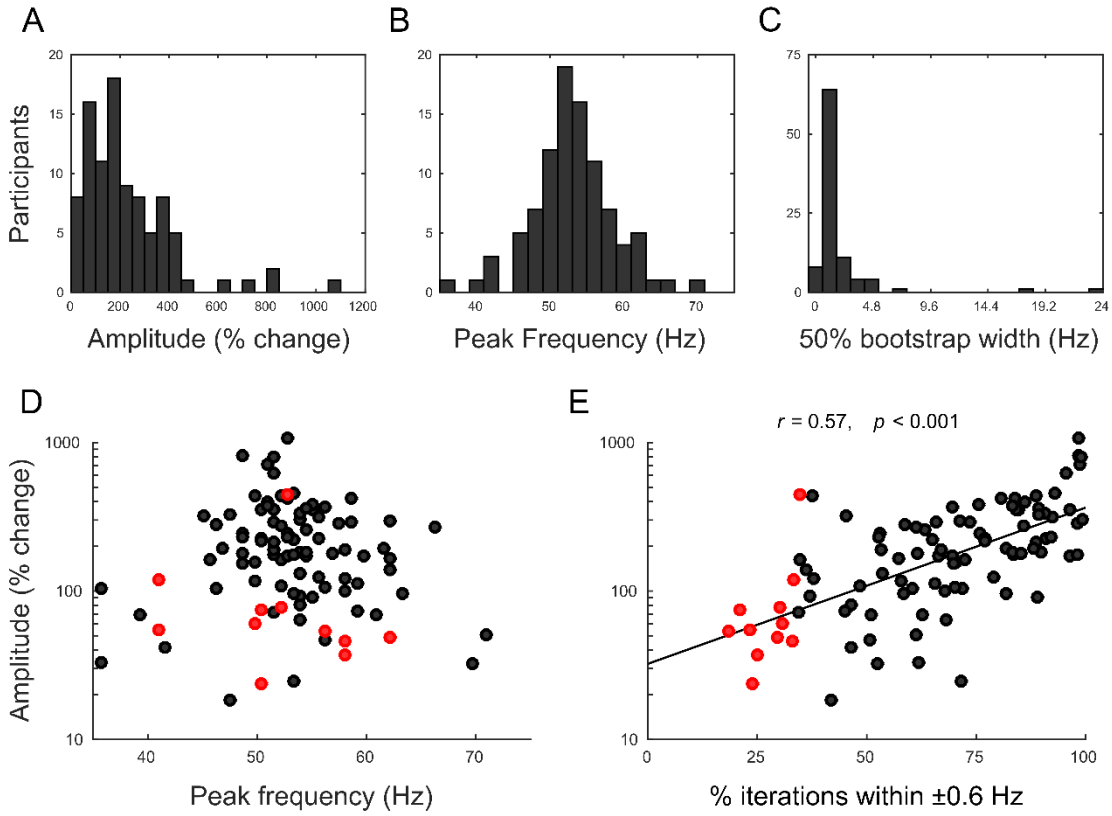

Figure 2.9. Distributions and correlations of the amplitude, frequency and quality parameters.

A) Distribution of gamma amplitude values (measured as percentage change from baseline) across participants. **B)** The same as in A), but for the gamma peak frequency (bootstrap distribution mode). **C)** The same as in A), but for the width in Hz necessary to accommodate 50% iterations or more around the bootstrap distribution mode. Note the different y-axis scale compared to A) and B). **D)** Scatter plot illustrating the absence of a linear relationship between gamma peak frequency and gamma amplitude (plotted on a logarithmic scale). The dots in red represent participants with poor-quality data. **E)** Scatter plot illustrating the significant positive linear relationship (Pearson's $r = 0.57$) between gamma amplitude and data quality (as indexed by the percentage of iterations falling within ± 0.6 Hz around the distribution mode). Note that although the gamma amplitude is plotted on a logarithmic scale, the values were not log-transformed prior to calculating the correlation coefficient. The colours are the same as in D).

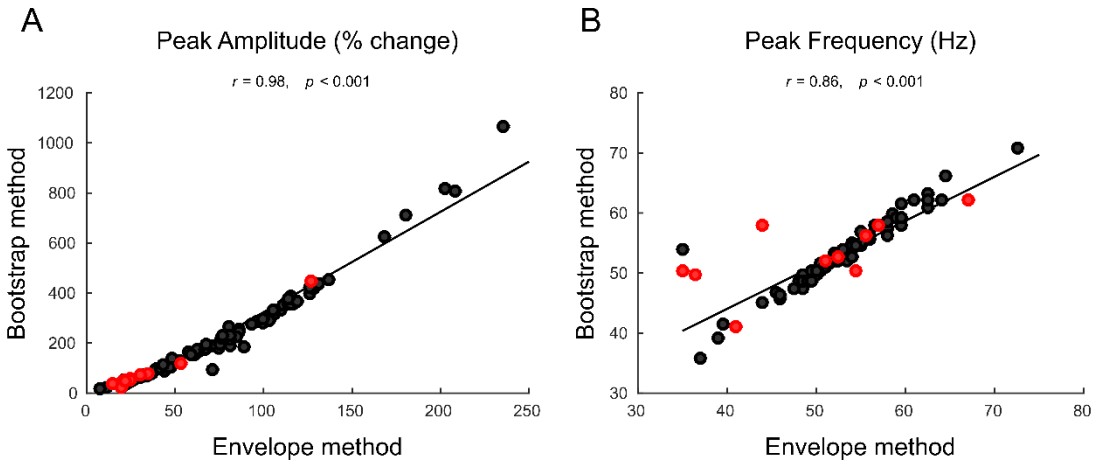

Figure 2.10. Comparison between bootstrap and envelope parameter estimates.

A) Scatter plot illustrating the significant positive linear relationship (Pearson's r = 0.98) between the gamma peak amplitude estimates obtained with the bootstrap and envelope methods. The dots in red represent participants with poor-quality data. **B)** The same as in A), but for the peak frequency parameter (Pearson's r = 0.86).

2.6.4 Comparison of parameter estimates

The comparison between the bootstrap and envelope estimates of the gamma peak amplitude and peak frequency parameters is illustrated in Figure 2.10A and Figure 2.10B, respectively. The amplitude values obtained with the bootstrap method were significantly higher, compared to the envelope method, but the two sets of amplitude estimates were highly correlated (r = 0.98, p < 0.001). Although statistically significant, however, the relationship between these two measures appeared quadratic rather than linear. It should be noted, in fact, that while the 'envelope peak amplitude' reflects actual *amplitude* measures, what we refer to as 'bootstrap peak amplitude' consists of percentage signal change between measures of spectral *power* density (i.e. amplitude squared). The linear relationship between the spectral *power* estimates obtained with the two methods is illustrated in Figure 2.11. In this additional analysis, the amplitude values obtained with the envelope method were squared before calculating the percentage change between stimulus and baseline epochs. The two measures, i.e.

bootstrap and envelope *power* estimates, resulted almost perfectly correlated ($r = 0.99$, $p < 0.001$).

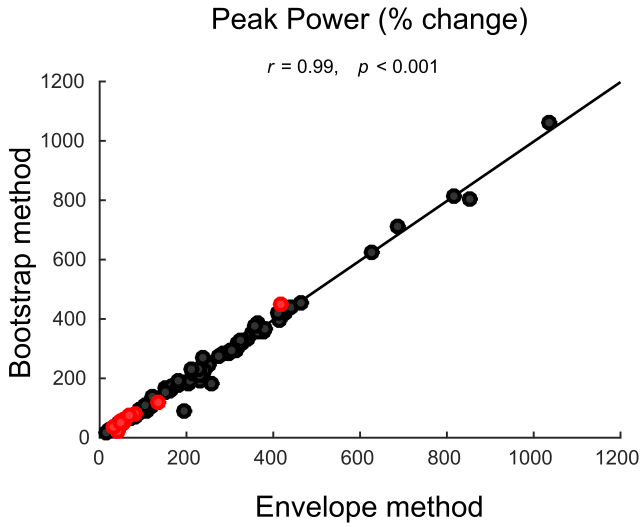

Figure 2.11. Comparison between bootstrap power and envelope power.

Scatter plot illustrating the almost perfect positive correlation (Pearson's $r = 0.99$) between bootstrap and envelope measures of spectral *power*. Colours are as in Figure 2.10.

The gamma peak frequency estimates (Figure 2.10B) were also highly correlated between the bootstrap and envelope methods ($r = 0.86$, $p < 0.001$). Furthermore, this significant positive relationship was strengthened after exclusion of poor-quality data from the correlational analysis ($r = 0.93$, $p < 0.001$). With inclusion of all participants, the bootstrap peak frequency was significantly higher than the envelope peak frequency ($t(93) = 2.14$, $p = 0.035$). However, after exclusion of the unreliable peak frequency estimates, this difference was no longer statistically significant ($t(82) = 1.58$, $p = 0.12$).

2.6.5 Data quality in the UK MEG Partnership (Cardiff data)

The power spectra calculated with the QC method for the UK MEG Partnership data collected at Cardiff University are illustrated in Figure 2.12, individually for each participant. A peak voxel in visual cortex could not be identified in five participants, which were thus excluded from the QC analysis. The QC reliability criterion, i.e. at

least 50% iterations falling within ± 1.2 Hz around the mode, was not met in ~13% of the remaining participants (10 out of 79). Overall, therefore, these results indicate that the QC results obtained in the 100 Brains dataset were replicated in a different sample of comparable size, using a similar visual gamma protocol.

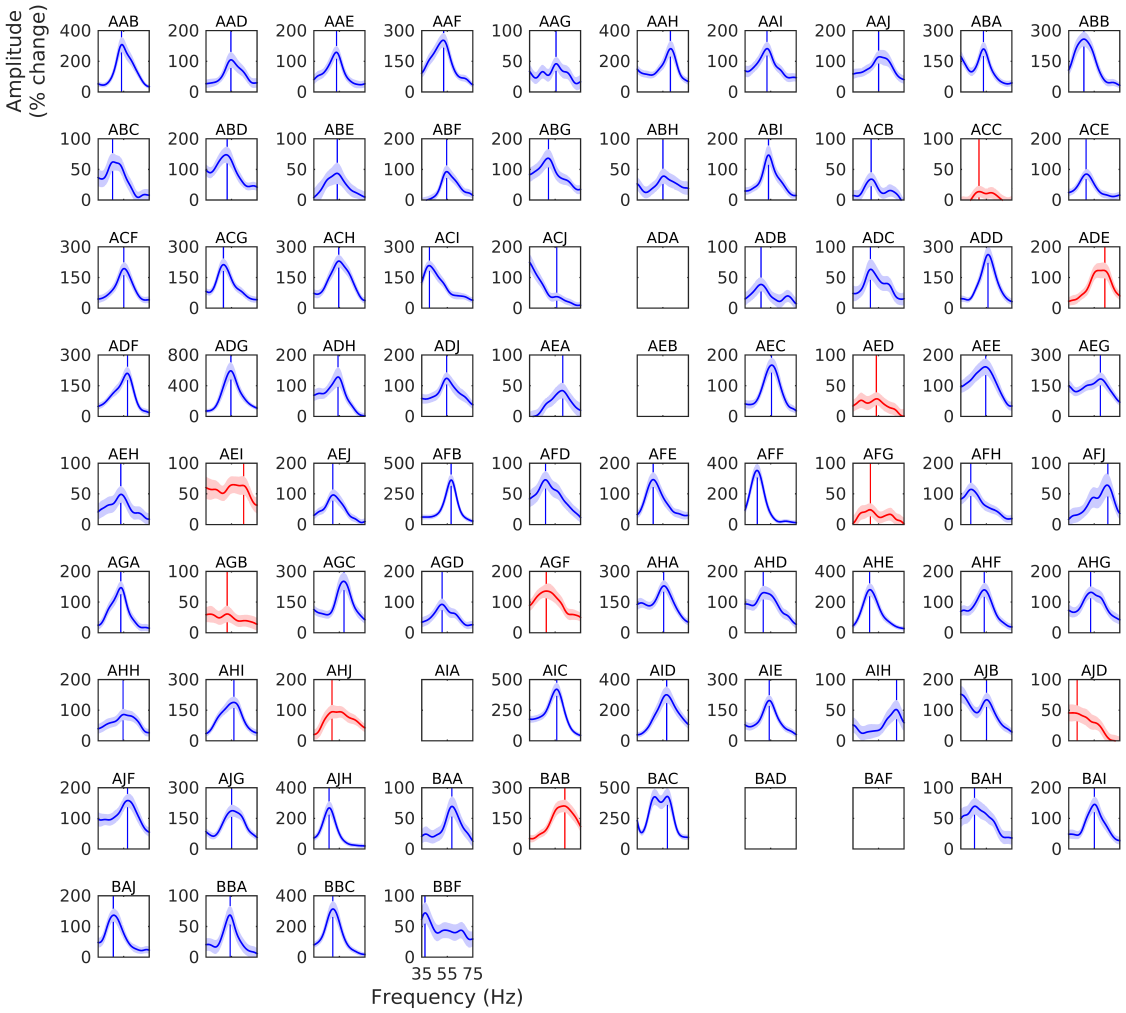

Figure 2.12. Individual visual gamma spectra (UK MEG Partnership).

The same as in Figure 2.7, but for the Cardiff data of the UK MEG Partnership.

2.7 Discussion

In the first part of this work, we developed a method based on bootstrapping across trials, which served two purposes: first, we measured the gamma peak frequency by averaging across the bootstrapped samples, and demonstrated the increased robustness of this measure relative to a more conventional alternative approach; second, we used a measure of spread in the distribution of bootstrapped peaks to estimate the reliability of the gamma peak frequency, which in turn allowed the identification of poorly estimated data. In the second part of this work, we used this QC approach to analyse real MEG data, which were collected as part of the '100 Brains' study at Cardiff University. We used this large-sample dataset to illustrate the distribution of oscillatory parameters such as the gamma peak amplitude and peak frequency, with particular emphasis on the estimates of peak frequency reliability.

2.7.1 Establishing quality-control criteria via bootstrapping

The peak frequency reliability estimates were obtained with two different but comparable approaches. The first option consisted of establishing a fixed proportion of bootstrap iterations, e.g., 50%, and calculating the width of the frequency window that was necessary to accommodate the requested percentage of iterations around the mode of the bootstrap distribution. This first approach is illustrated in Figure 2.4A, for the simulated data, and in Figure 2.9C, for participants of the 100 Brains. The second option was to define a fixed frequency window width around the bootstrap mode, e.g., ± 1.2 Hz, and calculate the proportion of iterations falling within the specified range. This second approach is illustrated in Figure 2.4B, for the simulated data, and in Figure 2.6, for participants of the 100 Brains.

The QC approach presented here should be treated as a framework for objective quantification of data quality. This neither establishes fixed criteria, nor provides rigid

guidelines for data exclusion. Rather, by characterizing data quality with descriptive measures, the method can be used to define explicit exclusion criteria based on unambiguous thresholds, and could prove useful for comparing data across sites, studies, and designs. Importantly, both these two approaches to estimating peak frequency reliability depend on the frequency resolution of the spectral estimation method. In this work, power spectral density was estimated with a Fourier method, the smoothed periodogram (Bloomfield, 2000). The frequency resolution of the periodogram (Matlab function: *periodogram*) is determined by the ratio between the sampling frequency (i.e. 1200 Hz, both in the simulated and in the 100 Brains MEG data) and the next power of two greater than the signal length. For example, the 100 Brains data consisted of analysis epochs of 1.2 s length, sampled at 1200 Hz for a total of 1440 time points. The next power of two greater than 1440 is 2048, resulting in 'frequency steps' of 1200 / 2048 ≃ 0.6 Hz. At a sampling frequency of 1200 Hz, for analysis time-series shorter than ~850 ms (and longer than ~425 ms), the next power of two is 1024, resulting in frequency steps of 1200 / 1024 ≃ 1.2 Hz. Note, however, that if the time-series are zero-padded to the next power of two, the increased frequency resolution (as indexed by the smaller frequency step) is only apparent, as the intrinsic frequency resolution is still determined by the length of the trial time-series. In typical MEG analyses, the data epochs are often between 500 ms and a few seconds long and are usually acquired at sampling rates of approximately 1 kHz. Also for these reasons, the QC cut-off threshold that we used to define data as of poor quality in this study was set to ± 1.2 Hz, as opposed to ± 0.6 Hz. The latter criterion was considered both excessively conservative and less easily generalizable to the analysis of spectral estimates with lower frequency resolution. Furthermore, at a frequency window width of 2.4 Hz (Figure 2.6, middle panel), the distribution of percentage iterations across the sample showed a clear lower tail. This allowed us to identify the participants with the

lowest-quality data (less than 50% iterations within ± 1.2 Hz), which corresponded to 12% of the sample. Interestingly, when this analysis was repeated for the second cohort (the UK MEG Partnership data, Figure 2.12) a very similar rejection rate of 13% was also achieved. This is despite the fact that the stimulus used was a smaller quadrant, rather than central full-field, and the data were not visually inspected to reject contaminated trials. Future work could directly compare cleaned and non-cleaned datasets to assess whether this rejection procedure is necessary for the analysis of visual gamma, particularly when using spatial filtering techniques, such as the beamformer used here.

2.7.2 Optimal peak frequency estimation via bootstrapping

It is worth noting that the two QC approaches mentioned above (par. 2.7.1) assume that the bootstrap distribution mode represents the most accurate estimator of the real peak frequency in the data, although our simulation demonstrated the validity also of the bootstrap mean as an accurate measure of peak frequency. The bootstrap peak frequency, calculated from the bootstrap distribution, resulted in an optimal measure when inter-trial frequency consistency was low in our method validation. However, it is possible that other methods, such as the envelope approach, could perform with better accuracy under different circumstances, such as when oscillation frequency cannot be assumed stationary. In the 100 Brains dataset, the exclusion of poor-quality data increased the strength of the correlation between the bootstrap and envelope peak frequency estimates (from $r = 0.86$ to $r = 0.93$; Figure 2.10B). This suggests that the uncertainty in peak frequency estimation was reduced by removing the estimates that were classified as unreliable with our QC criterion.

After visual inspection of the scatter plot in Figure 2.10B, it can be noted that the peak frequency in one participant was estimated differently by the two methods despite being

classified as of good quality, while a number of participants appeared to be estimated consistently between the two methods despite being classified as of poor quality. This is likely to reflect the balance between sensitivity and specificity of the QC approach. In particular, sensitivity and specificity can be affected by the width criterion, which determines the threshold for marking data as of poor quality. If a strict criterion is chosen, good but not perfect frequency estimates could be inappropriately excluded, potentially leading to a loss of statistical power. On the contrary, the choice of a loose criterion could lead to inclusion of poor estimates and, for example, increased likelihood of false negative results. In the future, work on either simulated data or similar large-sample datasets will have the opportunity to optimise the current approach. For example, optimal QC criteria could be determined empirically by systematically varying the method parameters (e.g., spectral estimation, tapering, number of bootstrap iterations, bootstrap width criterion, etc.) and testing how each of these changes impacts on the sensitivity and specificity of the QC results.

2.7.3 Considerations on gamma amplitude

In this study, we found a significant positive correlation between the gamma peak amplitude and the peak frequency reliability estimates, indicating higher data quality in participants showing higher-amplitude gamma responses. This suggests that the reliability of peak frequency could be inferred using a QC approach that is simply based on the response amplitude. However, as illustrated in the scatter plot in Figure 2.9E, the peak frequency was measured with high consistency across bootstrap iterations in several participants who showed relatively low-amplitude gamma responses (~20–30% increase). Vice versa, in some of the poor-quality participants, the consistency of peak frequency across bootstrap samples was low despite the response amplitude being high. The power spectra of individual participants illustrate how the latter scenario can sometimes result from gamma responses spanning relatively broad frequency ranges at

the highest amplitude values, which can make a clear peak frequency difficult to discern (e.g., see participants labelled as C33, C50 and C84 in Figure 2.7).

Finally, it is also worth noting that the estimates of peak amplitude derived with the smoothed periodogram in the bootstrap method were consistently higher than those obtained with the envelope approach. This is because the measures obtained with the periodogram reflect *power* spectral density, whereas in the envelope approach the analytic signal is used to derive *amplitude* envelopes. Nevertheless, when the estimates of gamma amplitude calculated with the envelope method turned into envelope *power* estimates (i.e. they were squared), the bootstrap and envelope *power* measures resulted almost perfectly correlated ($r = 0.99$; Figure 2.11). Similarly, when bootstrap *power* and envelope *amplitude* were correlated (Figure 2.10A), the two methods differed for the absolute values returned, but the relative differences across individuals were preserved.

2.7.4 Method applications

Overall, we believe that the QC approach proposed here will be most useful when noisy estimates of peak frequency can affect the statistical inferences made on this parameter. In particular, the modulation of the gamma peak frequency by extrinsic factors often occurs with small effect sizes and thus represents a challenge for the relatively noisy recordings obtained with MEG. One such example is the study by Perry et al. (2013) on the relationship between gamma frequency and stimulus size (see Introduction), where the large inter-individual variability in the relationship between these two parameters could be attributed also to external factors, such as measurement noise. Additionally, the use of relatively large stimulus sizes, which is typically necessary in order to elicit gamma responses of measurable amplitude in MEG (Muthukumaraswamy and Singh, 2013; Perry et al., 2013), could in principle result in complex, rather than coherent, oscillatory patterns across the visual cortex (Perry et al., 2013; van Pelt and Fries,

2013). In turn, oscillatory responses with different spectral profiles, such as those that are recorded from neurons with receptive fields for different eccentricities (Lima et al., 2010), could 'leak' into the spatially summated MEG signal, resulting in complex spectral responses. Together, measurement noise and spectral/spatial 'leakage' could explain the presence of multiple gamma peaks that is sometimes observed in MEG recordings (Muthukumaraswamy and Singh, 2013) and which can affect statistical inference. The QC approach proposed in this chapter provides a framework for objective quantification of data quality, which can contribute to reducing the uncertainties in the estimation and interpretation of the gamma peak frequency estimates obtained with MEG. The next chapter of this thesis (Chapter 3) will demonstrate the power of this approach when applied to the estimation of peak frequency modulations induced by pharmacological manipulation.

Chapter 3.

Peak frequency estimation and quality control in pharmacological MEG studies of visual gamma oscillations

Parts of this Chapter have been published in the form of a peer-reviewed journal article:

Magazzini, L., Muthukumaraswamy, S. D., Campbell, A. E., Hamandi, K., Lingford-Hughes, A., Myers, J. F., ... & Singh, K. D. (2016). Significant reductions in human visual gamma frequency by the GABA reuptake inhibitor tiagabine revealed by robust peak frequency estimation. *Human Brain Mapping*. doi:10.1002/hbm.23283

3.1 Abstract

The peak frequency of visual gamma oscillations is determined by both the neuronal excitation-inhibition balance and the time constants of GABAergic processes. In this study, we used the quality control (QC) approach developed in the previous chapter of this thesis (Chapter 2) to re-analyse MEG data from two pharmacological studies of visual gamma with alcohol (Campbell et al., 2014) and tiagabine (Muthukumaraswamy et al., 2013a). In the first study, disruption of the excitation-inhibition balance by alcohol was found to increase the peak amplitude and decrease the peak frequency of visual gamma oscillations. Here, our QC method revealed unreliable estimates of peak frequency in the same participants who were originally excluded by Campbell et al. (2014) using different qualitative criteria. Furthermore, the alcohol-induced reduction in peak frequency was replicated using the gamma peak frequency estimates derived with the bootstrap approach. The second study by Muthukumaraswamy et al. (2013a) had previously reported that GABAergic enhancement by tiagabine had surprisingly no effect on visual gamma oscillations – an unexpected finding given the strong evidence from both animal models and recent human studies. In our re-evaluation of this study, unreliable data were excluded using the QC method and the gamma peak frequency was estimated with the bootstrap approach. As originally predicted, we found that the GABA reuptake inhibitor tiagabine did produce a marked decrease in visual gamma oscillation frequency. These results demonstrate the potential impact of objective QC approaches in pharmacological MEG studies. Additionally, the tiagabine results provide new translational evidence for the mechanisms of GABAergic transmission generating gamma oscillations in humans.

3.2 Introduction

Synchronization of rhythmic neuronal firing in the gamma frequency range (~30–90 Hz) is a potential mechanism for information coding in the brain (Buzsáki and Wang, 2012; Fries, 2009). Pyramidal cell populations synchronized by inhibitory GABAergic interneurons produce intra-cortical LFP oscillations (Gonzalez-Burgos and Lewis, 2012), which can be recorded with high consistency between primates and humans (Fries et al., 2008a). Through translational research (Hall et al., 2005), gamma oscillations have been implicated in human sensory and cognitive function, as well as in neuropsychiatric disease (for reviews, see Bosman et al., 2014; Phillips and Uhlhaas, 2015; Sedley and Cunningham, 2013). In the MEG signal, sustained narrow-band gamma oscillations are generated in visual cortex in response to simple contrast pattern stimuli (Adjamian et al., 2004b; Hoogenboom et al., 2006). These responses arise from the interaction between local excitatory and inhibitory networks, which are believed to shape the amplitude, as well as the peak frequency of gamma oscillations (Bartos et al., 2007; Gonzalez-Burgos and Lewis, 2012).

In-vitro and in-vivo animal studies have demonstrated a dependency of the gamma peak frequency on the time constants of GABAergic processes (Bartos et al., 2007; Gonzalez-Burgos and Lewis, 2012). In very recent years, a limited number of studies combining MEG with pharmacological modulation of neurotransmission have provided initial compelling evidence for the translation of such models to humans. Reduced frequency of gamma oscillations was observed following administration of alcohol (Campbell et al., 2014) and lorazepam (Lozano-Soldevilla et al., 2014), drugs which enhance GABAergic transmission through different mechanisms. These findings largely support animal models in which IPSCs of prolonged duration result in synchronized pyramidal neurons firing at slower rhythms, generating gamma oscillations at lower frequencies and with higher amplitudes (Gonzalez-Burgos and Lewis, 2012).

However, not all human studies are entirely consistent with the animal literature. For example, the $GABA_A$ positive allosteric modulator propofol was found to increase gamma amplitude, but left gamma frequency unchanged (Saxena et al., 2013). More surprisingly, a recent study reported that neither the amplitude nor the frequency of visual gamma were modulated by tiagabine (Muthukumaraswamy et al., 2013a), a drug that prolongs IPSC duration by selectively inhibiting the re-uptake of GABA from the synapse. To date, the reasons behind such inconsistencies remain unknown.

In the present work, we build upon previous research in which the robustness of gamma oscillatory measures was studied with respect to systematic variations of the stimulus configuration (Muthukumaraswamy and Singh, 2013). Despite the use of optimised experimental designs, gamma responses in certain participants can be barely detectable or scarcely quantifiable (Hoogenboom et al., 2006; Muthukumaraswamy et al., 2010). Since the inclusion of weakly estimated parameters can lead to enhanced risk of both spurious findings and false negative results, here we applied our novel QC approach to two previous MEG studies of visual gamma modulations by pharmacological agents.

We re-analysed a study of alcohol by Campbell et al. (2014) and a study of tiagabine by Muthukumaraswamy et al. (2013a). Alcohol has a complex mechanism of action, affecting several different neurotransmitter systems, but primarily it decreases neuronal excitation by NMDA blockade (Grant and Lovinger, 1995) and increases neuronal inhibition via GABAergic enhancement (Weiner and Valenzuela, 2006). Tiagabine, in contrast, has a well-understood mechanism of action, which consist of inhibiting the reuptake of GABA from the synapse via GAT-1 blockade, resulting in elevated synaptic GABA concentrations (Dalby, 2000; Fink-Jensen et al., 1992). Despite these substantial pharmacological differences between alcohol and tiagabine, both drugs produce $GABA_A$-mediated IPSPs and IPSCs of prolonged duration (Roberto et al., 2003;

Roepstorff and Lambert, 1994; Thompson and Gähwiler, 1992). For this reason, and because of the dependency of gamma oscillations on the time constants of GABAergic inhibition (Bartos et al., 2007; Gonzalez-Burgos and Lewis, 2012), we hypothesised that modulations of the gamma peak frequency comparable to those observed with alcohol (Campbell et al., 2014) could be observed also with tiagabine (Muthukumaraswamy et al., 2013a), after controlling for data quality.

First, we tested the method on the study of alcohol, replicating the drug-induced reduction in peak frequency as well as providing objective quantitative measures that confirmed the authors' original observations on data quality (Campbell et al., 2014). Second, we re-evaluated the study by Muthukumaraswamy et al. (2013a), in which GABAergic enhancement by tiagabine had previously demonstrated a null effect on visual gamma oscillations. After exclusion of participants with unreliably measured data, we found that GABAergic enhancement by tiagabine produced a marked decrease in the peak frequency of visual gamma oscillations. This result supports the authors' original predictions (Muthukumaraswamy et al., 2013a), and provides additional translational evidence for the neurophysiological mechanisms generating gamma oscillations in humans (Bartos et al., 2007; Buzsáki and Wang, 2012).

3.3 Materials and Methods

3.3.1 Alcohol study design and data acquisition

We re-analysed data from a previous pharmacological MEG study of alcohol (Campbell et al., 2014). A detailed description of the experimental procedures, including participants, experimental design, MEG acquisition and analysis are reported in Campbell et al. (2014). Here we provide a summary. Sixteen healthy volunteers took part in a single-blind, placebo-controlled, crossover study. The study was divided into two days, each consisting of two sessions. Each day began with a 'pre-drink' session, followed by either placebo or alcohol consumption (0.8 g/kg), and by a 'post-drink' session.

In each MEG session, participants performed a visual paradigm known to robustly induce gamma oscillations in primary visual cortex. The visual stimulus consisted of a vertical, stationary, maximum contrast, three cycles per degree, square-wave grating covering 8 × 8° of visual angle. The grating was presented centrally, on a mean luminance background, for 1.5 s and was followed by an ITI of 2 s. Participants were instructed to fixate a red dot positioned at the centre of the grating and to press a button once the grating disappeared. A warning would be presented if no response was detected within 750 ms. The paradigm consisted of 100 trials, for a total duration of ~10 min. The stimulus presentations were programmed in Matlab (The Mathworks) using the Psychophysics Toolbox (Kleiner et al., 2007). Stimuli were displayed on a Mitsubishi Diamond Pro 2070 monitor operating at a refresh rate of 100 Hz.

The MEG recordings were performed using a 275-channel CTF axial gradiometer system (VSM MedTech), located inside a magnetically shielded room. An additional 29 reference channels were recorded for noise cancellation purposes and the primary sensors were analysed as synthetic third-order gradiometers (Vrba and Robinson, 2001).

The sampling rate was 1200 Hz. Three electromagnetic coils were placed on three fiduciary locations (nasion, left and right pre-auricular) and their position relative to the MEG sensors was localised before and after each session. For source-localization purposes, the MEG data were co-registered to the individual anatomical MRI of each participant by marking the MRI voxels corresponding to the position of the three fiducial coils. The individual anatomical MRIs (1-mm isotropic, T1-weighted FSPGR) were acquired as part of a different study, using a 3.0 T MRI scanner (General Electric).

3.3.2 Analysis of alcohol MEG data

The virtual sensor data that were re-analysed in this study were courtesy of Dr Anne Campbell (Campbell et al., 2014). For each dataset, the individual trial epochs (-2–2 s) were visually inspected and trials containing excessive artefacts (e.g., head movements, jaw clenches and eye blinks) were excluded. This resulted in the inclusion of the following average number of trials for analysis: pre-alcohol 82.6 (SD = 17.8), post-alcohol 85 (SD = 11.2), pre-placebo 82.4 (SD = 14.5), post-placebo 77.2 (SD = 16.1).

The source localization analysis was performed using the SAM beamformer algorithm (Robinson and Vrba, 1999). A multiple local-spheres volume conductor model (Huang et al., 1999) was computed by fitting spheres to the brain surface extracted by FSL's Brain Extraction Tool (Smith, 2002). The beamformer weights were computed at 4 mm isotropic voxel resolution using a global covariance matrix calculated on the bandpass-filtered data. The difference in gamma power (30–80 Hz) between stimulus (0–1.5 s) and baseline (-1.5–0 s) was calculated with a paired t-statistic at each voxel location. Virtual sensors were generated at the peak voxel location in the occipital lobe, for each participant and each session separately.

3.3.3 Quality control of alcohol data

The gamma peak frequency was calculated using the bootstrap approach described in the previous chapter of this thesis (Chapter 2), by averaging over 10,000 bootstrap iterations. In brief, the raw periodogram was computed separately for baseline (-1.4 to -0.1 s) and stimulus (0.3 to 1.5 s), smoothed with a Gaussian kernel (SD = 2 Hz) and averaged across trials, separately for baseline and stimulus spectra. The average amplitude spectrum was calculated as percentage signal change from baseline and the peak frequency in each bootstrap iteration was measured as the spectral peak of greatest amplitude, in the 30–90 Hz range. To obtain the peak frequency reliability estimates, the QC criterion was defined using a frequency window width of 2.4 Hz. In other words, if 50% or more of the bootstrapped peak frequencies in a given dataset fell within ± 1.2 Hz around the bootstrap distribution mode, the peak frequency in that dataset was considered reliably estimated. Otherwise, the dataset was marked as of poor quality.

For comparison, the analysis of the gamma peak frequency with alcohol was performed also using the 'envelope peak frequency'. As described in Chapter 2, the envelope peak frequency was calculated by bandpass-filtering the individual frequencies between 30–90 Hz in steps of 0.5 Hz, then calculating the magnitude of the analytic signal, to yield the amplitude envelope for this frequency range. The envelopes were baselined, in order to express the response as a percentage change from baseline. From the time-frequency spectrogram, amplitude was averaged over the stimulus time-range, within each frequency, yielding the average amplitude spectrum from which the envelope peak frequency was calculated.

3.3.4 Tiagabine study design and data acquisition

We re-analysed data from a previous pharmacological MEG study of tiagabine (Muthukumaraswamy et al., 2013a). A detailed description of the experimental

procedures, including participants, experimental design, MEG acquisition and analysis are reported in Muthukumaraswamy et al. (2013a). Here we provide a summary. Eighteen healthy volunteers took part in a single-blind, placebo-controlled, crossover study. Three women were unable to complete the study (see Hamandi et al., 2014), leaving complete datasets from fourteen men and one woman. The study was divided into two days, each consisting of four sessions. Each day began with a 'pre' measurement session, followed by oral administration of either placebo or tiagabine (15 mg; Gabitril®), and by three 'post' measurement sessions at 1, 3, and 5 hours after ingestion.

The visual gamma paradigm was very similar to the one used in the alcohol study (Campbell et al., 2014). The visual stimulus (par. 3.3.1) was presented in the lower left visual field, covering 8 × 8° of visual angle, for a shorter period compared to the study by Campbell et al. (2014), with a jittered duration between 1–1.5 s and an ITI of 1.5 s. Participants were instructed to fixate a red dot positioned at the top right-hand edge of the grating and to press a button once the grating disappeared, within 750 ms. The paradigm consisted of 120 trials, for a total duration of ~10 min. The stimulus presentations were programmed in Matlab (The Mathworks) using the Psychophysics Toolbox (Kleiner et al., 2007). Stimuli were displayed on a Mitsubishi Diamond Pro 2070 monitor operating at a refresh rate of 100 Hz.

The MEG recordings and MEG/MRI co-registration procedures were performed as described in the alcohol study (par. 3.3.1).

3.3.5 Analysis of tiagabine MEG data

The virtual sensor data that were re-analysed in this study and the SAM beamformer images illustrated in Figure 3.8 were courtesy of Dr Suresh Muthukumaraswamy (Muthukumaraswamy et al., 2013a). For each dataset, the individual trial epochs (-1–1

s) were visually inspected and trials containing gross artefacts (e.g., head movements and muscle clenching) were excluded. For each participant, the number of trials included in the analysis of each session was equalised by removing trials from the end of each recording. This resulted in an average number of trials for analysis of 105.5 per participant (range 82–117).

The beamformer source localization analysis was performed using SAM (Robinson and Vrba, 1999), as described in the alcohol study (par. 3.3.2). The difference in gamma power (30–80 Hz) between stimulus (0–1 s) and baseline (-1–0 s) was calculated with a paired t-statistic at each voxel location and virtual sensors were generated at the peak voxel location in the occipital lobe, for each participant and each session separately.

To compare the spatial distribution of gamma responses between placebo and tiagabine conditions, the SAM beamformer images were averaged, separately for accepted and rejected participants (par. 3.4.3 and 3.4.4). These average SAM maps were produced by spatially normalising the individual SAM images onto the MNI template brain using FMRIB's Linear Affine Registration Tool (Jenkinson and Smith, 2001). The warping parameters were first obtained by registering the participant's anatomical MRI with the template brain and then applied to each individual SAM image of that participant.

3.3.6 Quality control of tiagabine data

The QC analysis was performed as described in the alcohol study (par. 3.3.3). The gamma peak frequency was calculated by averaging over bootstrap iterations, using a baseline of -0.8 to -0.1 s and a stimulus period of 0.3 to 1.0 s. With this relatively short analysis time-range (700 ms), the QC criterion used to calculate the peak frequency reliability estimates coincided with the frequency resolution of the periodogram (~1.2 Hz). Peak frequency was considered reliably estimated if 50% or more of the

bootstrapped peaks in a given dataset fell within ± 1.2 Hz around the bootstrap mode, otherwise, the dataset was marked as of poor quality.

For comparison, the analysis of the gamma peak frequency with tiagabine was performed also using the 'envelope peak frequency', as described for the alcohol study (par. 3.3.3).

3.4 Results

3.4.1 Data quality in the alcohol study

The QC analysis of the alcohol data revealed, according to a QC reliability criterion of 50% iterations within ± 1.2 Hz, poor estimates of peak frequency in 5 out of 64 datasets, across all participants and conditions (Figure 3.1). This resulted in poor-quality data in 4 out of 16 participants. The same observation was also reported by Campbell et al. (2014) based on the absence of a clear peak in at least one of the MEG sessions, within participants. Poor-quality datasets were treated as missing observations, and excluded from further statistical analysis according to a list-wise deletion approach.

3.4.2 Peak frequency modulations by alcohol

To test the effect of alcohol on the frequency of visual gamma oscillations, the gamma peak frequency was analysed using a 2×2 repeated measures ANOVA, with factors *Drug* (two levels: placebo and alcohol) and *Time* (two levels: pre and post), with the *Drug* × *Time* interaction term being of most interest. To compare how the exclusion of participants and the bootstrap approach to peak frequency estimation affected the results, the analysis was repeated using the bootstrap peak frequency (Figure 3.2A and Figure 3.2B), and the envelope peak frequency (Figure 3.2C and Figure 3.2D), with inclusion of good-quality data only (Figure 3.2A and Figure 3.2C), and with all data included (Figure 3.2B and Figure 3.2D). For reference, the interaction effect observed by Campbell et al. (2014), where the gamma peak frequency was estimated in twelve participants using skewed Gaussian function fits, was $F(1,11) = 13.31$, $p = 0.004$.

The bootstrap method in the twelve participants with complete data, illustrated in Figure 3.2A, resulted in no significant effect of *Drug* ($F(1,11) = 2.44$, $p = 0.15$), a significant effect of *Time* ($F(1,11) = 5.34$, $p = 0.041$), and a significant *Drug* × *Time* interaction effect ($F(1,11) = 15.58$, $p = 0.002$). Peak frequency was significantly reduced by

alcohol in the post-alcohol session compared to both the pre-alcohol ($t(11) = -4.68$, $p = 0.001$) and the post-placebo session ($t(11) = -3.63$, $p = 0.004$). There were no significant differences in peak frequency between pre- and post-placebo ($t(11) = 0.58$, $p = 0.57$) or between pre-placebo and pre-alcohol ($t(11) = 0.44$, $p = 0.67$). The absence of a significant difference between pre- and post-placebo indicated that the significant main effect of *Time* was driven by the significant difference between pre- and post-alcohol alone.

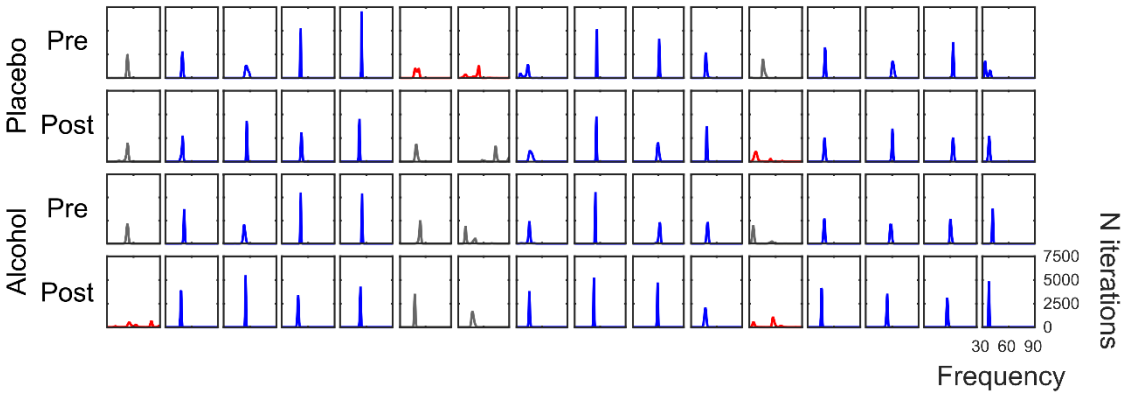

Figure 3.1. Data quality in the alcohol study.

Individual bootstrap distributions of the gamma peak frequency, calculated over 10,000 bootstrap iterations. The distributions are arranged column-wise by participants, in the placebo (top two rows) and alcohol (bottom two rows) conditions. The QC results are displayed in red (poor-quality datasets) and in blue (good-quality datasets). List-wise exclusions are displayed in grey.

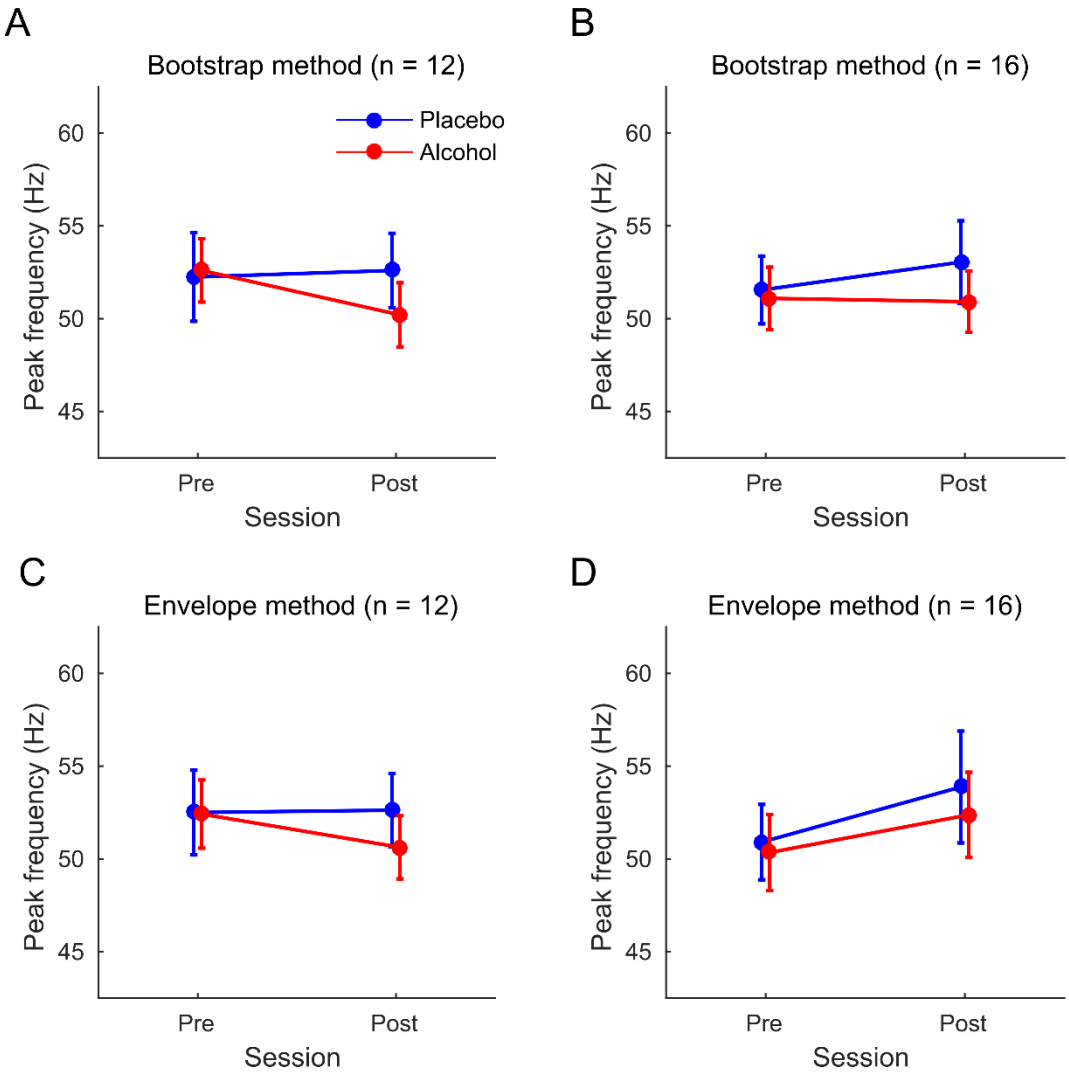

Figure 3.2. Peak frequency modulations with alcohol.

A) Peak frequency calculated using the bootstrap method, after exclusion of poor-quality data. **B)** The same as in A), but with all participants included. **C)** Peak frequency calculated using the envelope method, after exclusion of poor-quality data. **D)** The same as in C), but with all participants included. The average peak frequency across participants is plotted in blue for placebo and in red for alcohol. Vertical bars represent ± 1 SEM.

The results of the bootstrap method with inclusion of all sixteen participants (Figure 3.2B) showed no significant effect of *Drug* ($F(1,15) = 1.04$, $p = 0.32$) or *Time* ($F(1,15) = 0.31$, $p = 0.59$), and no significant *Drug* × *Time* interaction effect ($F(1,15) = 0.58$, $p = 0.46$).

The envelope method in the twelve participants with complete data (Figure 3.2C) resulted in no significant effect of *Drug* ($F(1,11) = 2.51$, $p = 0.14$) or *Time* ($F(1,11) = 2.30$, $p = 0.16$), and a significant *Drug* × *Time* interaction effect ($F(1,11) = 9.16$, $p = 0.012$). Peak frequency was significantly reduced by alcohol in the post-alcohol session compared to both the pre-alcohol ($t(11) = -2.57$, $p = 0.026$) and the post-placebo session ($t(11) = -2.71$, $p = 0.020$). There were no significant differences in peak frequency between pre- and post-placebo ($t(11) = 0.22$, $p = 0.83$) or between pre-placebo and pre-alcohol ($t(11) = -0.12$, $p = 0.91$).

The results of the envelope method with inclusion of all sixteen participants (Figure 3.2D) showed no significant effect of *Drug* ($F(1,15) = 0.40$, $p = 0.53$) or *Time* ($F(1,15) = 1.26$, $p = 0.30$), and no significant *Drug* × *Time* interaction effect ($F(1,15) = 0.05$, $p = 0.82$).

To summarise, using the bootstrap method to estimate the gamma peak frequency and after exclusion of participants based on the QC approach, the interaction effect reported by Campbell et al. (2014) was replicated at a higher level of significance compared to both the envelope method and the Gaussian function fits. Furthermore, our QC approach resulted in the exclusion of four participants, as also reported by Campbell et al. (2014) based on the absence of a clear peak in at least one of the conditions. No significant interaction was observed, with either the bootstrap or the envelope method, when all participants were included in the analysis.

3.4.3 Data quality in the tiagabine study

In the tiagabine study, the QC reliability criterion of 50% iterations within ± 1.2 Hz was not met in 22.5% of the datasets, across all participants and conditions (Figure 3.3). Across the eight recording sessions, the rate of within-subject data rejection was as high as 62.5% in four participants. Poor-quality datasets were treated as missing observations, and excluded from further statistical analysis according to a list-wise deletion approach.

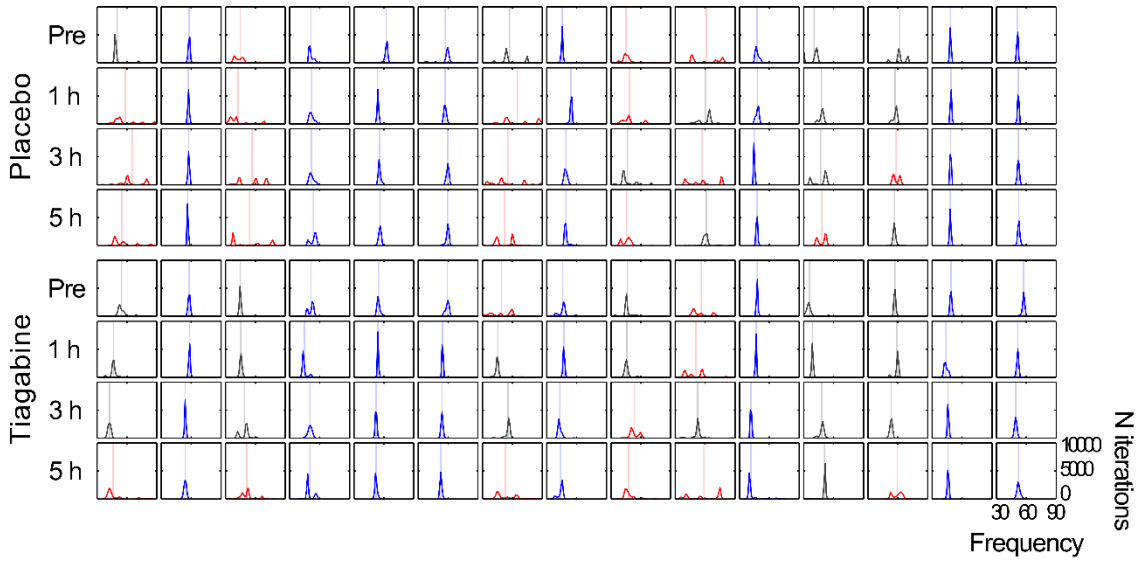

Figure 3.3. Data quality in the tiagabine study.

Individual bootstrap distributions of the gamma peak frequency, calculated over 10,000 bootstrap iterations. The distributions are arranged column-wise by participants in the placebo (top four rows) and tiagabine (bottom four rows) conditions. The QC results are displayed in red (poor-quality datasets) and in blue (good-quality datasets). List-wise exclusions are displayed in grey. The gamma peak frequency (bootstrap distribution mean) is indicated with a vertical line in each dataset.

3.4.4 Spectral modulations by tiagabine

To test the main hypothesis of a shift in the frequency of visual gamma oscillations, the bootstrap peak frequency was analysed in the eight participants with complete data using a 2×4 repeated measures ANOVA, with factors *Drug* (two levels: placebo and tiagabine) and *Time* (four levels: pre, 1 h, 3 h, and 5 h). In this analysis design, a significant effect of tiagabine is demonstrated by a significant *Drug* × *Time* interaction. Results, illustrated in Figure 3.4A, showed a significant effect of *Drug* ($F(1,7) = 18.8$, $p = 0.003$), a marginally non-significant effect of *Time* ($F(3,21) = 2.9$, $p = 0.057$), and a significant *Drug* × *Time* interaction effect ($F(3,21) = 3.7$, $p = 0.028$). The correspondence between bootstrap peak frequencies and peaks in the gamma range of the raw spectra, across all participant and conditions, is illustrated in Figure 3.5.

To investigate the temporal profile of drug modulation, given the significant interaction, we analysed the simple effects of *Drug* using paired-sample t tests at each of the four time points. There was no difference in peak frequency between the pre-ingestion sessions of the tiagabine and placebo treatments ($t(7) = -0.2$, $p = 0.87$). In contrast, the gamma peak frequency was significantly reduced with tiagabine, compared to the corresponding placebo sessions, at 1 h ($t(7) = 2.4$, $p = 0.048$), at 3 h ($t(7) = 6.5$, $p = 0.0003$), and at 5 h post-ingestion ($t(7) = 5.0$, $p = 0.002$).

Next, we analysed the simple effects of *Time* with two 1×4 repeated measures ANOVAs, separately for each of the two treatments. There was no effect of time in the placebo treatment ($F(3,21) = 0.1$, $p = 0.97$), suggesting that peak frequency was estimated reliably over repeated placebo sessions. In contrast, the effect of *Time* was significant in the tiagabine treatment ($F(3,21) = 7.3$, $p = 0.002$). Compared to the pre-tiagabine session, peak frequency was significantly reduced at 1 h ($t(7) = 2.6$, $p = 0.036$), at 3 h ($t(7) = 5.2$, $p = 0.001$), and at 5 h post-tiagabine ($t(7) = 5.5$, $p = 0.001$).

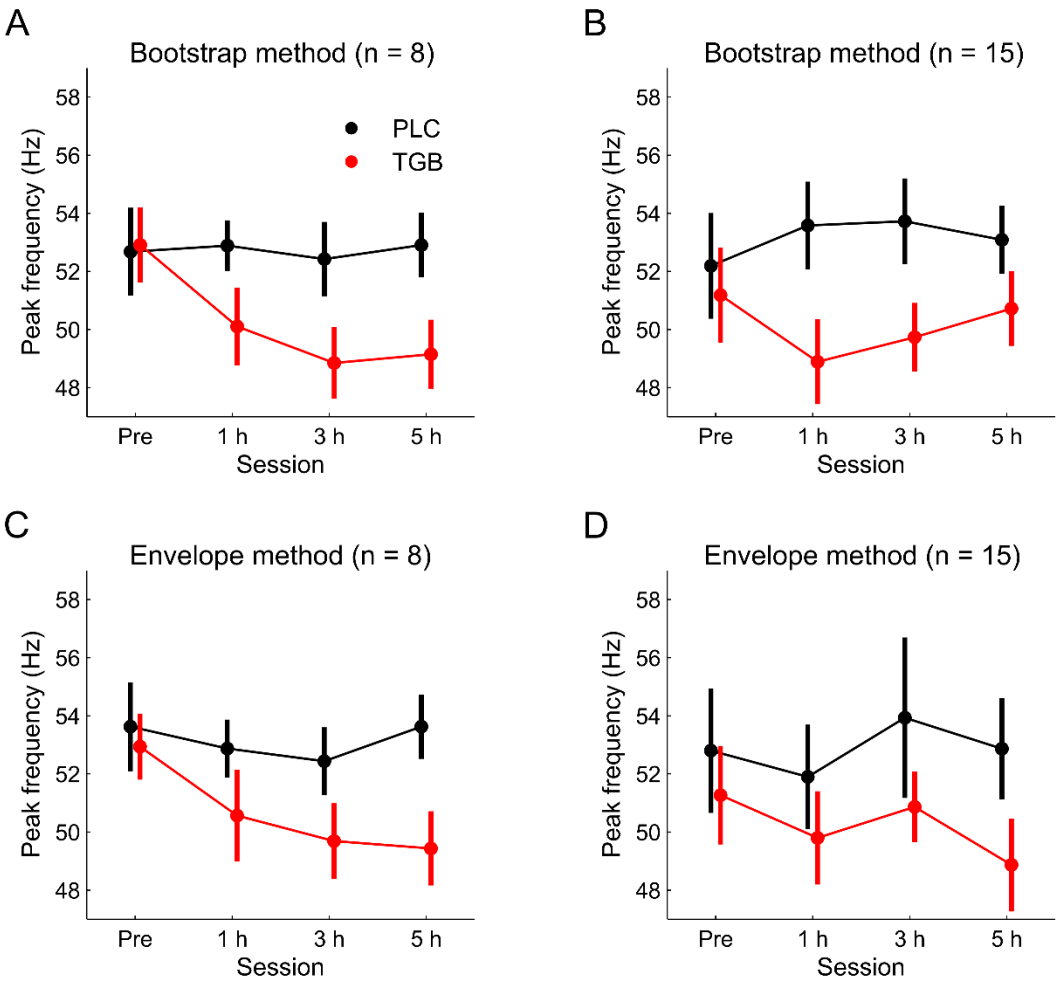

Figure 3.4. Peak frequency modulations with tiagabine.

A) Peak frequency calculated using the bootstrap method, after exclusion of poor-quality data. **B)** The same as in A), but with all participants included. **C)** Peak frequency calculated using the envelope method, after exclusion of poor-quality data. **D)** The same as in C), but with all participants included. The average peak frequency across participants is plotted in black for placebo (PLC) and in red for tiagabine (TGB). Vertical bars represent ± 1 SEM.

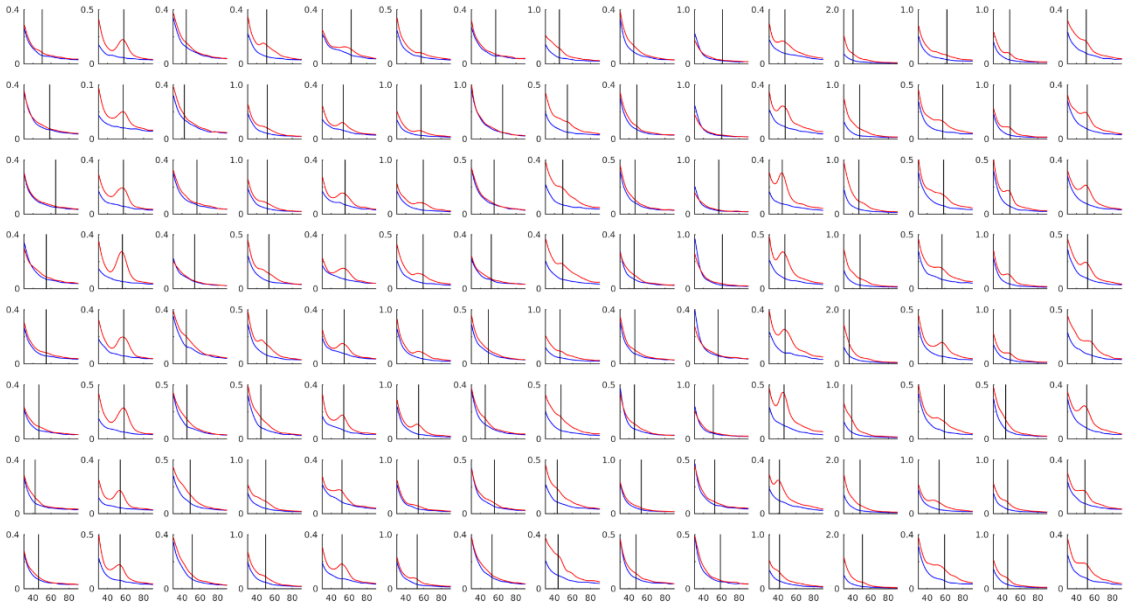

Figure 3.5. Tiagabine raw spectra.

Amplitude spectra of baseline (in blue) and stimulus (in red) in the gamma range (30–90 Hz), arranged column-wise by participants, in the placebo (top four rows) and tiagabine (bottom four rows) conditions. The gamma peak frequency (bootstrap distribution mean) is indicated with a vertical line in each dataset.

The amplitude spectra of percentage change from baseline in the gamma range are illustrated in Figure 3.6, averaged across participants. It can be noted that the averaged bootstrap peaks (vertical lines) appear just to the left of the peak in the average spectra. This effect, which appears particularly marked in the right-hand panels, is a result of the averaging procedure. Specifically, the individual spectra of higher amplitude tended to peak at higher frequencies, resulting in increased amplitude of the portion of the spectrum on the right side of the average peak frequency. The effect is explained with an illustrative example in Figure 3.7.

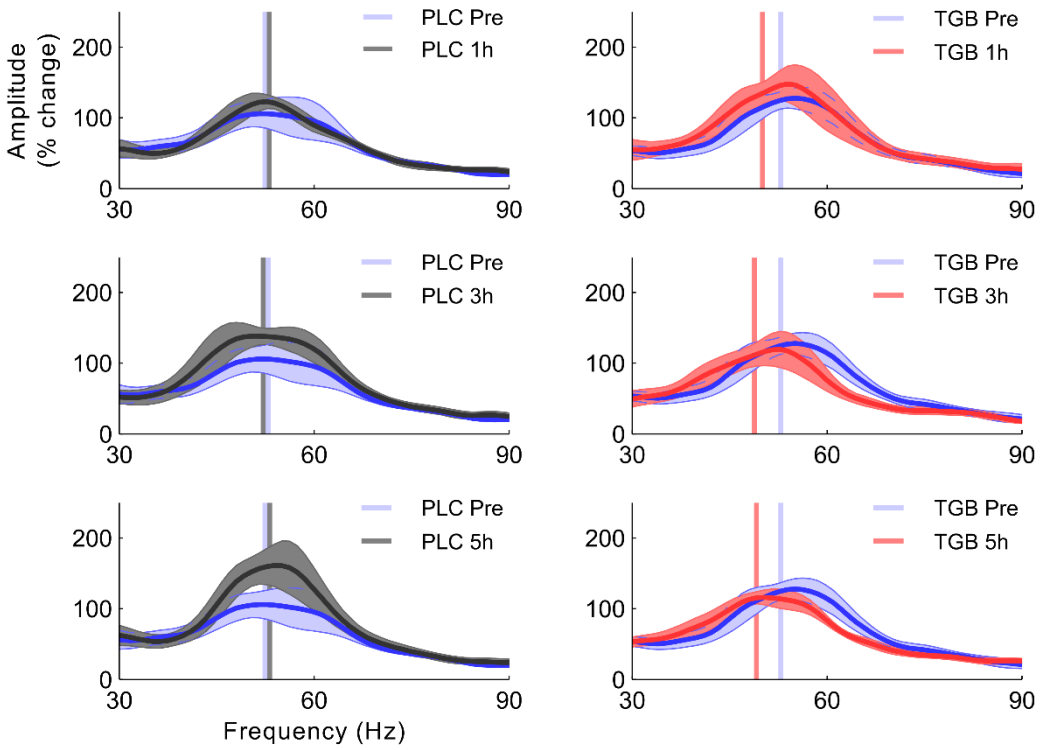

Figure 3.6. Tiagabine average spectra.

Amplitude spectra of percentage change from baseline averaged over participants (n = 8). Shaded areas represent ± 1 SEM across participants. Vertical bars indicate the bootstrap peak frequency, averaged across participants, in the pre- (blue) and post-drug sessions of placebo (PLC; black) and tiagabine (TGB; red).

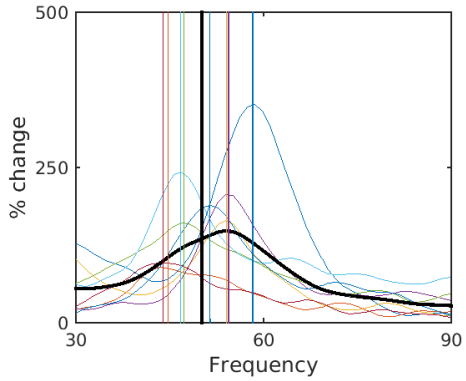

Figure 3.7. Relationship between individual and average spectra.

Illustrative example of the relationship between the individual spectra (colour lines) and their average (black thick line) in one of the conditions. The vertical lines indicate the bootstrap peak frequency. Despite the tight correspondence between the individual bootstrapped peaks and the peaks in the individual spectra, because amplitude is higher at higher frequencies, the peak in the average spectrum appears shifted rightwards of the actual average peak frequency.

Subsidiary to our main hypothesis, we tested the effect of tiagabine on the gamma peak amplitude with the same statistical analysis used for the gamma peak frequency (i.e. a 2×4 repeated measures ANOVA in the eight accepted participants). The results showed no significant effect of *Drug* ($F(1,7) = 1.7$, $p = 0.24$), or *Time* ($F(3,21) = 1.5$, $p = 0.24$), and no significant *Drug* × *Time* interaction ($F(3,21) = 2.6$, $p = 0.08$). This null result of gamma amplitude was suggested also by the visual inspection of the average SAM spatial maps (par. 3.3.5). As illustrated in Figure 3.8, the SAM images did not show any apparent difference between tiagabine and placebo, or across measurement sessions. However, as expected, the average gamma amplitude in the occipital cortex appears to be consistently higher in the QC-accepted participants, compared to those whose data were rejected.

Overall, these results indicated that the gamma peak frequency was significantly reduced by tiagabine at each of the three time points measured after drug administration, whereas gamma amplitude was not affected. Furthermore, peak frequency did not differ statistically across the four measurements in the placebo conditions, or between the pre-tiagabine and the pre-placebo sessions. Therefore, peak frequency was estimated reliably both at repeated intervals of 2 h, and between sessions as far as 1 week apart. For comparison, results are shown in Figure 3.4 after the analysis was repeated using the bootstrap peak frequency (Figure 3.4A and Figure 3.4B), and the envelope peak frequency (Figure 3.4C and Figure 3.4D), with inclusion of good-quality data only (Figure 3.4A and Figure 3.4C), and with all data included (Figure 3.4B and Figure 3.4D). Despite the session of maximal decrease in frequency differed among the four combinations of method and sample used, the pattern of results appeared qualitatively comparable, apart from when the envelope method was used with inclusion of all participants (Muthukumaraswamy et al., 2013a).

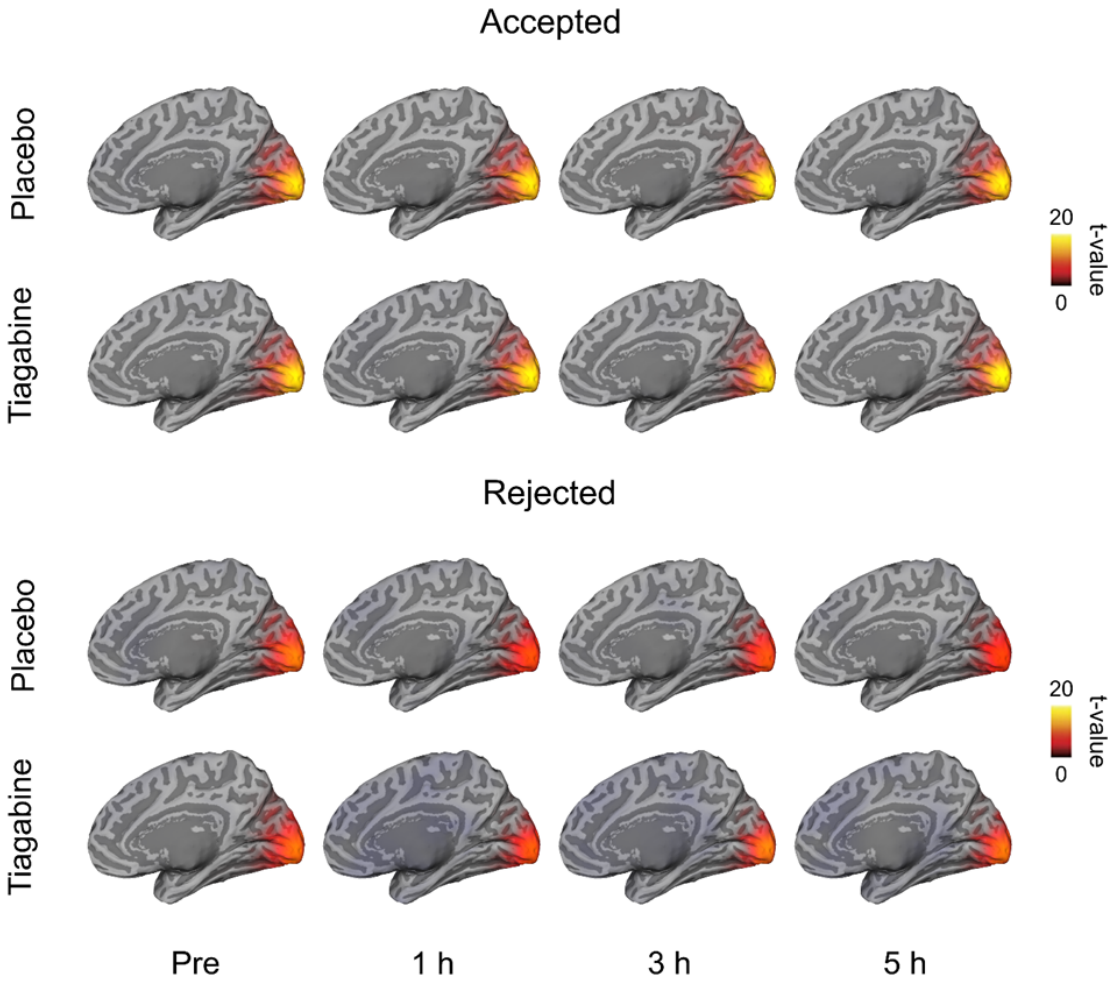

Figure 3.8. Tiagabine SAM spatial images.

SAM beamformer images contrasting gamma power (30–80 Hz) between baseline (-1 to 0 s) and stimulus (0 to 1 s), at 4 mm isotropic voxel resolution. The t-statistic values were averaged, within each condition, separately for accepted and rejected participants (eight and seven, respectively) and displayed on the right hemisphere of an inflated grey-matter cortical mesh reconstruction of a template-space MRI volume.

3.4.5 Correlations of the gamma peak frequency in the tiagabine study

We asked the question of whether differences in gamma quality could be related to differences in the individual peak frequency, across participants. The latter measure has been proposed as an index of local GABA concentration (Muthukumaraswamy et al., 2009) and $GABA_A$ receptor density (Kujala et al., 2015), two factors that could potentially influence the variability of our peak frequency reliability estimates. We used Pearson's *r* coefficient to correlate the gamma peak frequency, in each experimental session, with the estimates of peak frequency reliability, as measured by the percentage of bootstrap iterations within ± 1.2 Hz around the bootstrap distribution mode. As illustrated in Figure 3.9A, we found no evidence for a consistent relationship between these two measures, suggesting that the estimated reliability of peak gamma frequency did not depend on the frequency at which the gamma peaks occurred.

We also investigated the relationship between gamma quality and the magnitude of change in peak frequency. We first calculated the peak frequency change (or so-called 'delta peak frequency') by subtracting the pre-placebo (or pre-tiagabine) peak frequency from each of the post-placebo (or post-tiagabine) sessions, and then correlated this measure with the peak frequency reliability estimates. For this purpose, the percentage of bootstrap iterations in the 'pre' and 'post' sessions were averaged, separately for each correlation. Once again, we found no significant correlations between the reliability of peak frequency and the drug-induced changes in peak frequency. The correlation at 1 h post-tiagabine was the only positive correlation, and its uncorrected p-value approached statistical significance ($r = 0.48$, $p = 0.067$). As illustrated in Figure 3.9B (bottom row, first plot from the left) participants whose peak frequency decreased the most tended to show the lowest reliability estimates, at 1 h post-tiagabine. This would explain why, after participant exclusion, the greatest reduction in peak frequency was observed in the session at 3 h, rather than 1 h after tiagabine (cf. Figure 3.4A and Figure 3.4B).

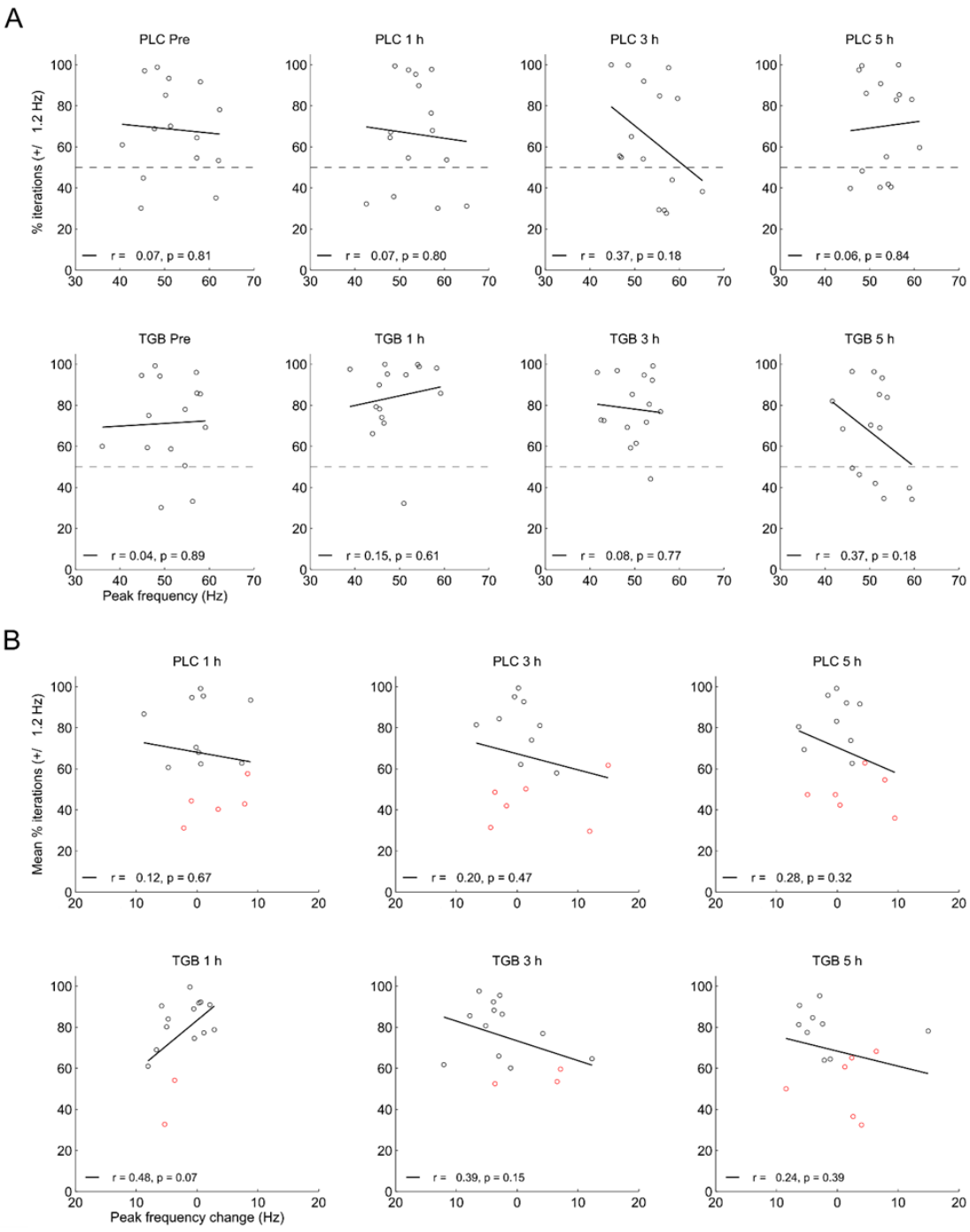

Figure 3.9. Correlations of the peak frequency reliability estimates.

A) Correlations between the gamma peak frequency and the estimates of peak frequency reliability (percentage of iterations within ± 1.2 Hz around the bootstrap mode). Observations falling below the horizontal dashed line in each plot, the horizontal dashed (i.e. the QC criterion) represent poor-quality estimates. **B)** Correlations between the change in peak frequency (i.e. peak frequency in the 'pre' session subtracted from the 'post' session), and the reliability estimates, averaged between 'pre' and 'post' sessions. Circles plotted in red represent participants with poor-quality estimates in either one or both of the 'pre' and 'post' sessions being correlated.

Finally, in the hypothesis that baseline GABA levels (as indexed by the gamma peak frequency in the pre-tiagabine session) could have an influence on the peak frequency modulations by tiagabine, we also tested whether the change in peak frequency was correlated with the gamma peak frequency in the pre-tiagabine session. As illustrated in Figure 3.10A, we found two significant negative correlations, indicating that individuals with a higher peak frequency at baseline showed larger reductions after tiagabine, particularly in the sessions at 3 h (r = -0.77, p = 0.004) and at 5 h post-tiagabine (r = -0.81, p = 0.008). However, the statistical significance of these correlations appeared to be determined by a single observation (cf. Figure 3.10B). This individual represented an outlier in terms of the gamma peak frequency in the pre-tiagabine session (~35 Hz) and showed an increase in frequency after tiagabine, rather than a decrease. It could be hypothesised that for this individual a high-beta peak prevailed (i.e. gamma amplitude was low in the pre-tiagabine session) and their gamma peak (~45–50 Hz) was revealed only in the post-tiagabine sessions, by a tiagabine-induced boost in gamma amplitude. However, we neither found evidence for an increase in gamma amplitude with tiagabine (par. 3.4.4), nor had a chance to test this hypothesis more formally, given the limited sample size in this study.

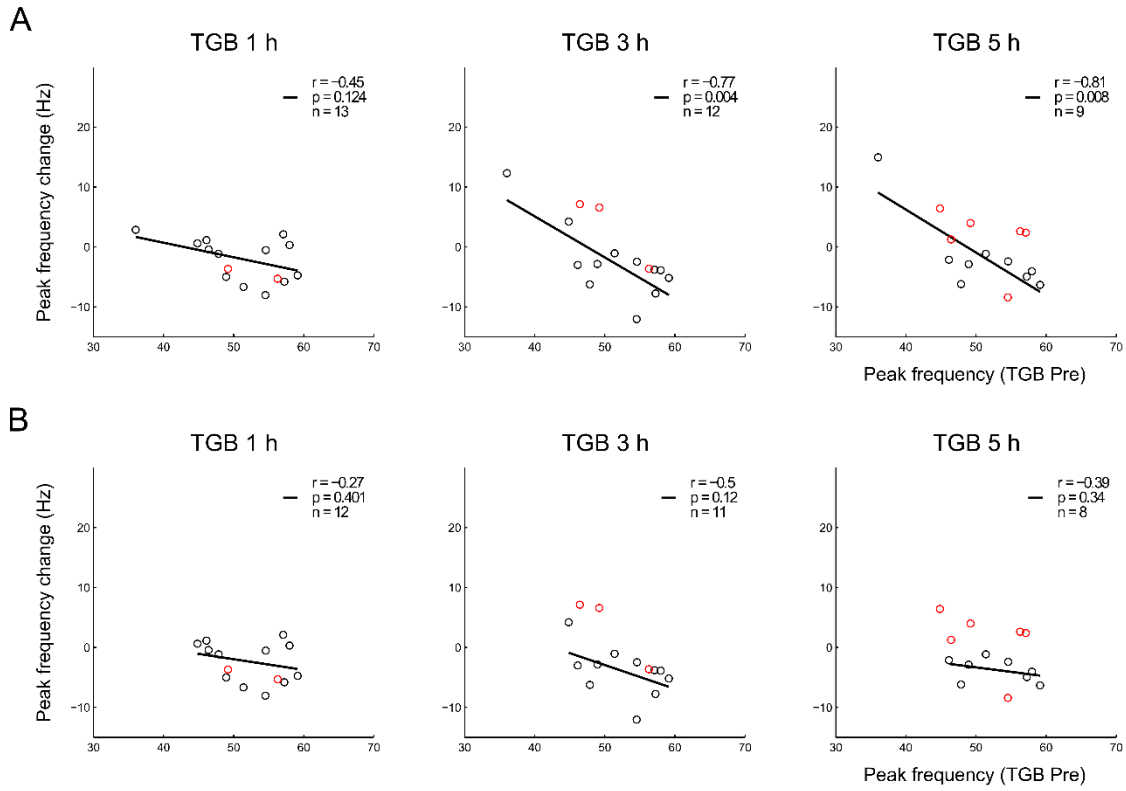

Figure 3.10. Correlations of peak frequency at baseline.

A) Correlations between the change in gamma peak frequency and the gamma peak frequency at baseline (TGB Pre). Circles plotted in red represent participants with poor-quality estimates in either one or both of the 'pre' and 'post' sessions being correlated. **B)** The same as in A), but after exclusion of one observation.

3.5 Discussion

The true nature of neuronal oscillations in the gamma frequency range has been long disputed in neuroscience (Brunet et al., 2014b). Correspondingly, the choice of spectral method for the analysis of electrophysiological data has also been highly debated (Bruns, 2004; Le Van Quyen and Bragin, 2007; Le Van Quyen et al., 2001; van Vugt et al., 2007). In this work, we used a newly developed method based on bootstrapping across trials, which served two purposes. First, we used a measure of spread in the distribution of bootstrapped peaks to estimate the reliability of the gamma peak frequency, which in turn allowed the identification of poorly estimated data. Second, we measured the gamma peak frequency by averaging across the bootstrapped samples, as this measure was demonstrated more robust compared to a more conventional alternative approach (see Chapter 2). This QC method was used to re-analyse data from two pharmacological MEG studies, one in which alcohol was demonstrated to produce a marked decrease in the peak frequency of visual gamma oscillations (Campbell et al., 2014), and one in which tiagabine was reported to modulate stimulus-evoked responses, but to have no effect on neuronal oscillatory dynamics (Muthukumaraswamy et al., 2013a).

3.5.1 Methodological considerations

The pharmacological MEG dataset that we re-analysed in the first part of this work, i.e. the alcohol data by Campbell et al. (2014), was considered as a benchmark to test the validity of our QC approach on real data. In the original publication, the peak frequency and amplitude parameters were estimated by fitting skewed Gaussian functions to the gamma range of the power spectra. In our analysis, the success of the QC approach was demonstrated in two ways. First, it revealed the presence of poor-quality data in the same number of participants as originally reported by the authors, who blind-screened

the data for low-amplitude gamma responses with no clear peak (Campbell et al., 2014). Second, it replicated the drug-induced modulations, which consisted of a decrease in the peak frequency of visual gamma with alcohol. Together, the results of our validation study on simulated data presented in the previous chapter of this thesis (Chapter 2) and our replication of the findings by Campbell et al. (2014) supported the validity of our QC approach to fulfil two purposes; first, to identify reliably measured data in the study by Muthukumaraswamy et al. (2013a) and, second, to re-test the effect of tiagabine using optimal estimates of peak frequency.

In our re-analysis of these two pharmacological MEG studies, the use of ANOVA tests required the inclusion of complete data from each participant. This resulted in good-quality data being excluded from both the alcohol (11 out of 48) and the tiagabine datasets (29 out of 120). In other words, approximately 25% of the recorded sessions provided reliable peak frequency estimates, but had to be excluded from analysis according to the list-wise deletion approach. It should be noticed that, by applying a standard analysis pipeline and avoiding participant exclusion, Muthukumaraswamy et al. (2013a) adopted the least biased approach possible. On the one hand, the rejection of complete datasets is questionable when each individual represents a precious or rare observation and the sample size cannot be readily increased. On the other hand, our proposed approach offers the advantage of basing statistical inference on reliably estimated peak frequency measures. However, if missing observations (i.e. unreliable peak frequency estimates) are handled by list-wise deletion (i.e. only participants with complete data are included in the analysis), it is important to consider whether the probability of the data missing is related to other independent variables or on the dependent variable itself.

Our QC approach circumvents the limits of setting simple rejection criteria based on the amplitude of the response, which could remove sources of intra- and inter-individual variability, such as drug-induced reductions in amplitude or disease-related impairments of oscillatory rhythms. Nevertheless, rejecting datasets based on the estimates of peak frequency reliability is still dependent on the signal-to-noise ratio and hence amplitude (see Chapter 2). Any QC approach is thus vulnerable to low generalizability of results. In this study, in particular, the peak frequency reduction induced by tiagabine can be demonstrated only for those participants who showed gamma responses of high consistency across trials. Despite the comparability of results illustrated in Figure 3.4A and Figure 3.4B, the gamma peak frequency measures must be of sufficient quality in order for the drug-induced modulations to be statistically significant. Results, instead, cannot be generalised to individuals who showed high inter-trial variability in their response frequency. The factors underlying such differences in the variability of the gamma response frequency are largely unexplored, and remain an open question for future research.

3.5.2 Gamma peak frequency reduction by tiagabine

After identification and exclusion of datasets that yielded unreliable estimates of peak frequency, we observed a marked tiagabine-induced reduction in visual gamma frequency. The gamma peak frequency appeared to be significantly reduced both at 1 hour and at 3 hours after oral administration (par. 3.4.4), in line with the pharmacokinetics of tiagabine showing maximum plasma concentrations occurring between 45 and 150 minutes after drug ingestion (Leach and Brodie, 1998; Murphy, 2011; Snel et al., 1997). The average decrease in frequency induced by tiagabine, as measured with the bootstrap method (Figure 3.4A) relative to a pre-tiagabine peak frequency of 52.9 ± 5.0 Hz (mean ± SD across participants), was 2.8 Hz, 4.1 Hz and 3.8 Hz at 1 h, 3 h and 5 h, respectively. Interestingly, a comparable effect was observed

with alcohol, with the gamma peak frequency being reduced on average by 2.4 Hz at less than 1 h after drug consumption, relative to a pre-alcohol peak frequency of 52.6 ± 5.9 Hz (Figure 3.2A).

Overall, these novel tiagabine results are strongly supportive of previous studies of animal models, which demonstrate a close dependency of gamma frequency on the time constants of GABAergic inhibition (Faulkner et al., 1998; Oke et al., 2010; Traub et al., 1996; Whittington et al., 1995, 1996; Xing et al., 2012a). In relatively simple models, the generative mechanisms of gamma oscillations consist of pyramidal cells firing synchronously under the inhibitory control of GABAergic interneurons (Bartos et al., 2007; Buzsáki and Wang, 2012; Gonzalez-Burgos and Lewis, 2012; Tiesinga and Sejnowski, 2009). At the synaptic level, tiagabine exerts its effects by selectively inhibiting GAT-1, the most abundantly expressed GABA transporter in the cerebral cortex (Borden et al., 1994; Conti et al., 2004). By blocking the reuptake of GABA from the synapse, tiagabine elevates the synaptic concentrations of GABA (Dalby, 2000; Fink-Jensen et al., 1992) and increases the duration of the $GABA_A$ receptor-induced IPSCs (Roepstorff and Lambert, 1994; Thompson and Gähwiler, 1992). Thus, IPSCs of prolonged duration result in synchronization of neuronal firing at slower rhythms, which in turn translates to LFP oscillations at lower gamma frequencies.

3.5.3 Relationship between gamma frequency and GABA

In non-invasive human studies, the use of MRS to measure the relationship between GABA and gamma frequency has produced controversial results (cf. Cousijn et al., 2014; Muthukumaraswamy et al., 2009). Invigorating this debate, a very recent flumazenil-PET study demonstrated a positive correlation between the frequency of visually induced gamma oscillations and the density of $GABA_A$ receptors in early visual areas (Kujala et al., 2015). Further contribution to the translation of animal models to

humans has come from studies combining MEG, to record cortical activity, with the use of pharmacological agents, to modulate neurotransmission (Hall et al., 2010; Muthukumaraswamy, 2014). Decreased visual gamma frequency in humans was observed after administration of alcohol, which affects GABA and NMDA receptor activity (Campbell et al., 2014), and lorazepam, a positive allosteric $GABA_A$ modulator (Lozano-Soldevilla et al., 2014). More recently, comparable results were obtained with the NMDA receptor antagonist ketamine (Shaw et al., 2015). In addition to the frequency modulation, these studies found gamma responses of increased amplitude with GABAergic enhancement, replicating previous results obtained with administration of the $GABA_A$ agonist propofol (Saxena et al., 2013).

Increased gamma amplitude accompanying a shift towards lower gamma frequencies may be related to the recruitment of larger pyramidal cell populations achieved under longer periods of inhibition (Gonzalez-Burgos and Lewis, 2012). In the current study, however, no significant effects were observed when, subsidiary to our main hypothesis, gamma amplitude was tested with the same analysis used for peak frequency. This could suggest that tiagabine has a specific effect on oscillation frequency via modulation of inhibitory time constants, while leaving other network parameters unaltered. In support of this, animal studies have demonstrated that the duration of IPSCs is prolonged by tiagabine, but IPSC amplitude is not increased (Roepstorff and Lambert, 1994; Thompson and Gähwiler, 1992). Alternatively, the absence of an effect of drug on gamma amplitude might be explained by a lack of sensitivity of the amplitude measures themselves. Compared to gamma frequency, gamma amplitude is a less repeatable measure (Tan et al., 2016) and could be more vulnerable to noise, particularly when differences in head movement or head distance from the sensor array in repeated recording sessions are not explicitly controlled for.

3.5.4 Relationship between gamma frequency and other parameters

A partially unresolved question is whether the changes in frequency associated with GABAergic neurotransmission are unique to gamma oscillations, or extend to other frequency ranges. Likewise, it is unclear whether the GABAergic influences on oscillatory dynamics are specific to visual areas or extend to other cortices. In sensorimotor regions, administration of a benzodiazepine $GABA_A$ positive allosteric modulator produced an alteration of the beta rhythm consisting of decreased frequency and increased amplitude (Jensen et al., 2005). In other studies, no differences in gamma frequency were observed over motor regions using alcohol (Campbell et al., 2014), lorazepam (Lozano-Soldevilla et al., 2014), ketamine (Shaw et al., 2015), or tiagabine (Muthukumaraswamy et al., 2013b). Overall, therefore, the functional significance of shifts in oscillation frequency remains a subject of significant interest.

The frequency of gamma oscillations has been previously related to differences in behavioural performance (Dickinson et al., 2015; Edden et al., 2009), and in cognitive traits of possible clinical relevance (Dickinson et al., 2015; Kahlbrock et al., 2012a). For example, a recent study showed that the normal velocity-dependent modulation of visual gamma frequency appeared to be impaired in children with autism spectrum disorders (Stroganova et al., 2015). Although the inter-individual differences in visual gamma frequency have been related to the structural properties of visual cortical areas (Muthukumaraswamy et al., 2010; Schwarzkopf et al., 2012), other studies do not show a clear dependence (Kujala et al., 2015; Robson et al., 2015). Gamma frequency in visual cortex is modulated by sensory input strength, increasing monotonically with respect to stimulus contrast (Jia et al., 2013; Perry, 2015; Perry et al., 2015; Ray and Maunsell, 2010; Roberts et al., 2013). Increased peak gamma frequency has been reported also for stimuli of smaller size, in both LFP (Gieselmann and Thiele, 2008; Jia et al., 2013; Ray and Maunsell, 2011) and MEG recordings (van Pelt and Fries, 2013;

although, see also Perry et al., 2013). This could be explained with smaller stimuli being represented by smaller neuronal ensembles, which in turn could be synchronized at a higher frequency over a shorter cortical distance (Gieselmann and Thiele, 2008). Interestingly, gamma responses in monkey visual areas are induced at higher frequencies in response to repeated stimulus presentations compared to novel stimuli (Brunet et al., 2014a), and functionally synchronous networks appear to be tuned to higher frequencies when representing stimuli that are under the focus of attention (Bosman et al., 2012). Attentional modulations of narrow-band gamma oscillations in early visual areas are not typically observed with MEG (e.g., Koelewijn et al., 2013), perhaps due to the different sensitivity of MEG compared to LFPs. However, since GABAergic drugs can be expected to induced altered cognitive states, the next chapter (Chapter 4) will explore the suggested link between attention and gamma frequency (Bosman et al., 2012).

3.5.5 Conclusions

The work presented here highlights the potential impact of objective data quality quantification and paves the way for future methodological developments in this direction. Using our novel approach to peak frequency estimation, we demonstrated a reduction in gamma frequency by tiagabine, in those participants with reliable peak frequency estimates. This result is supported by animal models, and provides additional translational evidence of the GABAergic mechanisms generating gamma oscillations in humans.

Chapter 4.

Changes in peak gamma amplitude and frequency with visual spatial attention assessed using optimised quality-control procedures

4.1 Abstract

Oscillatory synchronization in the gamma frequency range has been proposed as a neuronal mechanism to prioritize processing of relevant stimuli over competing ones. Recent studies in animals found that selective spatial attention enhanced gamma-band synchronization in high-order visual areas (V4) and increased the gamma peak frequency in V1. The existence of such mechanisms in the human visual system is yet to be fully demonstrated. In this study, we used MEG, in combination with an optimised stimulus design, to record visual gamma oscillations from human early visual cortex, while participants performed a visuospatial attention cueing task. First, we reconstructed virtual sensors in V1/V2, where gamma oscillations were strongly induced by visual stimulation alone. Second, following the results of a statistical comparison between conditions of attention, we reconstructed cortical activity in inferior occipital-temporal regions (V4). The results indicated that gamma amplitude was modulated by spatial attention across the cortical hierarchy, both in the early visual cortex and in higher-order regions of the ventral visual pathway. Attentional effects in V1/V2 preceded those in V4 by approximately 70 ms, consistent with a feed-forward role of gamma-band activity in propagating sensory representations across the visual cortical hierarchy. Although we found no evidence for an increase in the gamma peak frequency in V1/V2 with attention, the centroid of the power spectra tended to shift towards higher frequencies by ~1 Hz, on average. Across individuals, the gamma peak frequency correlated negatively with the response time in the attention task, suggesting a link between this oscillatory parameter and behaviour. Together, these findings suggest that differences in experimental design or methodology can account for the inconsistencies in previous animal and human studies. Furthermore, our results support the hypothesis of enhanced gamma-band synchronization as an attentional mechanism in the human visual cortex.

4.2 Introduction

The ability to direct attention to selected, relevant stimuli in a visual scene is crucial to adaptive behaviour. One proposed mechanism by which visual spatial attention is implemented at the cortical level is oscillatory synchronization in the gamma frequency range (~30–80 Hz). The action potentials of synchronized pre-synaptic neurons arrive at the post-synaptic dendrites closer in time and sum up more effectively than those from asynchronous pre-synaptic neurons, hence increasing their downstream impact. For this reason, synchronization of neuronal firing could represent a top-down attentional mechanism to prioritize processing of attended, relevant stimuli over competing, irrelevant ones (see Fries, 2015; Gregoriou et al., 2015 for recent reviews).

The evidence in support of this model comes from studies of monkey visual area V4, where local gamma-band synchronization, measured as spectral power in the LFP (Fries et al., 2001; Taylor et al., 2005), spike-field coherence (Bichot et al., 2005; Fries et al., 2001) or spike-spike coherence of MUA (Fries et al., 2008b), is consistently stronger for attended, compared to ignored stimuli. Yet, the attentional modulation of visual gamma oscillations in the primary visual cortex is less clear. One study in monkey unexpectedly found a small, but statistically significant, increase in gamma amplitude in V1 when spatial attention was directed to stimuli outside, rather than inside, the receptive field of the recorded neurons (Chalk et al., 2010). Other studies have found no obvious effects of attention on gamma amplitude in V1 (Bosman et al., 2012; Buffalo et al., 2011). One study also found that attention modulated the gamma peak frequency in V1, which was higher in response to relevant, compared to irrelevant stimuli (Bosman et al., 2012).

Across studies in human, the effect of spatial attention on gamma-band oscillatory activity in the early visual cortex is variable and unclear. In MEG studies, the amplitude

of visually induced gamma oscillations is typically reported to increase with attention in the occipital lobe contralateral to the attended hemi-field, with sources normally extending from high-order extrastriate areas to lateral occipital and parietal cortices (Bauer et al., 2012, 2014, Marshall et al., 2015a, 2015b; Siegel et al., 2008). In the early visual cortical areas, i.e. presumed V1/V2, gamma oscillations are often reported to be unaffected by attention (e.g., Siegel et al., 2008). Although one study reported attentional modulations of the high-frequency gamma-band response (~60–90 Hz) in the medial visual cortex (Koelewijn et al., 2013), this frequency range is thought to reflect different neuronal mechanisms, compared to those underlying narrow-band visual gamma oscillations (Ray and Maunsell, 2011).

Overall, the effects of spatial attention on gamma oscillations in the human early visual cortex, and in particular on the spectral properties of the V1 response, remain largely unexplored. As the uncertainties in the geometry of the source distribution can be partly attributed to the choice of stimulus configuration (see Koelewijn et al., 2013), the visuospatial attention cueing paradigm used in this MEG study was designed to induce sustained visual gamma oscillations with clear sources in the contralateral visual cortex. The accurate choice of stimulus parameters, such as size (Jia et al., 2013), spatial frequency (Adjamian et al., 2004b) and eccentricity (van Pelt and Fries, 2013), allowed us to record gamma responses with a clearly quantifiable spectral profile and to test the effect of attention also on the gamma peak frequency.

4.3 Materials and Methods

4.3.1 Participants

Twenty healthy volunteers took part in the study (mean age, 28.6 years; range, 22–42 years; seven males; two left-handed). All participants provided informed consent and received monetary reimbursement in agreement with the guidelines of the local ethics committee. Two participants showed no measurable gamma response to visual stimulation (par 4.3.8) and hence they were excluded from the analysis. The eye-tracker data were not recorded in one participant due to technical difficulties (par. 4.3.4).

4.3.2 Experimental design and paradigm

Participants performed a visuospatial attention cueing paradigm, the task consisting of discriminating the change in orientation of the attended stimulus. The trial structure is illustrated in Figure 4.1. Each trial started with a cue, an arrow pointing either to the left or to the right side of the screen, presented centrally for 500 ms and followed by a fixation cross (0.3° of visual angle). After a jittered interval of 1–1.5 s, two stimuli (a grating and a vertical line; par. 4.3.3) were presented, one in the left and one in the right visual hemi-field, centred horizontally at an eccentricity of 3°. Participants were instructed to attend the stimulus in the cued hemi-field, whilst fixating centrally throughout the trial. After an unpredictable interval of 1–3 s, the attended stimulus, i.e. the one in the cued hemi-field, changed from the vertical to a tilted orientation, either clockwise or counter-clockwise. The tilted stimulus was presented for 30 ms and, to increase task difficulty, it was followed by a mask (a plaid or a cross; par. 4.3.3), presented for 120 ms. After a further 350 ms, a question mark prompted participants to perform a forced-choice orientation discrimination. Participants indicated whether the stimulus orientation had changed counter-clockwise or clockwise via a button-press, using the index and middle fingers of their right hand, respectively. Participants were

allowed up to 1.5 s to respond and, if they had not perceived the direction of the orientation change, they were instructed to guess it. Participants were also instructed to withhold their response to any trial in which they had not complied with the task (e.g., if they had not attended the cued hemi-field). After an inter-trial interval of 1.5 s, the next trial started.

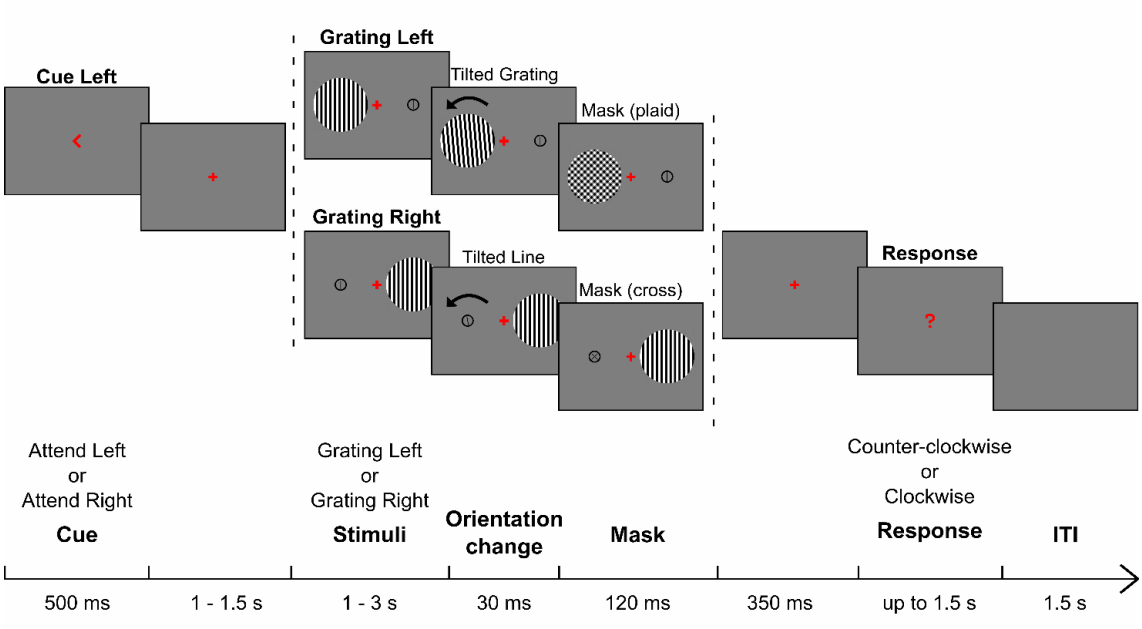

Figure 4.1. Trial structure of the experimental paradigm.

The trials started with a cue, presented for 500 ms, instructing participants which hemi-field to attend. After 1–1.5 s, two stimuli were presented, a grating and a line. After 1–3 s, the stimulus in the cued hemi-field was first presented at a tilted orientation (30 ms) and then replaced by a mask (120 ms), a plaid or a cross, depending on which stimulus was presented in the cued hemi-field. After 350 ms, participants were prompted to respond to the task by indicating whether the attended stimulus was tilted counter-clockwise or clockwise. For convenience, only the attend-left condition is illustrated in this figure, however, all four possible combinations of cue hemi-field (attend-left and attend-right) and stimulus hemi-field (grating-left and grating-right) were presented.

The experimental session consisted of 400 trials in total, divided into four blocks. Within each block, trials were counterbalanced across all possible combinations of four factors, namely, stimulus hemi-field (grating left vs. grating right), cued hemi-field (attend left vs. attend right), change direction (counter-clockwise vs. clockwise) and change magnitude (par. 4.3.3). Importantly, depending on which hemi-field was cued to attend and in which hemi-field the grating was presented, each trial fell into one of two main conditions of interest (attend grating vs. ignore grating), which were also counterbalanced. Trials were presented in pseudo-random order. To prevent habituation effects, the same combination of stimulus hemi-field and cued hemi-field was never presented for more than five times consecutively. Participants were allowed to take breaks between blocks. Each participant completed between two and four blocks (3.5 blocks on average), for a total duration of the experimental session of up to 1 hour.

4.3.3 Stimuli

The stimuli consisted of a grating and a line, the grating being the stimulus of interest for the analysis of visual gamma. The grating stimulus consisted of a vertical square-wave grating (maximum contrast, three cycles per degree), presented through a circular aperture with a diameter of 4°. The line stimulus consisted of a vertical black line (0.9° length, 0.05° width) enclosed in a black circle (1.1° diameter, 0.05° width). The parameters of the grating stimulus, such as size and eccentricity (4° and 3°, respectively), were designed to induce gamma oscillations with both unambiguous cortical sources (i.e. in the contralateral visual cortex; e.g., Muthukumaraswamy et al., 2009) and clearly measurable spectral properties (i.e. high-amplitude responses; see van Pelt and Fries, 2013). In contrast, the absence of high-contrast edges and the smaller size of the line stimulus were chosen to produce gamma responses of only minimal, or non-measurable, amplitude. This prevented the gamma response to the grating from being contaminated by sources in the other hemisphere, as would have happened, for

example, if gratings were presented in both visual hemi-fields. Therefore, by carefully designing the psychophysical properties of both the relevant and the irrelevant stimulus, we were able to obtain uncontaminated gamma responses to the grating, whilst preserving the behavioural relevance of both stimuli to the attention task.

The difficulty of the task was varied on a trial-by-trial basis, with five possible magnitudes of orientation change increasing logarithmically from 0.3° to 5° to the vertical. To account for the different properties of the two stimuli and based on behavioural piloting, the magnitudes of orientation change of the line stimulus were increased by a factor of four compared to the grating stimulus (i.e. orientation change from 1.2° to 20° to the vertical). To increase task difficulty and hence engage participants further in the allocation of spatial attention, the orientation change was backward masked. The grating was masked by a plaid and the line was masked by a cross, both masks being presented at a tilted orientation of 45° to the vertical.

Stimuli were displayed on a gamma-corrected Mitsubishi Diamond Pro 2070 CRT monitor placed at a viewing distance of 2 m. The refresh rate was 100 Hz. Stimuli were programmed in Matlab (The Mathworks) using the Psychophysics Toolbox (Kleiner et al., 2007).

4.3.4 Eye-tracker data acquisition and analysis

To monitor eye movements, monocular recordings were obtained from the right eye with an iViewX MEG250 eye-tracker (SensoMotoric Instruments) in nineteen out of twenty participants (par. 4.3.1). The video camera, operating at a sampling rate of 250 Hz, was positioned at a distance of 120 cm in front of the participant, with an infrared light placed 60 cm to the right of the camera. The gaze direction was determined based on the position of the pupil. The system was initially calibrated before the beginning of

the first experimental block and then recalibrated between blocks if the head position had changed after the break.

The eye-tracker data were analysed to identify and exclude trials in which the eye gaze position deviated from the central fixation. In principle, eye gaze position or eye movements could differ between conditions, depending on which hemi-field is cued to attend. If so, any difference between the visual gamma response to attended and ignored gratings could be a spurious result of an associated difference in stimulus eccentricity (van Pelt and Fries, 2013), rather than a true effect of attention. In particular, if participants were to move their gaze towards the cued hemi-field, the eccentricity of the grating would decrease when the grating is attended, compared to when it is ignored. As such, the analysis explained below ensured that eye gaze position did not differ when participants attended the left or the right hemi-field and, consequently, towards or away from the grating (both for left- and right-presented gratings; see counterbalancing procedures, par. 4.3.2). Thus, we ruled out the possibility that differences in visual gamma could arise from differences in stimulus eccentricity.

The eye-tracker data analysis was performed using the EYE-EEG extension (Dimigen et al., 2011) of EEGLAB (Delorme and Makeig, 2004) and custom Matlab scripts. The raw data were cut into 2–2.5 s epochs, from cue offset (between -1 and -1.5 s) to 1 s around stimulus onset. The same pre-processing parameters were applied separately to the X and Y coordinates of gaze position, with the horizontal component being the one of interest in the analysis, for the reasons explained above. First, the data were demeaned based on the median position within each epoch. Second, short segments of missing data caused by blinks or temporary signal loss were reconstructed by linear interpolation. Third, high-frequency noise was suppressed by smoothing the data with a moving average over a window of 10 data samples. Finally, the epochs were shortened

to include only the time-range in which the visual gamma response could be affected, i.e. 0–1 s around stimulus onset (par. 4.3.8). To identify trials containing artefactual ocular activity, two measures were derived using these stimulus epochs. First, the horizontal gaze position (hereafter referred to as 'horizontal fixation') was calculated as the within-trial median X coordinate and trials were excluded if the horizontal fixation deviated more than ± 2.5 SD (from the average horizontal fixation across trials). Second, horizontal eye movements (e.g., saccades) were defined as X coordinate values in a trial larger than ± 2.5 SD (SD measured on the concatenated trials) and trials were excluded if they contained horizontal eye movements. The outcome of these two control procedures was visually inspected for each participant and stricter SD-based thresholds were implemented if necessary (e.g., ± 1.5 SD in one participant). Additionally, the horizontal fixation was compared between cue conditions (attend left vs. attend right), within each participant. For this purpose, trials surviving artefact rejection were first pooled according to their condition and then contrasted with unpaired t-tests. This resulted in no significant difference in eye gaze position of right vs. left cue conditions, in any of the participants (mean t = -0.44 across participants). Altogether, therefore, these procedures ensured that the eccentricity of the gratings did not differ, because of fixation or eye movements, when they were presented in the attended or ignored hemi-field.

4.3.5 MEG data acquisition

The MEG recordings were performed using a 275-channel axial gradiometer CTF system (VSM MedTech), located inside a magnetically shielded room. The data were acquired continuously, with a sampling rate of 1200 Hz (low-pass filtered online at 300 Hz). An additional 29 reference channels were recorded for noise cancellation purposes and the primary sensors were analysed as synthetic third-order gradiometers (Vrba and Robinson, 2001). Three electromagnetic coils were placed on three fiduciary locations

(nasion, left and right pre-auricular) and their position relative to the MEG sensors was recorded continuously during each experimental block.

4.3.6 MEG/MRI co-registration

An anatomical MR image (1-mm isotropic, T1-weighted FSPGR) acquired with a 3.0 T MRI scanner (General Electric) was available for each participant. For source-localization purposes, the anatomical MRI and the MEG data were co-registered by marking the voxels on the MR image corresponding to the position of the three fiducial coils (par. 4.3.5).

4.3.7 MEG data pre-processing

For each participant, the data were concatenated over experimental blocks and the median head position was used as reference position for the entire dataset. The continuous dataset was then cut into epochs (± 1.5 s around stimulus onset), the epochs were visually inspected and trials containing gross artefacts (e.g., muscular activity) were excluded. The position of the head within and between blocks was also visually inspected, by concatenating the continuous head position data over trials. Trials were excluded if, at any time within the trial, the distance of any of the coils from the reference position exceeded a threshold. This threshold, for the maximum distance of the head from the reference position, was defined individually for each participant (mean threshold 4.65 mm, range 2.5–7.5 mm), based on the amount of head motion. Trial exclusion did not result in a different number of trials between attend-grating and ignore-grating conditions.

4.3.8 Source localization

Source analysis was performed in Matlab, using the FieldTrip toolbox (Oostenveld et al., 2011). In order to reconstruct oscillatory activity at brain locations directly

comparable across participants, 1) the MNI template brain was divided into a 5 mm isotropic voxel resolution grid, 2) the individual anatomical MRI was warped to the template MRI and 3) the inverse transformation matrix was used to warp the template grid onto an individual grid for each participant. The leadfield was calculated using a semi-realistic volume conduction model based on the individual anatomy (Nolte, 2003). The optimal dipole orientation at each voxel was calculated by SVD and power was estimated using an LCMV beamformer algorithm (Van Veen et al., 1997).

To localize the sources of visual gamma oscillations in each hemisphere optimally, the beamformer weights were calculated separately for left- and right-presented gratings. For each participant, trials were combined according to the stimulus hemi-field (left-grating or right-grating trials) and irrespective of the attention condition (both attend-grating and ignore-grating trials). To compute the weights, the covariance matrices were calculated on a time-range from -1 to 1 s around stimulus onset, between 30–70 Hz. The peak voxel in each hemisphere was then identified by selecting the voxel of greatest increase in gamma power (30–70 Hz), measured as percentage change between stimulus (0.3–1 s) and baseline (-0.7–0 s). The use of two separate sets of weights allowed for optimal localization of the gamma source in each hemisphere. Yet, when reconstructing the virtual sensor data (par. 4.3.10), the same weights were used to reconstruct trials of both conditions, within each hemisphere, thereby allowing the responses to attended and ignored gratings to be compared.

To compare the spatial localization of the visual gamma response to attend-grating and ignore-grating trials, the difference between the two conditions was quantified as a percentage change at each voxel location. In line with the previous source localization procedure, gamma power (30–70 Hz) was estimated during the stimulus epoch (0.3–1 s) and contrasted between attended and ignored gratings. This procedure was performed

separately for left- and right-presented gratings, using the two sets of optimised weights, as described above.

4.3.9 Statistical analysis at the source level

The consistency of the visual gamma response across participants was tested statistically using a non-parametric cluster-based permutation approach, which controls for multiple comparisons across voxels (Maris and Oostenveld, 2007). First, the estimates of gamma power (30–70 Hz) in the baseline (-0.7–0 s) and stimulus (0.3–1 s) epochs were contrasted with paired-sample t-tests across participants at each voxel location. Second, significant t-statistics ($p < 0.05$) were grouped into clusters based on spatial adjacency and the t-values summed within clusters to produce a cluster-level statistic. Third, the maximum cluster-level statistic was measured in each of 10,000 Monte Carlo permutations, yielding a non-parametric null distribution that was then used to calculate the p-value of the clusters observed in the original data.

This method was applied using two different approaches. First, to compare the response to attended and ignored gratings in each hemisphere, gamma power (30–70 Hz) in the stimulus epoch (0.3–1 s) was contrasted between attend-grating and ignore-grating conditions, separately for left- and right-presented gratings. Second, to test for any sources of visual gamma insensitive to the stimulus hemi-field, the beamformer weights were re-computed after pooling trials across all conditions (calculating the covariance matrix from -1 to 1 s, between 30–70 Hz) and gamma power (30–70 Hz; 0.3–1 s) was contrasted between the two conditions of attention, irrespective of the grating hemi-field. In both procedures, the number of trials was equalized between conditions by random sub-sampling.

4.3.10 Source reconstruction

To analyse the effect of attention on the spectral properties of gamma oscillations in the early visual cortex (i.e. V1/V2; par. 4.4.3), virtual sensors were reconstructed, individually for each participant and separately for each of the two peak voxel locations, by multiplying the sensor-level data by the corresponding set of optimised weights. The reconstructed single-trial time-series were first combined between left- and right-hemisphere virtual sensors and then sorted between attend-grating and ignore-grating trials. The effect of attention was analysed statistically both in the time-frequency (par. 4.3.11) and in the frequency domain (par. 4.3.12).

To investigate the time-course of gamma activity in downstream regions and based on the results of the statistical comparison between attention conditions, virtual sensors were reconstructed also in higher-order visual cortex. For this purpose, target locations were identified within the V4 complex (Bartels and Zeki, 2000) by selecting the voxel in the fusiform gyrus that was closest to the observed peak t-statistic, separately in the left (MNI coordinates: [-38 -65 -15]) and in the right hemisphere (MNI coordinates: [38 -45 -10]). To remove the effect of possible spatial leakage between V1/V2 and V4, , the raw virtual sensor time-series were first orthogonalised to remove zero-lag correlation (Colclough et al., 2015).

4.3.11 Time-frequency analysis and statistics

To investigate the spectral evolution of the visual gamma response over time, the virtual sensor data were represented in the time-frequency domain. For this purpose, the orthogonalised time-series from -1.5 to 1.5 s were bandpass-filtered at each frequency between 4–100 Hz, in steps of 0.5 Hz (8 Hz bandpass, 3rd order Butterworth filter) and the amplitude envelope of the analytic signal (Matlab function *hilbert*) averaged across trials (e.g., Muthukumaraswamy et al., 2010). The time-frequency maps were calculated

separately for attend-grating and ignore-grating trials. A non-parametric cluster-based permutation test was then used to compare the two conditions statistically, whilst controlling for multiple comparisons across time and frequency bins (Maris and Oostenveld, 2007). In brief, first, the two conditions were contrasted with paired-sample t-tests across participants at each time-frequency bin (from -0.5 to 1 s, between 4–100 Hz). Second, significant t-statistics ($p < 0.05$) were grouped into clusters based on temporal and spectral adjacency and then summed within clusters to produce a cluster-level statistic. Third, the maximum cluster-level statistic was measured in each of 10,000 Monte Carlo permutations, yielding a non-parametric null distribution that was then used to calculate the p-value of the clusters observed in the original data.

To illustrate the changes in gamma power over time, the amplitude values from -0.5 to 1 s were averaged between 30–70 Hz, converted into percentage change from baseline (-0.5–0 s) and averaged across participants, separately for attend-grating and ignore-grating conditions.

4.3.12 Spectral analysis and quality control

The peak frequency and peak amplitude parameters of sustained visual gamma oscillations were calculated using the bootstrap procedure illustrated in the first experimental chapter of this thesis (Chapter 2), which allowed also for inspection of data quality (Magazzini et al., 2016). Spectral analysis was performed using a Fourier method, the smoothed periodogram, separately for baseline (-0.7–0 s) and stimulus (0.3–1 s) epochs. The power spectrum was calculated as percentage change from baseline and the gamma peak frequency was measured, in the 30–70 Hz range, by averaging across 10,000 bootstrap iterations. The QC was performed by calculating the width in frequency that was necessary to accommodate at least 50% of the bootstrap iterations around the bootstrap distribution mode. The data were considered of poor

quality if less than 50% of the bootstrap iterations fell within ± 1.2 Hz around the distribution mode (i.e. based on the frequency resolution of the periodogram).

4.3.13 Behavioural data and correlational analysis

The behavioural data were analysed in terms of accuracy rates, measured as percentage of correct orientation discriminations, and RTs, calculated as time in seconds from the onset of the tilted stimulus (par. 4.3.2). Trials with omissions were excluded from the analysis. Accuracy rates and RTs were calculated separately for attend-grating and attend-line (i.e. ignore-grating) conditions and separately for each magnitude of orientation change. The relationship between accuracy/RT and the gamma peak amplitude/frequency parameters was measured using the Pearson's correlation coefficient (r). For this purpose, and based on the results of the QC analysis (par. 4.4.7), the gamma peak amplitude and peak frequency were measured in the attend-grating condition only, using data from all eighteen participants, and the accuracy and RT measures were averaged across the five magnitudes of orientation change.

4.4 Results

4.4.1 Behavioural results

The behavioural responses were analysed in order to remove trials with omissions (mean ± SEM, 4 ± 1%; range, 0–20%) from the analysis of both the behavioural and the MEG data. Trials containing gross artefacts in the MEG data, excessive head motion, or eye movements (par. 4.3.7 and 4.3.4) were also excluded from the MEG data analysis. The orientation of the tilted stimulus was reported correctly in 84 ± 3% (mean ± SEM) of the attend-grating trials and in 75 ± 3% (mean ± SEM) of the attend-line (i.e. ignore-grating) trials. The accuracy rates were clearly modulated by the magnitude of orientation change of both grating and line stimuli (Figure 4.12A), demonstrating that participants complied with the task. The RTs were highly comparable between attend-grating (750 ± 5 ms, mean ± SEM) and ignore-grating trials (800 ± 5 ms, mean ± SEM) and were slightly modulated by the magnitude of orientation change (Figure 4.12D).

4.4.2 Source localization

The results of the source analyses reported below refer to the localization of the sustained component (0.3–1 s) of visual gamma oscillations, as opposed to the transient gamma response (0–0.3 s), which was not the focus of this investigation. Anatomical labels were defined by integrating the AAL atlas (Tzourio-Mazoyer et al., 2002), the Anatomy Toolbox probabilistic atlas (Eickhoff et al., 2005) and the Talairach atlas (Lancaster et al., 2007). MNI coordinates are expressed in mm throughout.

4.4.3 Visual gamma sources in left and right visual cortex irrespective of attention

The source analysis was performed separately for left- and right-presented gratings, by contrasting stimulus and baseline epochs irrespective of the attended hemi-field (Figure 4.2). The left and right peak voxels were identified individually for each participant (see

Table 4.1 and Figure 4.4). Here, results refer to the average across participants. When grating stimuli were presented in the left visual hemi-field (Figure 4.2A), the gamma peak response (~38% increase from baseline) was localized to the calcarine fissure and surrounding cortex in the right hemisphere (MNI coordinates: [12 -96 -2]). When gratings were presented in the right hemi-field (Figure 4.2B), the gamma peak response (~43% increase from baseline) was localized to the calcarine fissure and surrounding cortex in the left hemisphere (MNI coordinates: [-14 -96 -2]). The peaks of these visual gamma responses are illustrated on orthogonal slices in Figure 4.3.

These results confirmed the effectiveness of the stimulus parameters (e.g., size and eccentricity of the grating) in eliciting visual gamma oscillations of clearly measurable amplitude in eighteen out of twenty participants (par. 4.3.1). Out of these eighteen participants, the right peak voxel was localized in V1 (BA17) in five and in V2 (BA18) in twelve; the left peak voxel was localized in V1 (BA17) in ten and in V2 (BA18) in eight participants. Sporadic variations in the localization of these sources (e.g., BA19 in one participants) were most likely caused by MEG-MRI co-registration errors or imperfect co-registration to the MNI template (Perry et al., 2011). Thus, to summarise, the gamma sources were unambiguously localized in the hemisphere contralateral to the stimulus hemi-field, with peaks in close proximity to V1. Hereafter, these sources will be also referred to as the "early visual cortex".

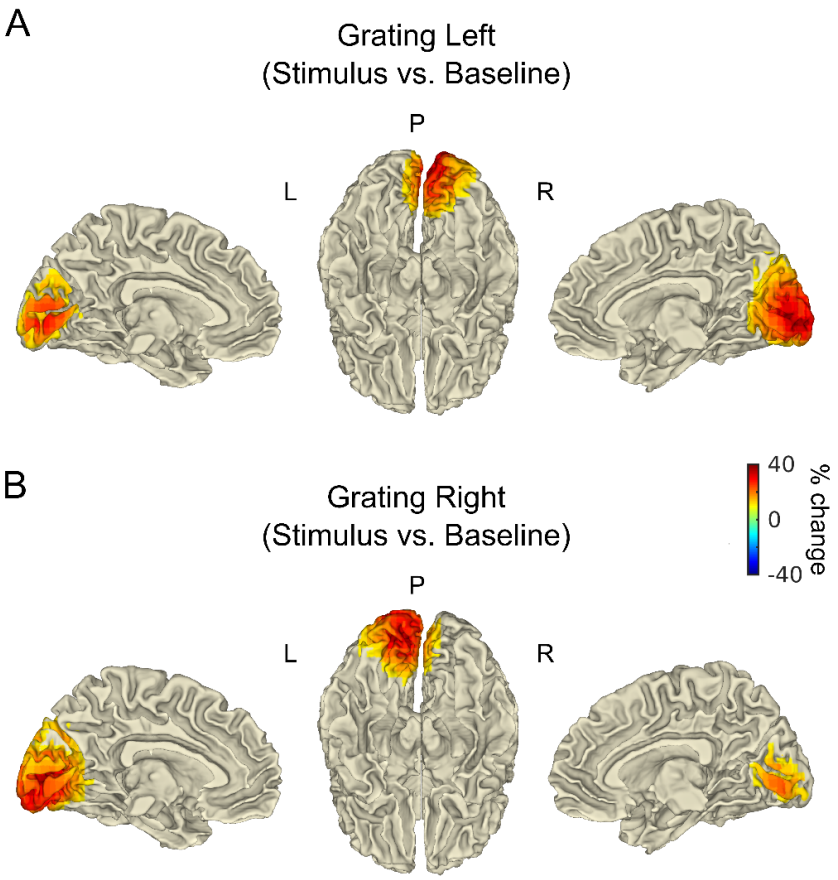

Figure 4.2. Visual gamma response in V1/V2 irrespective of the attended hemi-field.

Beamformer source localization, projected onto the surface of an MNI template brain (left medial, bilateral inferior and right medial views, respectively). The effect of visual stimulation was measured as percentage change in gamma power (30–70 Hz) between stimulus (0.3–1 s) and baseline (-0.7–0 s), irrespective of attention and separately for gratings presented in the left (**A**) and in the right hemi-field (**B**). For visualization purposes, percentage values between ±10% were masked. P, Posterior; L, Left; R, Right.

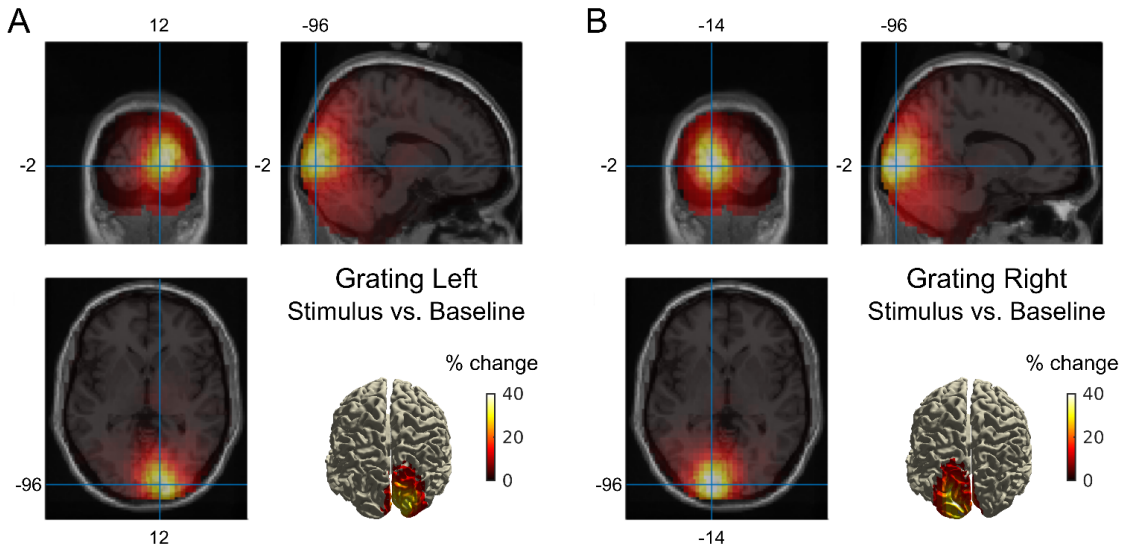

Figure 4.3. Visual gamma response in V1/V2 irrespective of attention (orthogonal slices).

Beamformer source localization of gamma power (30–70 Hz), measured as percentage change between stimulus (0.3–1 s) and baseline (-0.7–0 s), for gratings presented in the left (**A**) and right hemi-field (**B**). Trials were pooled irrespective of whether the grating was attended or ignored. The individual responses were averaged across participants and plotted on orthogonal slices of a template brain. The crosshairs indicate the voxel of greatest increase in gamma power (MNI coordinates in mm). The results were also projected onto the brain surface (posterior view). For visualisation purposes, only values higher than 10% increase were projected.

Table 4.1. Individual peak voxel coordinates.

Grating Left				**Grating Right**			
x	**y**	**z**	**BA**	**x**	**y**	**z**	**BA**
8	-90	10	18	-28	-100	10	17
8	-90	10	18	-12	-100	-4	17
8	-90	-4	17	-18	-90	-4	18
12	-94	-10	18	-12	-94	-14	18
18	-90	10	18	-8	-84	6	17
12	-94	16	18	-12	-90	10	17
22	-90	10	18	-12	-100	6	17
22	-100	10	17	-2	-100	0	17
12	-100	-10	18	-12	-94	16	18
12	-94	6	17	-22	-90	20	18
22	-94	-4	18	-8	-100	0	17
12	-70	40	19	-12	-74	26	18
22	-94	10	18	-18	-94	6	18
8	-100	26	18	-18	-94	0	18
28	-90	-10	18	-18	-94	-14	18
12	-90	10	17	-12	-94	0	17
18	-100	0	17	-12	-94	0	17
22	-94	6	18	-12	-100	0	17

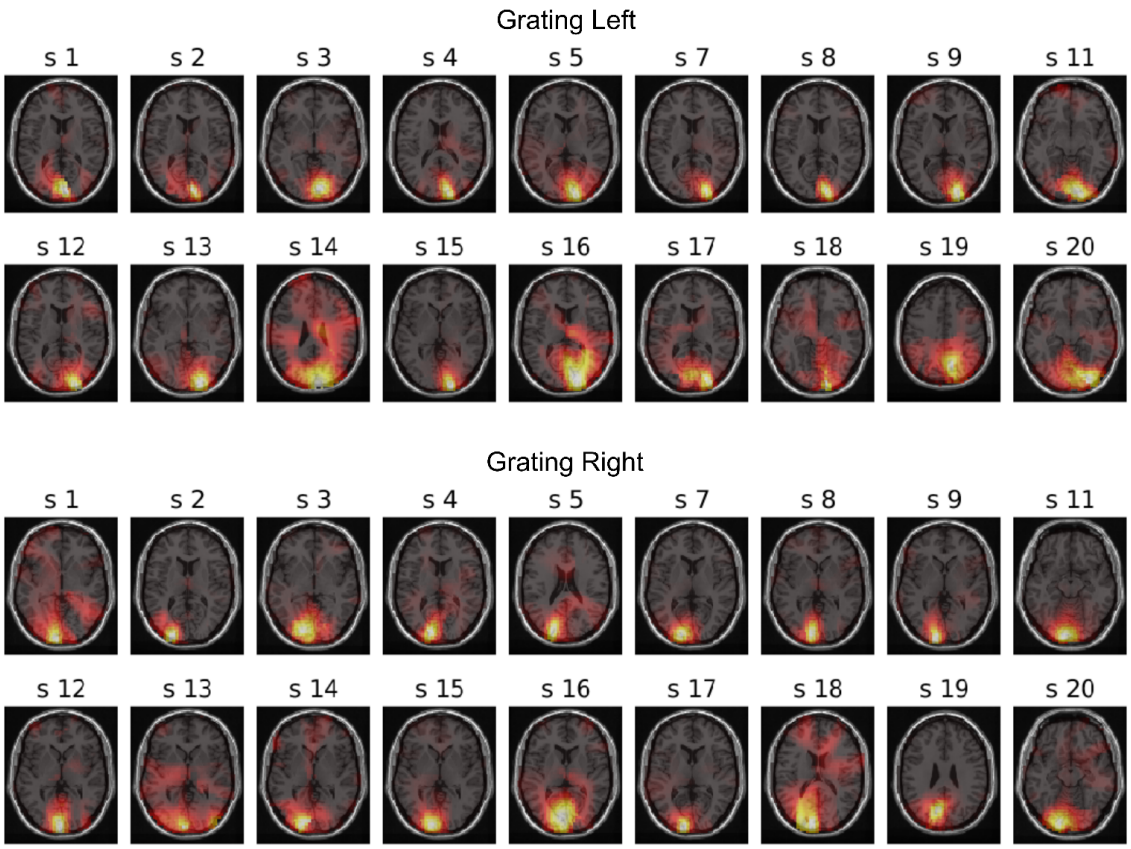

Figure 4.4. Individual source localization images.

Beamformer source localization of gamma power (30–70 Hz), measured as percentage change between stimulus (0.3–1 s) and baseline (-0.7–0 s). Results were plotted on orthogonal slices of a template brain, individually for each participant, separately for gratings presented in the left (top) and right hemi-field (bottom). Trials were pooled irrespective of whether the grating was attended or ignored. For visualisation purposes, colours were scaled to the maximum in each participant and negative values were masked.

4.4.4 Attentional modulation of visual gamma sources in left and right visual cortices

The effect of attention on the visual gamma sources in the left and right hemispheres was tested by comparing the response to attended and ignored gratings, separately for left- and right-presented stimuli. On average, attending the grating resulted in a 5–10% increase in gamma power in V1/V2, compared to attending the line stimulus in the opposite hemi-field (Figure 4.7). The increase in gamma power with attention peaked in the right calcarine (MNI coordinates: [22 -96 4]), when gratings were presented in the left hemi-field (Figure 4.7A), and in the left middle occipital gyrus (MNI coordinates: [-28 -96 14]), when gratings were presented in the right hemi-field (Figure 4.7B). These peak locations were ~1 cm more lateral, compared to the peaks identified for the effect of visual stimulation irrespective of the attended hemi-field (par. 4.4.3). Nevertheless, this increase in gamma power with attention is consistent with sources in contralateral V1/V2. These results are illustrated also in Figure 4.5.

To quantify the effect statistically at the source level, the contrast between attend-grating and ignore-grating conditions was performed using a cluster-based permutation test (par. 4.3.9), separately for left- and right-presented gratings. This analysis revealed a significant difference between conditions, for both left-presented (Figure 4.6A, associated cluster: p = 0.014) and right-presented gratings (Figure 4.6B, associated cluster: p = 0.041). When gratings were presented in the left hemi-field (Figure 4.6A), the greatest difference within the cluster was observed in close proximity to the right inferior/middle temporal, right fusiform and right inferior occipital gyri (t = 5.14, MNI coordinates: [44 -44 4]) and the voxels within the cluster extended to the right calcarine and surrounding cortex. When gratings were presented in the right hemi-field (Figure 4.6B), the greatest differences were observed in the posterior portion of the left fusiform gyrus (t = 5.17, MNI coordinates: [-44 -80 -14]). Figure 4.8 illustrates these results on multiple axial slices.

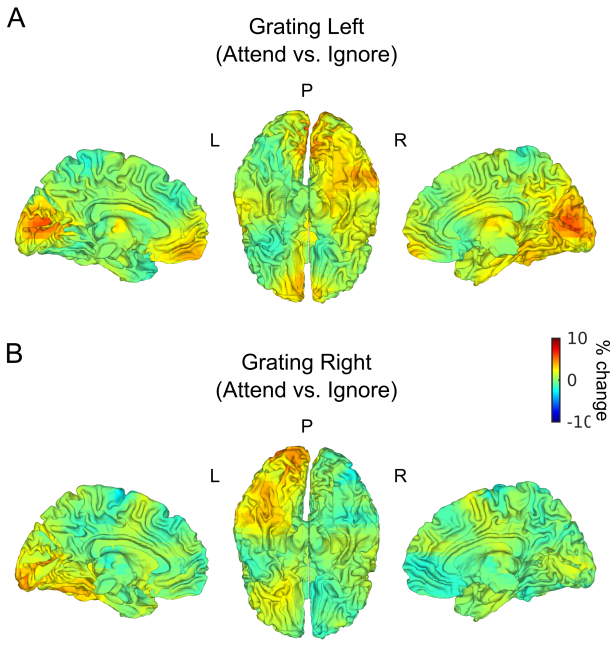

Figure 4.5. Percentage change in gamma power with attention at source level.

The same as in Figure 4.2, but for the contrast between attended and ignored gratings.

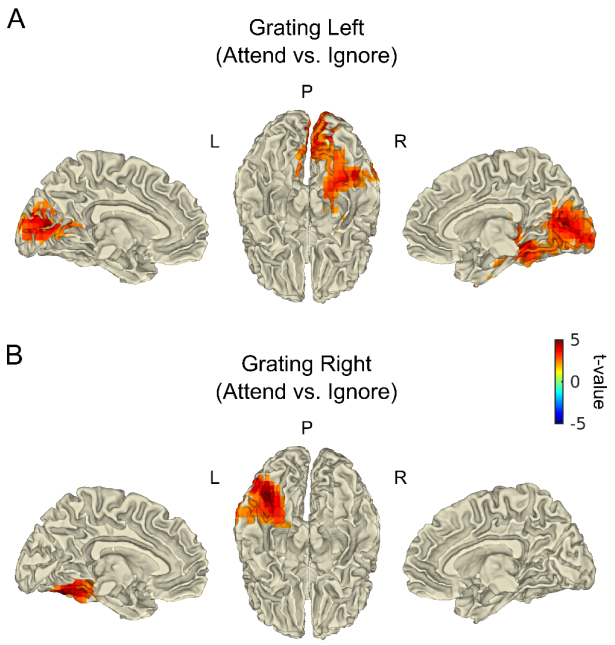

Figure 4.6. Cluster-based statistics of the effect of attention at source level.

Results of the non-parametric permutation test contrasting gamma power (30–70 Hz; 0.3–1 s) between attended and ignored gratings, separately for gratings presented in the left (**A**) and in the right hemi-field (**B**). The significant paired-sample t-statistics ($p < 0.05$, uncorrected) were masked according to the results of the cluster-based permutation ($p < 0.05$, corrected) and projected onto the surface of an MNI template brain (left medial, bilateral inferior and right medial views, respectively). P, Posterior; L, Left; R, Right.

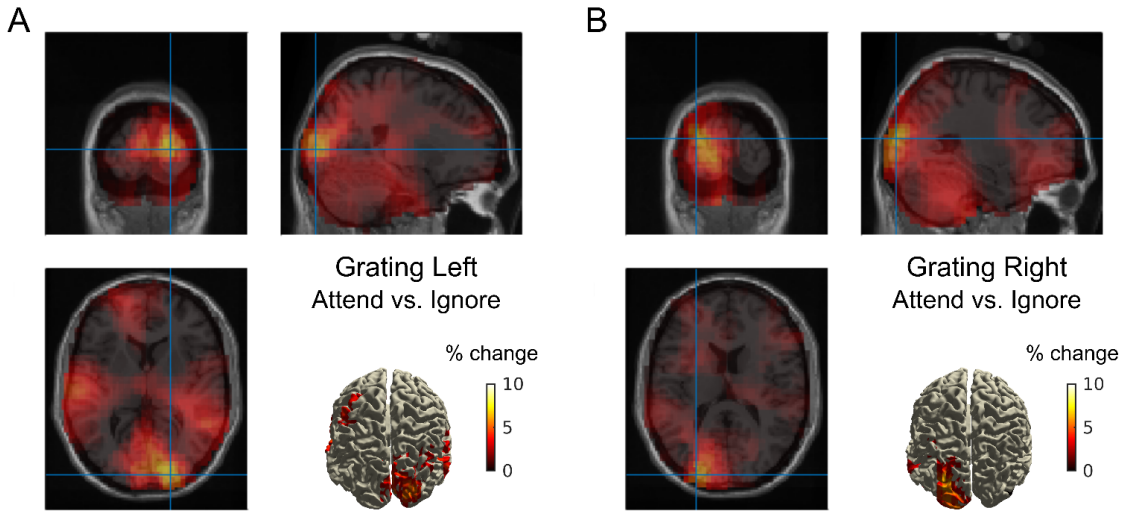

Figure 4.7. Increased visual gamma response in V1/V2 with attention (orthogonal slices).

Beamformer source localization of gamma power (30–70 Hz; 0.3–1 s), measured as percentage change between attend-grating and ignore-grating conditions, for gratings presented in the left (**A**) and right (**B**) hemi-field. The individual responses were averaged across participants and plotted on orthogonal slices of an MNI template brain. The crosshairs indicate the voxel of greatest increase in gamma power. For visualisation purposes, only values higher than 3% increase were projected onto the brain surface (posterior view).

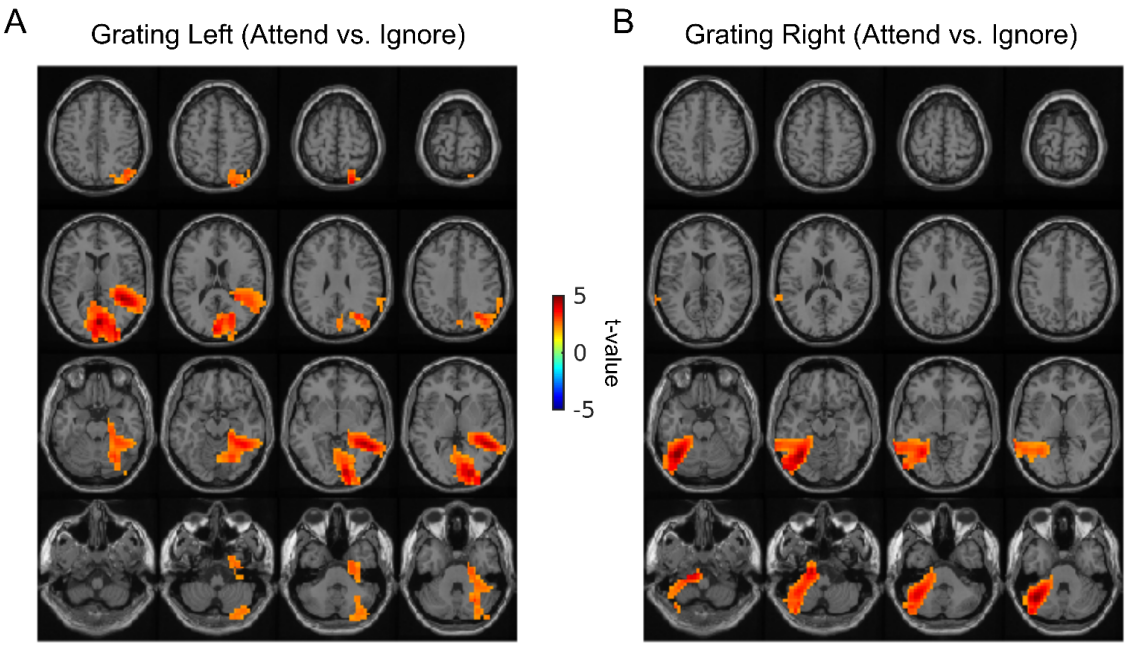

Figure 4.8. Statistical analysis of the effect of attention (axial slices).

The same results as in Figure 4.6, but plotted on axial slices of an MNI template brain.

4.4.5 Attentional modulation of visual gamma sources irrespective of stimulus hemi-field

To test whether any sources of gamma oscillations were modulated in a non-lateralised fashion (i.e. irrespective of the stimulus hemi-field), the effect of attention was tested statistically at source level by first pooling left-grating and right-grating trials and then contrasting the gamma response to attend-grating and ignore-grating conditions. The effect was tested statistically using a cluster-based permutation approach (par. 4.3.9). Results are illustrated in Figure 4.9. The cluster with the lowest associated p-value (p = 0.078) comprised voxels confined to the early visual cortex bilaterally and the greatest difference between conditions (t = 4.99) was localized to the calcarine fissure (MNI coordinates: [0 -82 14]). In other words, V1 (BA17) showed an increase in gamma power with attention that was consistent across stimulation of both left and right hemispheres.

It should be clarified here that this analysis approach cannot be used to infer the spatial localization of the visual gamma sources. By pooling trials across left and right grating presentations, statistical significance is biased towards those voxels showing an increase in amplitude consistently across the two hemispheres, rather than those voxels showing the strongest response to either of the two conditions. In other words, this statistical approach 'favoured' statistical significance for voxels that are closest to the midline and, thus, will not be discussed further.

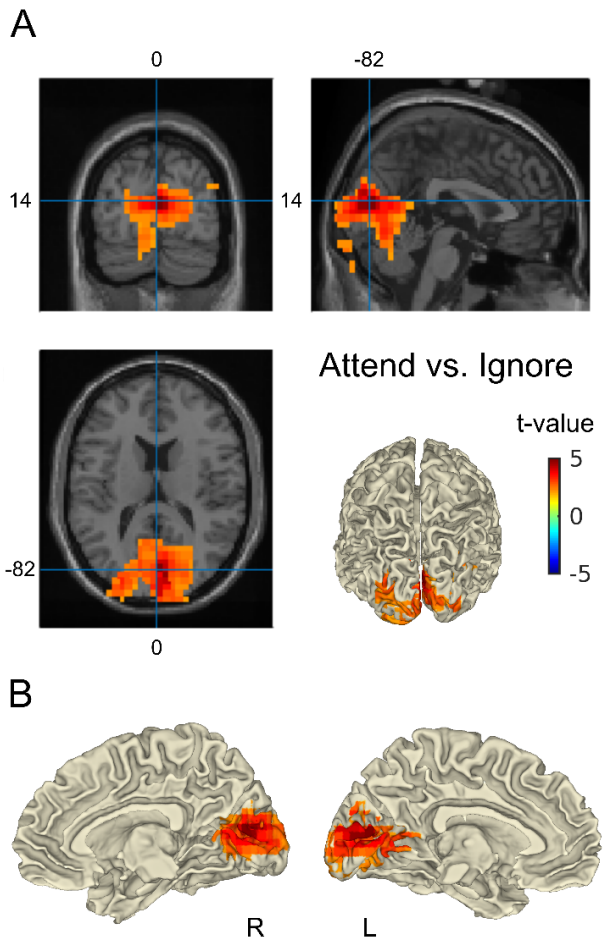

Figure 4.9. Statistical analysis irrespective of the grating hemi-field.

A) Results of the statistical analysis of gamma power (30–70 Hz; 0.3–1 s), contrasting attended and ignored gratings, irrespective of the hemi-field (i.e. trials pooled across left and right grating presentations). The paired t-values were masked according to the results of the permutation test (cluster p = 0.078, corrected). The crosshairs indicate the voxel with largest t-value (t = 4.99, MNI: [0 -82 14]). In the bottom-right panel, results were projected onto the surface of an MNI template brain. **B)** Medial views of the surface projection, right (R) and left (L) hemispheres.

4.4.6 Attentional modulations in the time-frequency domain

The time-frequency analysis of the virtual sensor time-series reconstructed in left and right early visual cortex (par. 4.4.3) was performed separately for attend-grating and ignore-grating conditions (Figure 4.10A and Figure 4.10B). The effect of attention was tested using a cluster-based permutation approach, which revealed a significant difference between the response to attended and ignored gratings (Figure 4.10C), with two associated positive clusters (p = 0.006, ~200–600 ms, ~50–65 Hz and p = 0.018, 500–800 ms, ~48–60 Hz) and one associated negative cluster (p = 0.002, ~0.35–1, ~4–18 Hz). To understand the nature of the difference between conditions, this result was followed up by performing a spectral analysis of the sustained visual gamma response in V1/V2 (par. 4.4.7).

The cluster-based permutation approach also revealed that the visual gamma response in V4 (Figure 4.10D and Figure 4.10E) was significantly higher in power when gratings were attended (Figure 4.10F), with one associated positive cluster (p = 0.042, ~200–400 ms, ~30–45 Hz) and one positive cluster approaching statistical significance (p = 0.092, ~300–500 ms, ~50–60 Hz). This increase in V4 gamma is unlikely to reflect spatial leakage from V1 for two reasons. First, the time-series were orthogonalised to remove any zero-lag correlation between the signals. Second, the evolution of gamma power (30–70 Hz) over time differed between the two regions, with the gamma response to attended gratings showing a peak earlier in V1/V2 (~170 ms; Figure 4.10G) and later in V4 (~240 ms; Figure 4.10H).

4.4.7 Spectral modulations by attention and data quality control

The QC analysis revealed that the spectral data in V1/V2 were generally of very good quality, with poor estimates of the gamma peak frequency in only 2 out of 36 datasets. The individual bootstrap peak frequency distributions are illustrated in Figure 4.11A, separately for attend-grating and ignore-grating conditions. The individual spectra of percentage change from baseline in the gamma frequency range (30–70 Hz) are illustrated in Figure 4.11B. The effect of attention on the gamma peak amplitude and peak frequency in early visual cortex was tested after exclusion of the two participants with poorly estimated gamma. Attending to the grating resulted in visual gamma responses of significantly higher amplitude ($t(15) = 4.04$, $p = 0.001$), compared to attending to the line stimulus in the opposite hemi-field. On the contrary, no significant effect of attention on the gamma peak frequency was observed ($t(15) = 0.94$, $p = 0.36$). The same pattern of results was found when all eighteen participants were included in the analysis, for both gamma amplitude ($t(17) = 4.61$, $p = 0.0002$) and gamma frequency ($t(17) = -0.14$, $p = 0.89$).

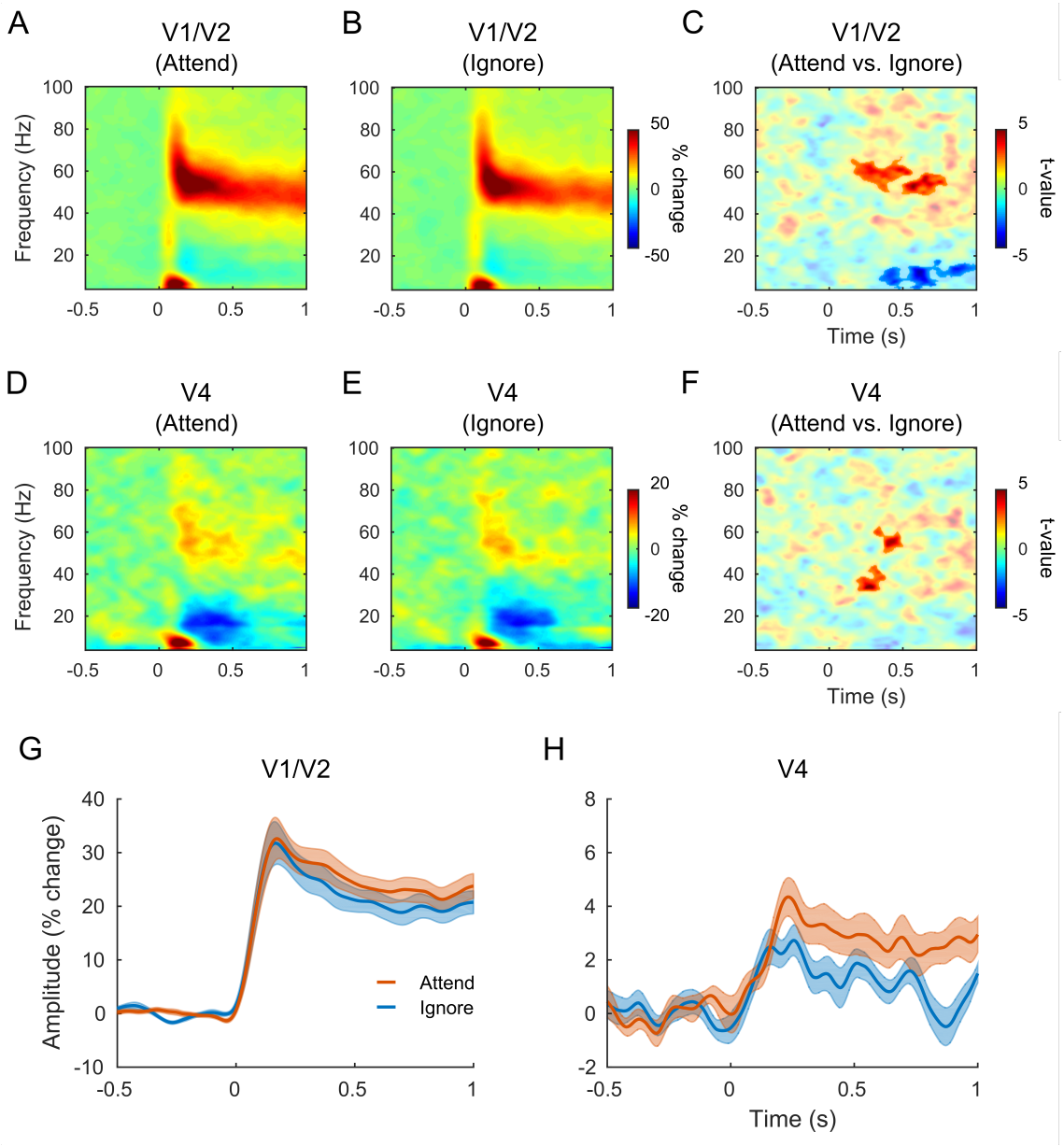

Figure 4.10. Time-frequency analysis of the visual gamma response in V1/V2 and V4.

The virtual sensor data were reconstructed at the left and right peak voxel locations in V1/V2 (**A**, **B**, **C** and **G**) and in left and right V4 (**D**, **E**, **F** and **H**). The data were analysed separately for attended (**A**, **D**, red line in **G** and **H**) and ignored gratings (**B**, **E**, blue line in **G** and **H**) and compared statistically with a cluster-based permutation test (**C**, **F**). The clusters ($p < 0.05$, corrected) were highlighted by changing the transparency value of the colours in the plots. Note that $p = 0.09$ for one of the two clusters in **F**. The thick lines in **G** and **H** represent the percentage change in gamma power (averaged between 30–70 Hz) and the shaded areas represent ±1 SEM, across participants.

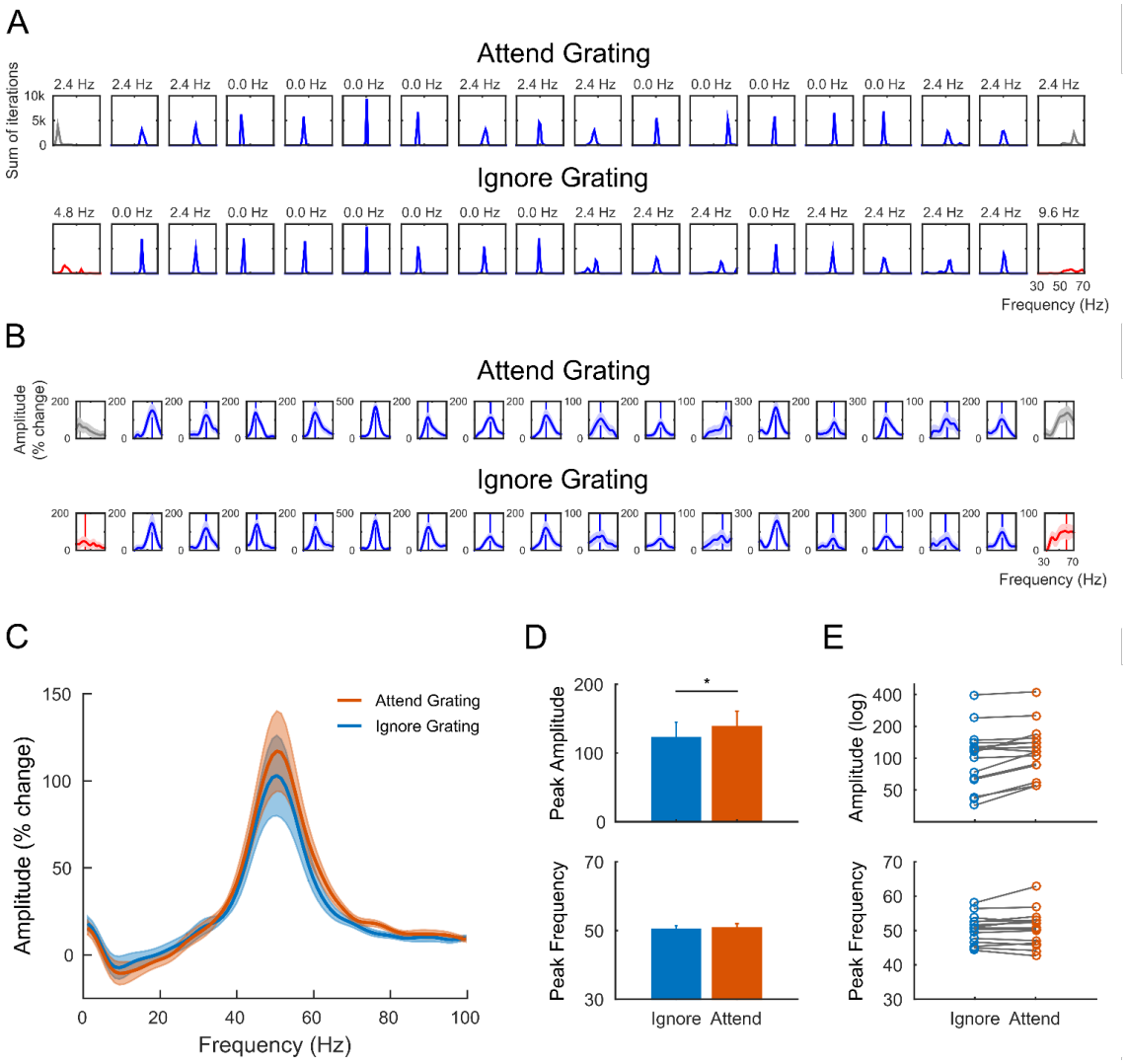

Figure 4.11. Quality control and spectral analysis of visual gamma responses in V1/V2.

A) Individual bootstrap peak frequency distributions, calculated separately in the attend-grating and ignore-grating conditions. Poor-quality data are shown in red, list-wise rejections are shown in grey. The width in frequency necessary to accommodate 50% or more of the bootstrap iterations is shown at the top of each individual panel. **B)** Individual spectra of percentage change from baseline in the gamma frequency range (30–70 Hz). The vertical line in each individual panel indicates the bootstrap peak frequency (i.e. averaged across bootstrap iterations). The colours are the same as in A). **C)** Power spectra of percentage change from baseline in the attend-grating and ignore-grating conditions, grand-averaged across participants, separately for the two conditions. **D)** Bar graph illustrating the average peak gamma amplitude (top) and peak gamma frequency (bottom), in the two conditions. The error bars indicate +1 SEM. **E)** The same as in D), but illustrating the individual participants.

To test whether the change in peak frequency co-varied with the change in gamma amplitude in V1/V2 (see Discussion), we calculated the difference in peak amplitude and peak frequency between attended and ignored stimuli and correlated the two measures across participants. This resulted in no evidence of a linear relationship between the two variables ($r = 0.16$, $p = 0.55$).

After visual inspection of the data, we tested the hypothesis that attention could modulate the so-called "centre of mass" or "spectral centroid" of the power spectra, rather than the gamma peak frequency. This measure differs from the peak frequency in that it weighs frequency (30–70 Hz) by its power across the gamma spectrum (see Lozano-Soldevilla et al., 2014 for a more detailed explanation). The result of a paired-sample t-test revealed a tendency for the centroid of the response to attended gratings (mean = 51.3 Hz) to be higher than the centroid of the response to ignored gratings (mean = 50.5 Hz; $t(15) = 1.95$, $p = 0.070$). This indicates that attention tended to shift the power spectra to higher frequencies by ~1 Hz, on average, without producing an evident change in the peak frequency of the response.

4.4.8 Correlations between visual gamma and behaviour

The relationship between behavioural performance at the orientation discrimination task and the oscillatory parameters in early visual cortex was tested by correlating accuracy and RT with the gamma peak amplitude and peak frequency. The accuracy rate showed a trend for a positive correlation with gamma amplitude ($r = 0.43$, $p = 0.078$; Figure 4.12B) and no relationship with gamma frequency ($r = 0.02$, $p = 0.94$; Figure 4.12C). The RT showed a non-significant negative correlation with gamma amplitude ($r = -0.20$, $p = 0.42$; Figure 4.12E) and a significant negative correlation with gamma frequency ($r = -0.48$, $p = 0.045$). Although the latter correlation would not survive

correction for multiple comparisons, it suggests that individuals whose visual gamma peaked at higher frequency tended to respond faster to the discrimination task.

As the sample size was not particularly large in this study, the correlations were followed up with median split tests. The gamma peak amplitude and peak frequency values were sorted across participants according to high/low accuracy rates and fast/slow RTs and the difference in amplitude and frequency between the resulting groups was tested with independent-sample t-tests. It is worth noting that the trend towards a positive linear relationship between amplitude and accuracy was most likely driven by an outlier value of gamma amplitude (Figure 4.12B; see also the correlation between amplitude and RT, Figure 4.12E). However, also the median split t-test approached statistical significance, as gamma amplitude tended to be higher for those participants who performed with better accuracy at the task ($t(16) = 1.91$, $p = 0.074$). In addition, the significant negative correlation between gamma frequency and RT was supported by a statistically significant difference in peak frequency between participants with fast and slow RTs ($t(16) = -2.71$, $p = 0.015$).

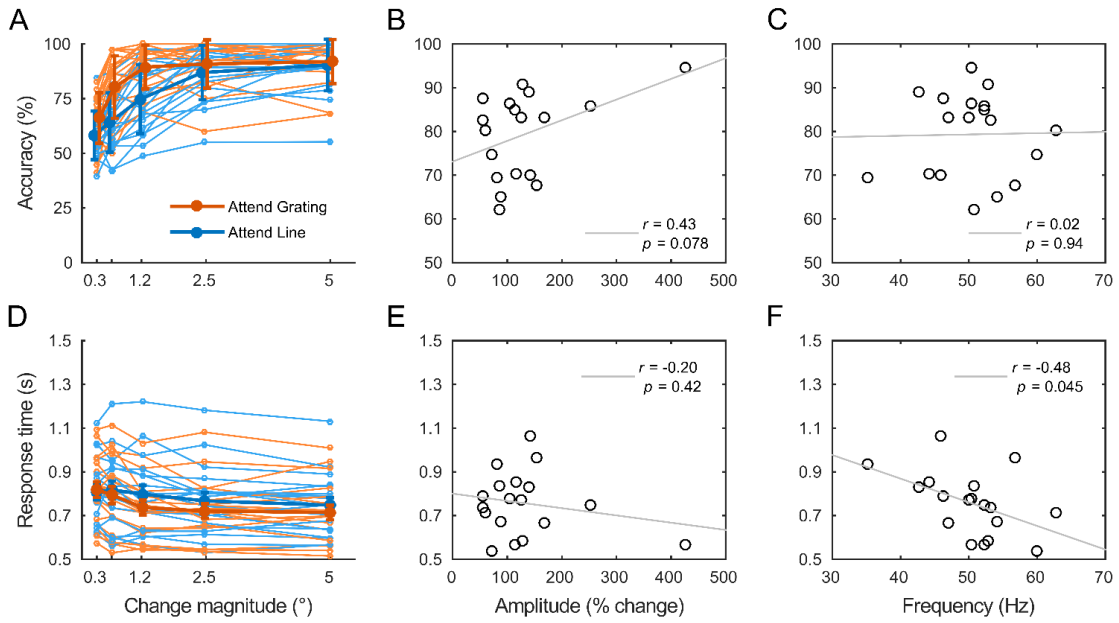

Figure 4.12. Behavioural data and correlations.

A) Accuracy (i.e. percentage of correct orientation discriminations) at each magnitude of orientation change, plotted separately for each participant and also as a group average (thick lines). The error bars indicate ±1 SEM. Note that each magnitude of orientation change was increased by a factor of four, for the line stimulus (par. 4.3.3). **B)** Scatter plot and line of best fit for the correlation between the V1/V2 gamma peak amplitude and accuracy. **C)** Scatter plot and line of best fit for the correlation between the V1/V2 gamma peak frequency and accuracy. **D)**, **E)** and **F)** The same as in A), B) and C), respectively, but for RT instead of accuracy.

4.5 Discussion

In this study, we investigated the effects of visual spatial attention on human visual gamma oscillations. We tested the hypothesis that attention can modulate the spectral profile of the gamma response induced by visual stimulation. Despite the use of an optimal method for robust peak frequency estimation (Magazzini et al., 2016), however, we found no evidence of an increase in the gamma peak frequency with attention. Instead, we found that attention modulated the amplitude of sustained visual gamma oscillations in V1/V2, as well as in V4, and shifted the centroid of the power spectra in V1/V2 towards higher frequencies by ~1 Hz on average. Together, these findings can provide a reconciling solution to the inconsistent results of previous research in both animals and humans.

By combining a beamformer approach to source localization with careful design of the visual stimulus properties, we were able to record gamma oscillations from the early visual cortex contralateral to the hemi-field in which a grating stimulus was presented (Figure 4.2). As expected based on evidence from previous studies in humans (e.g., Hoogenboom et al., 2006; Muthukumaraswamy et al., 2009), the individual visual gamma responses peaked in contralateral V1 or V2. The spectral analysis of the gamma response in V1/V2 revealed an increase in amplitude to attended gratings (i.e. gratings presented in the cued hemi-field) compared to ignored gratings (i.e. gratings presented contralateral to the attended hemi-field), whereas the gamma peak frequency resulted unaffected by attention. The spatial localization of this increase in gamma amplitude with attention was largely consistent with the sources of the gamma response induced by visual stimulation irrespective of attention (i.e. V1/V2; see Figure 4.7). Furthermore, a direct statistical comparison at source level revealed that the gamma response in higher-order visual cortices (i.e. V4) was also significantly modulated by attention (Figure 4.6). By reconstructing virtual sensors in V1/V2 and in V4, after removing the

effect of signal leakage with an orthogonalisation procedure (Colclough et al., 2015), these regions were confirmed as separate visual gamma sources. Thus, we can conclude that spatial attention modulates the amplitude of visual gamma oscillations across the human visual cortical hierarchy, both in the early visual cortex and in higher-order downstream regions.

These results are in line with recent theories on the role of gamma-band synchronization in attentional processing. From a theoretical perspective, post-synaptic processing stages would benefit from strongly synchronized pre-synaptic input (Engel et al., 2001). In particular, pre-synaptic neuronal groups that synchronize their firing more efficiently in response to attended stimuli can increase their post-synaptic drive, thereby facilitating the processing of attended stimulus features in downstream regions (Gregoriou et al., 2015). The attentional enhancement of gamma power in V4 observed here could thus reflect the increased efficacy by which the representation of attended stimuli in early visual cortex is propagated onto higher-order visual areas (Fries, 2015). In this view, the power increase in the early visual cortex could reflect either enhanced input from the thalamus, which would elicit the generation of higher amplitude gamma oscillations in V1 (van Kerkoerle et al., 2014), or stronger coupling between V1 and V2 (Roberts et al., 2013). Overall, this would be in line with recent theories of gamma-band activity as a mechanism for propagating sensory representations in a feedforward manner across the visual cortical hierarchy (e.g., Michalareas et al., 2016; van Kerkoerle et al., 2014).

In previous studies in animals, the strongest enhancements of gamma amplitude and gamma-band synchronization by attention have been reported in high-order visual areas, such as V4 (Bichot et al., 2005; Buffalo et al., 2011; Fries et al., 2001, 2008b; Taylor et al., 2005). Although not to such a large extent, attentional modulations of gamma synchrony have been observed also in V2 (Buffalo et al., 2011). In V1, gamma power

appears to be either decreased (Chalk et al., 2010) or unaffected by attention (Bosman et al., 2012; Buffalo et al., 2011), although the latter observation could be a result of response saturation effects due to the use of high-contrast stimuli (see Bosman et al., 2012). In the human early visual cortex, modulatory effects of gamma-band power by attention have been reported by one recent study (Koelewijn et al., 2013), though the frequency range of the effect (~60–90 Hz) could reflect an underlying increase in neuronal firing rate, rather than in rhythmic synchronization (see Ray and Maunsell, 2011). Attentional enhancement of narrow-band gamma oscillations, instead, has been observed in early visual cortex with manipulation of attention between different sensory modalities, rather than between different locations of the visual field (Kahlbrock et al., 2012b). Since other studies have not been able to implicate the early visual cortex as a source of gamma-band attentional modulations, we have identified hereafter a number of factors that could explain the (dis)similarities between our results and the existing evidence from both animals and humans.

In the human MEG literature, one study by Siegel et al. (2008), namely the first study to apply beamformer source localization in this context, investigated the effect of spatial attention on gamma oscillations induced by visual motion. The results revealed a relative increase in gamma power by attention, with extended sources in high-order visual areas that did not include the presumed V1/V2 (Siegel et al., 2008). This discrepancy with our results could be explained by the different stimulus used (i.e. random dot patterns vs. static gratings) and task required (i.e. motion direction vs. orientation discrimination) and both these factors also explain the involvement of ventral regions in our study, as opposed to the dorsal visual pathway in the study by Siegel et al. (2008). Furthermore, interpreting the sources in Siegel et al. (2008), as well as those reported by other studies (e.g., Bauer et al., 2012, 2014, Marshall et al., 2015a, 2015b), is complicated by the uncertainties in the source geometry underlying the

response to bilateral stimuli, a configuration that may lead to self-cancellation of medial bilateral sources, when reconstructed with a beamformer (Sekihara et al., 2002; see also Koelewijn et al., 2013).

The increase in gamma amplitude in V1/V2 could also be explained by our paradigm design. The behavioural results indicated that the orientation discrimination task was harder for the line stimulus than the grating, suggesting that the task demand was high not only in the attend-grating but also in the attend-line condition. Successful allocation of spatial attention was thus required both towards and away from the grating stimulus, in order to perform the task accurately. This, together with an eccentricity of the stimulus that was unlikely to cause response saturation effects (van Pelt and Fries, 2013), may have played an important role in revealing the attentional modulation of gamma amplitude in the early visual cortex. At the same time, though, this consideration also highlights one limitation of the study, namely that the effect we refer to as an increase in amplitude with attention could in theory be driven by an underlying decrease in gamma amplitude when grating stimuli were ignored. Future studies will have the opportunity to address this concern by including an experimental condition in which attention is not cued to either hemi-field. Despite this, the interpretation of an enhancement in V1/V2 gamma by attention appears the most consistent with the literature (Buffalo et al., 2011; Kahlbrock et al., 2012b).

One potential confounding factor in the interpretation of the gamma amplitude increase in V1/V2 is related to eye movements and gaze position, which, in principle, could introduce systematic differences in stimulus eccentricity between attention conditions. The visual gamma response is reduced for peripheral compared to foveal stimuli (van Pelt and Fries, 2013). For static gratings similar to those used in this study, gamma amplitude is drastically reduced at an eccentricity of 6° and less so for 3° eccentricity.

As estimated by Van Pelt and Fries (2013), the decrease in power is accompanied by a decrease in peak frequency of ~1 Hz/°. In our study, however, we did not observe a significant change in peak frequency with attention. In addition, the increase in gamma amplitude with attention was not significantly correlated with the change in peak frequency, across participants. For these reasons, we concluded that the procedure of trial exclusion based on changes in eye gaze position, as measured by eye-tracking, was successful in removing the possible influence of eye movements on the properties of the visual gamma response.

The second main hypothesis tested in this study concerned the peak frequency of visual gamma oscillations in V1/V2. Contrary to the effect on gamma amplitude, we found no evidence for an effect of spatial attention on the gamma peak frequency. Testing for this hypothesis was motivated by two recent studies, which reported increased gamma-band inter-areal synchronization across the visual cortical hierarchy (between V1 and V4) with selective spatial attention (Bosman et al., 2012; Grothe et al., 2012). In particular, Bosman et al. (2012) found that the gamma peak frequency in V1 was increased in response to relevant, compared to irrelevant stimuli. This suggested that the modulation of gamma frequency by top-down attentional mechanisms could serve to enhance the impact of selected upstream neurons (e.g., those in the V1 retinotopic space that represent the attended part of the visual field) on downstream neuronal groups (Cannon et al., 2014; Fries, 2015). Crucially, the shift to a higher gamma frequency with attention is thought to occur only when more than one neuronal group in V1 compete for the influence on the same neuronal group in a downstream area, such as V4 (Fries, 2015). Hence, the difference in experimental paradigm could explain why this effect was not observed here. In the study by Bosman et al. (2012; see also Grothe et al., 2012), monkeys were presented with two visual stimuli, each activating a separate recording site in V1 and the same site in V4. Due to the technical limitations of MEG,

however, it would be hard to achieve a stimulus configuration that can both activate two separate, unambiguous sites in V1 and produce gamma responses of measurable amplitude in humans. Additionally, although separate activations could be achieved by stimulating both hemispheres, the use of bilateral grating stimuli would have introduced possible source cancellation problems, which, as discussed above, may have obscured the gamma response in the early visual cortex. Overall, therefore, the absence of competition among different V1 neuronal groups could well explain the lack of evidence of an increase in peak frequency with attention.

In light of the different methodologies used in animal and human electrophysiology, the discrepancy between the result by Bosman et al. (2012) and our null finding could also arise from the difference in spatial resolution itself. The oscillations recorded invasively with LFPs in monkeys are very finely resolved in space, whereas the signals recorded in humans with MEG reflect the spatial summation of synchronous neurons across larger patches of the cortical sheet (reviewed in Muthukumaraswamy, 2014). Therefore, if the gamma peak frequency measured in this study reflected the contribution of spatially distributed sources, it is possible that the modulation by attention, if any at all, was not sufficiently consistent across the visual cortex to be detected in the spatially summated response. Speculatively, it could be hypothesized that smaller neuronal groups generated spectral power at higher frequencies in response to attended stimuli, while the dominating response frequency of larger neuronal groups remained unaltered. In line with this hypothesis, the centroid (centre of mass) of the power spectra tended to higher frequencies by ~1 Hz in response to attended stimuli, compared to ignored ones. Despite substantial inter-individual differences (see the individual spectra in Figure 4.11B) this effect can be observed also in the power spectra of attended and ignored gratings, grand-averaged across participants (Figure 4.11C). It is also worth noting that the gamma peak frequency differed remarkably between the two conditions of attention

in some participants, although not consistently across the sample (Figure 4.11E). While part of this variation is likely to reflect measurement error, the peak frequency reliability estimates obtained with our QC approach (Magazzini et al., 2016) were generally very high, within each condition. At the same time, though, the gamma peak frequency is also known to be highly repeatable within participants (Muthukumaraswamy et al., 2010; Tan et al., 2016), which leaves the individual between-condition variations observed here difficult to interpret.

Finally, we attempted to link the inter-individual differences in behavioural performance with the spectral properties of visual gamma oscillations. This was motivated by the evidence of a relationship between gamma-band synchronization and behaviour (e.g., response times) in both monkeys (Womelsdorf et al., 2006) and humans (Hoogenboom et al., 2010). In this study, we found a tendency for participants who performed better at discriminating the change in stimulus orientation to show higher-amplitude gamma oscillations in V1/V2 (Figure 4.12B). However, the positive linear relationship between these two variables appeared to be driven by one outlier observation and a follow-up median split test only approached statistical significance. The other behavioural measure considered, the RT, showed a more robust negative correlation with the gamma peak frequency in V1/V2 (Figure 4.12F). In a follow-up median split test, the gamma peak frequency of participants who responded faster to the task was significantly higher than that of slow responders. In previous studies, the gamma peak frequency has been shown to correlate with parameters of psychophysical performance, such as the individual orientation discrimination threshold (Dickinson et al., 2015; Edden et al., 2009). Overall, therefore, although the non-specificity of the RT as a measure of performance complicates the interpretation of this result, it suggests the existence of a link between the gamma peak frequency and functionally relevant parameters of behavioural performance.

Chapter 5.

A multi-site study of visual gamma oscillations using quality-control measures to compare data across three different MEG systems

5.1 Abstract

Recently, neuroimaging research has witnessed a rapid increase in sample size. This trend has been partly influenced by the benefits of data sharing, but driven primarily by criticisms of a lack of statistical power in cognitive neuroscience research and an associated failure to reproduce the findings of small studies. In this study, we describe the first multi-site collaborative project in the UK for the collection of standardised MEG protocols. We pooled data from a total of 80 individuals across four research centres and three different MEG systems (CTF, Elekta and 4-D). The data consisted of a visual gamma paradigm, which offered clear reference criteria for comparing the data among the four sites. The different data formats were brought to a common ground by applying the same source analysis pipeline to each MEG system. To test for differences among the four sites, we compared the classic oscillatory parameters such as the gamma peak amplitude and peak frequency and used the QC approach developed in the first experimental chapter of this thesis (Chapter 2) to compare data quality, measured as the reliability of peak frequency. While the gamma peak frequency was highly comparable among sites, the data from Glasgow resulted in higher gamma amplitude, which might be attributed to differences in sensor type between 4-D and the other MEG systems. Although gamma amplitude correlated positively with the estimates of peak frequency reliability, data quality did not differ remarkably among sites. Additionally, results were highly comparable when source analysis was performed with the LCMV and DICS beamformer algorithms. Although still preliminary, our results suggest that the gamma peak frequency is a suitable measure for the purpose of combining multi-site datasets. In contrast, differences in MEG sensor type may need to be controlled for, before measures of gamma amplitude can be pooled. Overall, the present work provides the first proof-of-concept for the establishment of shared multi-site MEG databases and the development of new large-scale collaborative MEG projects.

5.2 Introduction

In recent years, the field of neuroimaging has benefitted from very rapid advances in the methodological and theoretical approaches to studying brain structure and function, which together have led to increased interest in the collection of much larger samples, compared to the few dozen participants typical of studies from a decade ago (Eickhoff et al., 2016). While smaller samples still represent a pragmatic solution, for example when specific research questions need to be addressed, the advantages of large sample sizes are conspicuous. First and foremost, the increased statistical power and reduced vulnerability to spurious effects paves the way for transparent and reproducible science (Eickhoff et al., 2016), which is most effectively achieved by making not only the data but also the analysis code available to other researchers (Gorgolewski and Poldrack, 2016). As highlighted in a recent special issue of the journal *NeuroImage* (Eickhoff et al., 2016), data sharing has seen a rapid growth in the field of neuroimaging. In some cases, sharing neuroimaging data is aimed at establishing normative databases for clinical use (Poline et al., 2012), whereas in other circumstances the use of large samples simply facilitates the generation of novel hypotheses, which can be rigorously tested with the necessary statistical power (Milham, 2012). Furthermore, shared datasets can serve as a test bed for new analysis methods, providing benchmarks against which novel approaches can be compared, thereby enhancing the reproducibility of results (Poldrack and Gorgolewski, 2014).

To date, the majority of the existing large-scale collaborative studies and shared neuroimaging repositories consist primarily of structural or functional MRI data (e.g., Herrick et al., 2016; Hodge et al., 2016; Poldrack and Gorgolewski, 2015; Walker et al., 2016). However, there are several reasons for also establishing similar large-scale databases for MEG data. For example, MEG data consist of complex and mixed neural signals, which are not yet fully understood and would be best interpreted by the

development of new advanced analysis methods. Furthermore, although some first steps have been made towards establishing recommended practices in MEG research (Gross et al., 2013), there is still no standardised approach to data analysis. For the reasons mentioned above, collaborative work on shared data could thus both facilitate and accelerate the achievement of this goal. To date, no large-scale MEG databases have been established. However, two large shared databases involving some MEG data are available. The first, the Human Connectome Project (HCP), consists of both task-based and task-free MEG recordings from approximately 100 individuals (Larson-Prior et al., 2013), as well as structural and functional MRI, behavioural and genetics data (Van Essen et al., 2013). The second, the Omega project, offers a similar sample size to that of the HCP, but consists of resting-state MEG data only (Niso et al., 2016).

In the UK, the first whole-head MEG system was installed at Aston University in 2001 and since then research in this field has been expanding rapidly, with the establishment of nine (prospectively ten) other MEG laboratories in the following fifteen years. In chronological order, MEG centres have opened in York, London, Cardiff, Nottingham, Glasgow, Oxford, Cambridge and Ulster, with the University of Birmingham being currently in the process of establishing the tenth MEG laboratory in the UK (the second in the city of Birmingham). In 2013, eight of these Universities started a collaborative project known as the 'UK MEG Partnership'. By coming together as a research partnership, the sites have been facilitated in their academic networking activities, including setting up collaborative training programmes and PhD studentships. One of the aims was to agree on standard experimental paradigms to be collected from a cohort of healthy individuals. In principle, these standard protocols could be used for clinical research purposes, thereby overcoming the challenges associated with recruiting large numbers of patients at a single site.

As well as adopting a unified approach to data collection, the Partnership also aimed at building a shared multi-site MEG database from a large number of healthy volunteers and to establish common pipelines for the analysis of each standard protocol. The idea was to provide a proof of principle for future large-scale collaborative projects on specific clinical populations, where data might be collected at different sites and with different MEG systems. In the present work, we aimed to demonstrate the feasibility of such an approach. We combined data from three different systems, providing an initial proof-of-concept for the establishment of shared MEG databases, which we believe will show the way forward in clinical MEG research.

5.3 Materials and Methods

5.3.1 The UK MEG Partnership project

The UK MEG Partnership is a large multi-site study led by Prof Krish Singh, Head of Human Electrophysiology at Cardiff University. The project was established in 2013 in collaboration among eight MEG laboratories in the UK and is supported by a five-year grant of £1.5 million from the Medical Research Council (MRC; Grant Numbers: MR/K005464/1 and MR/K501086/1). One of the key research goals of the collaboration is to establish a normative MEG database, yielding a total of 640 datasets (80 participants at each site) across three different MEG systems (CTF, Elekta Neuromag and 4-D Neuroimaging).

The project is based at the Cardiff University Brain Research Imaging Centre (CUBRIC) and the original seven partner sites are, in alphabetical order: the Aston Brain Centre (ABC) at Aston University; the Centre for Cognitive Neuroimaging (CCNi) at the University of Glasgow; the Cognition and Brain Sciences Unit (CBU), in collaboration with the University of Cambridge; the Oxford Centre for Human Brain Activity (OHBA) at the University of Oxford; the Sir Peter Mansfield Imaging Centre (SPMIC) at the University of Nottingham; the Wellcome Trust Centre for Neuroimaging (WTCN) at University College London (UCL); and the York Neuroimaging Centre (YNiC) at the University of York.

As of 2016, the University of Birmingham and the University of Ulster have also established, or are expected to establish, new MEG laboratories. These two UK Universities may thus join the MEG Partnership in the near future.

5.3.2 Participants

The participants of the UK MEG Partnership consisted of healthy individuals with no history of psychiatric or neurological conditions, who reported no use of psychoactive drugs and had normal or corrected vision. For the purpose of merging the data with the 100 Brains study (see Chapter 2), participants recruited at Cardiff University were required to be right-handed and of Caucasian ethnicity. Additionally, each recruitment site could choose whether or not to include site-specific psychometric questionnaires ahead of the MEG scan. On the day of the MEG scan, all sites screened their participants for caffeine, nicotine and alcohol intake, medications and hours of sleep.

In this study, we pooled data from four different MEG centres (Cardiff, Nottingham, Aston and Glasgow), twenty participants each, for a total of 80 participants. One individual from Nottingham had to be excluded (par. 5.4.1), for a total of 79 participants included in the analysis. The mean, SD and range of age of the participants recruited at each site is illustrated in Table 5.1.

Table 5.1. Participants' age (mean, SD and range, in years).

MEG site	**Mean (years)**	**SD (years)**	**Range (years)**
Cardiff	30.3	8.1	21–55
Nottingham	30.5	10.4	19–56
Aston	23.2	5.2	18–37
Glasgow	26.5	4.8	19–35

5.3.3 Visual gamma paradigm

The visual gamma paradigm was standardised across MEG centres in order to control for the physical properties of the stimuli that could influence the spectral properties of the visual gamma response. The paradigm is illustrated schematically in Figure 5.1. The

visual stimulus consisted of a vertical, stationary, maximum contrast, three cycles per degree, square-wave grating, presented in the lower left visual field, subtending 4° of visual angle both horizontally and vertically. The grating was presented on a mean luminance background for a jittered duration between 1.5–2 s. The ITI was 4 s in one half and 8 s in the other half of the trials. Although this was not the focus of the present investigation, the use of both long and short ITIs was aimed at fully capturing the temporal dynamics of the post-movement beta rebound (e.g., Fry et al., 2016), whilst optimising the total duration of the paradigm. Short and long ITIs were presented in random order. Participants were instructed to fixate a red dot positioned at the top right-hand edge of the grating and to perform a simple abduction of the index finger of their right hand once the grating disappeared. The paradigm consisted of 100 trials, for a total duration of ~13 min.

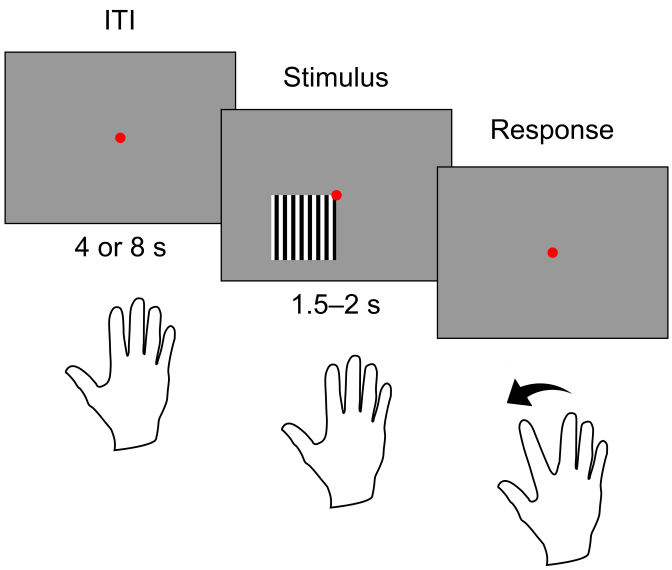

Figure 5.1. Visual gamma paradigm.

Schematic illustration of the visual gamma paradigm. Participants were instructed to perform the index finger abduction movement as soon as the grating disappeared. The stimulus duration was jittered (1.5–2 s) to prevent participants from anticipating the response. The ITI (4 or 8 s) started at stimulus offset.

The stimulus presentations were programmed in Matlab (The Mathworks) using the Psychophysics Toolbox (Kleiner et al., 2007). The projection systems used to display the stimuli differed among the four MEG centres, but all projectors were gamma-corrected and operated at the same refresh rate of 60 Hz.

5.3.4 Data acquisition in Cardiff

The MEG recordings at Cardiff University were performed using a 275-channel axial gradiometer CTF system (VSM MedTech), located inside a magnetically shielded room. An additional 29 reference channels were recorded for noise cancellation purposes and the primary sensors were analysed as synthetic third-order gradiometers (Vrba and Robinson, 2001). The sampling rate was 1200 Hz. Three electromagnetic coils were placed on three fiduciary locations (nasion, left and right pre-auricular) and their position relative to the MEG sensors was localized before and after each session. For source-localization purposes, the MEG data were co-registered to the individual anatomical MRI of each participant by marking the MRI voxels corresponding to the position of the three fiducial coils. The individual anatomical MRIs (1-mm isotropic, T1-weighted FSPGR) were acquired using a 3.0 T MRI scanner (General Electric).

5.3.5 Data acquisition in Nottingham

The MEG data collected at the University of Nottingham were courtesy of PhD Student Benjamin Hunt, who also performed the MEG/MRI co-registration and MEG source analysis. The MEG recordings were performed using a 275-channel axial gradiometer CTF system identical to the one used in Cardiff (par. 5.3.4). The position of three electromagnetic coils (nasion, left and right pre-auricular) was first measured relative to the subject's head shape using a Polhemus Isotrak 3D digitiser (Kaiser Aerospace Inc.) and then co-registered by matching the digitised head surface to the head surface

extracted from the individual anatomical MRI. The individual anatomical MRIs (1-mm isotropic, T1-weighted MPRAGE) were acquired using a 3.0 T MRI scanner (Philips).

5.3.6 Data acquisition in Aston

The MEG data collected at Aston University were courtesy of PhD Student Michael Hall, who also performed the MEG/MRI co-registration and MEG source analysis and contributed to developing the Matlab code for analysis of Elekta MEG data in Fieldtrip. The MEG recordings were performed using a 306-channel magnetometer and planar gradiometer system (Elekta Neuromag), located inside a magnetically shielded room. The data were sampled at 1 kHz, bandpass-filtered online between 1–300 Hz. The position of five electromagnetic coils was measured using a Polhemus Isotrak 3D digitiser (Kaiser Aerospace Inc.) and the subject's digitised head shape was co-registered to the head surface extracted from the individual anatomical MRI using a modified version of a multiple-iteration, least-error, surface-matching algorithm (Adjamian et al., 2004a). The individual anatomical MRIs (1-mm isotropic, T1-weighted) were acquired using a 3.0 T MRI scanner (Siemens).

5.3.7 Data acquisition in Glasgow

The MEG data collected at the University of Glasgow were courtesy of PhD Student Kevin Prinsloo, who also performed the MEG/MRI co-registration and MEG source analysis and contributed to developing the Matlab code for analysis of 4-D MEG data in Fieldtrip. The MEG recordings were performed using a 248-channel magnetometer system (MAGNES 3600 WH, 4-D Neuroimaging). An additional 28 reference channels were recorded for noise cancellation purposes. The data were sampled at 1017 Hz, highpass-filtered online at 0.1 Hz. The position of five electromagnetic coils was measured using a Fastrak 3D digitiser (Polhemus Inc.) and the subject's digitised head shape was co-registered to the individual anatomical MRI of each participant using a

semi-automatic procedure based on a modified version of the ICP algorithm (Besl and McKay, 1992). The individual anatomical MRIs (1-mm isotropic, T1-weighted) were acquired using a 3.0 T MRI scanner (Siemens).

5.3.8 MEG data pre-processing

For data collected with CTF MEG systems (Cardiff and Nottingham), environmental noise was reduced by transforming the primary sensors into third-order gradients (par. 5.3.4). The individual trial epochs were then visually inspected and trials containing large artefacts (e.g., muscle clenching) were excluded from the analysis.

The data collected with the Elekta MEG system (Aston) were pre-processed using Elekta software. Environmental noise was reduced using a temporal Signal Space Separation algorithm (tSSS; MaxFilter v2.2), with a subspace correlation limit of 0.9, and static bad channels were identified with Xscan 3.0. Trials were then visually inspected and epochs containing large artefacts removed.

The data collected with the 4-D MEG system (Glasgow) were de-noised by performing a PCA of the reference channels and regressing the principal components out of the primary MEG sensors.

Trials were cut into epochs from -2 to 2 s around stimulus onset and the pre-processed data were down-sampled to 300 Hz prior to covariance or CSD matrix computation (par. 5.3.9), but not prior to virtual sensor reconstruction. For the purpose of reconstructing virtual sensor data with the same number of trial samples, the pre-processed data from Elekta and 4-D were linearly interpolated to match the sampling rate of CTF, i.e. 1200 Hz.

5.3.9 Source localization analysis

Source analysis was performed in Matlab, using the Fieldtrip toolbox (Oostenveld et al., 2011) and with the same analysis pipeline for CTF, Elekta and 4-D data. In order to reconstruct oscillatory activity at brain locations directly comparable across participants, 1) the MNI template brain was divided into a 5 mm isotropic voxel resolution grid, 2) the individual anatomical MRI was warped to the template MRI and 3) the inverse transformation matrix was used to warp the template grid onto an individual grid for each participant. The leadfield was calculated using a semi-realistic volume conduction model based on the individual anatomy (Nolte, 2003) and source power was estimated twice, using two different beamformer algorithms, namely LCMV (Van Veen et al., 1997) and DICS (Gross et al., 2001).

For source analysis with LCMV, the covariance matrix was calculated on a time-range from -1.5 to 1.5 s around stimulus onset, after bandpass-filtering the data between 35–75 Hz. The optimal dipole orientation at each voxel was calculated by SVD. For each participant, the peak voxel was identified by selecting the voxel of greatest difference in gamma power (35–75 Hz), calculated with paired-sample t-test at each voxel location contrasting stimulus (0.3–1.5 s) and baseline (-1.2–0 s). Virtual sensors were reconstructed at the peak voxel location by multiplying the sensor-level data by the beamformer weights for that location.

For DICS, the frequency analysis was performed using multi-taper FFT with Slepian tapers, centred at 55 Hz with ±20 Hz smoothing, and the CSD was calculated from -1.5 to 1.5 s around stimulus onset. For each participant, the peak voxel was identified by selecting the greatest t-statistic across voxels, and virtual sensors were reconstructed at this location in the same way as the LCMV analysis (see above).

5.3.10 Time-frequency analysis

To illustrate the spectral evolution of the visual gamma response over time, the virtual sensor data were represented in the time-frequency domain. For this purpose, the time-series from -1.5 to 1.5 s were bandpass-filtered at each frequency between 4–100 Hz, in steps of 0.5 Hz (8 Hz bandpass, 3rd order Butterworth filter), the amplitude envelope of the analytic signal (Matlab function *hilbert*) was averaged across trials and expressed as percentage change from baseline (-1.5–0 s).

5.3.11 Spectral analysis and quality control

The peak frequency and peak amplitude parameters of sustained visual gamma oscillations were calculated using the bootstrap procedure illustrated in Chapter 2, which allowed also for inspection of data quality (Magazzini et al., 2016). Spectral analysis was performed using a Fourier method, the smoothed periodogram, separately for baseline (-0.7–0 s) and stimulus (0.3–1 s) epochs. The power spectrum was calculated as percentage change between stimulus (0.3–1.5 s) and baseline (-1.2–0 s) and the gamma peak frequency was measured in the 35–75 Hz range. The peak frequency reliability estimates were obtained by calculating the percentage of iterations falling within ±0.6 Hz around the bootstrap distribution mode, consistently with the analysis performed in Chapter 2.

5.4 Results

5.4.1 Visual gamma responses

The results of the source localization analysis are illustrated in Figure 5.2A, for LCMV, and in Figure 5.2B, for DICS. The difference in gamma power (35–75 Hz) between stimulus (0.3–1.5 s; sustained gamma) and baseline (-1.2–0 s) was calculated separately for each participant with a paired-sample t-tests across trials. The t-statistic values at each voxel location were then averaged across participants, separately for participants from each of the four sites (Cardiff, Nottingham, Aston and Glasgow).

The source topographies of the data from Cardiff, Aston and Glasgow were highly comparable. In these three sites, positive t-statistic values were confined to the occipital lobe bilaterally and peaked in the right calcarine fissure, i.e. contralateral to the visual hemi-field in which the grating was presented. The Glasgow data showed the highest average t-values and the Aston data the lowest. The data from Nottingham showed a similar lateralised pattern of activation, but the positive t-values were more broadly spread across the occipital and parietal lobes. After visual inspection of the individual source topographies, one participant from Nottingham was excluded from further analysis, as they did not show a clear gamma peak in the occipital lobe.

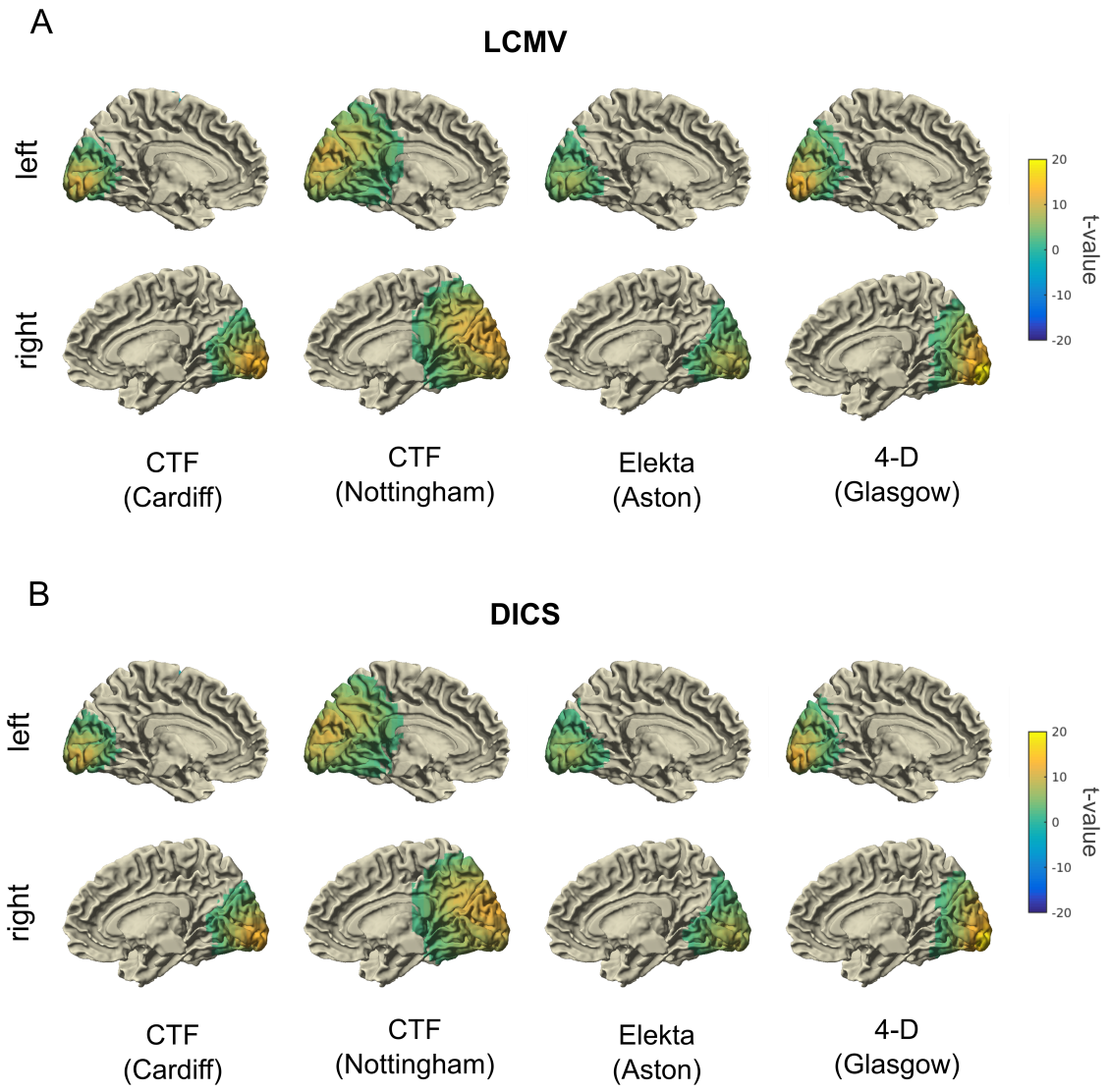

Figure 5.2. Source localization of visual gamma with LCMV and DICS.

A) LCMV beamformer source localization illustrating the difference in gamma power between stimulus and baseline, measured with paired-sample t-tests at each voxel location. The t-statistics were averaged over participants, separately for the twenty participants from each of the four MEG centres, and projected onto the surface of an MNI template brain. For illustration purposes, negative t-statistics were masked. **B)** The same as in A), but for the DICS beamformer.

5.4.2 Data comparison between beamformers

As illustrated in Figure 5.2, the results of the source analysis were highly comparable between LCMV (Figure 5.2A) and DICS (Figure 5.2B), for each of the four sites. At the group level, the source topographies produced by the two beamformer algorithms did not show any marked differences.

In line with the similarity observed in the spatial domain, the spectro-temporal properties of the visual gamma response reconstructed by the LCMV and DICS beamformers were also highly comparable. As illustrated by the time-frequency analysis of the virtual sensor time-series reconstructions (Figure 5.3A), the temporal evolution of the visual gamma response, averaged over participants, showed no marked differences between LCMV and DICS beamformers. The individual time-frequency maps are illustrated in Figure 5.4.

The power spectra derived from the LCMV and DICS virtual sensors are illustrated in Figure 5.3B, averaged over participants. Similar to the results of the time-frequency comparison, the results of spectral analysis performed with the smoothed periodogram method were also highly comparable between the two beamformer algorithms. The comparison of the gamma peak amplitude and peak frequency parameters between LCMV and DICS at the individual level is illustrated in Figure 5.5. This confirmed the tight correspondence of the peak parameter estimates obtained with the two beamformers.

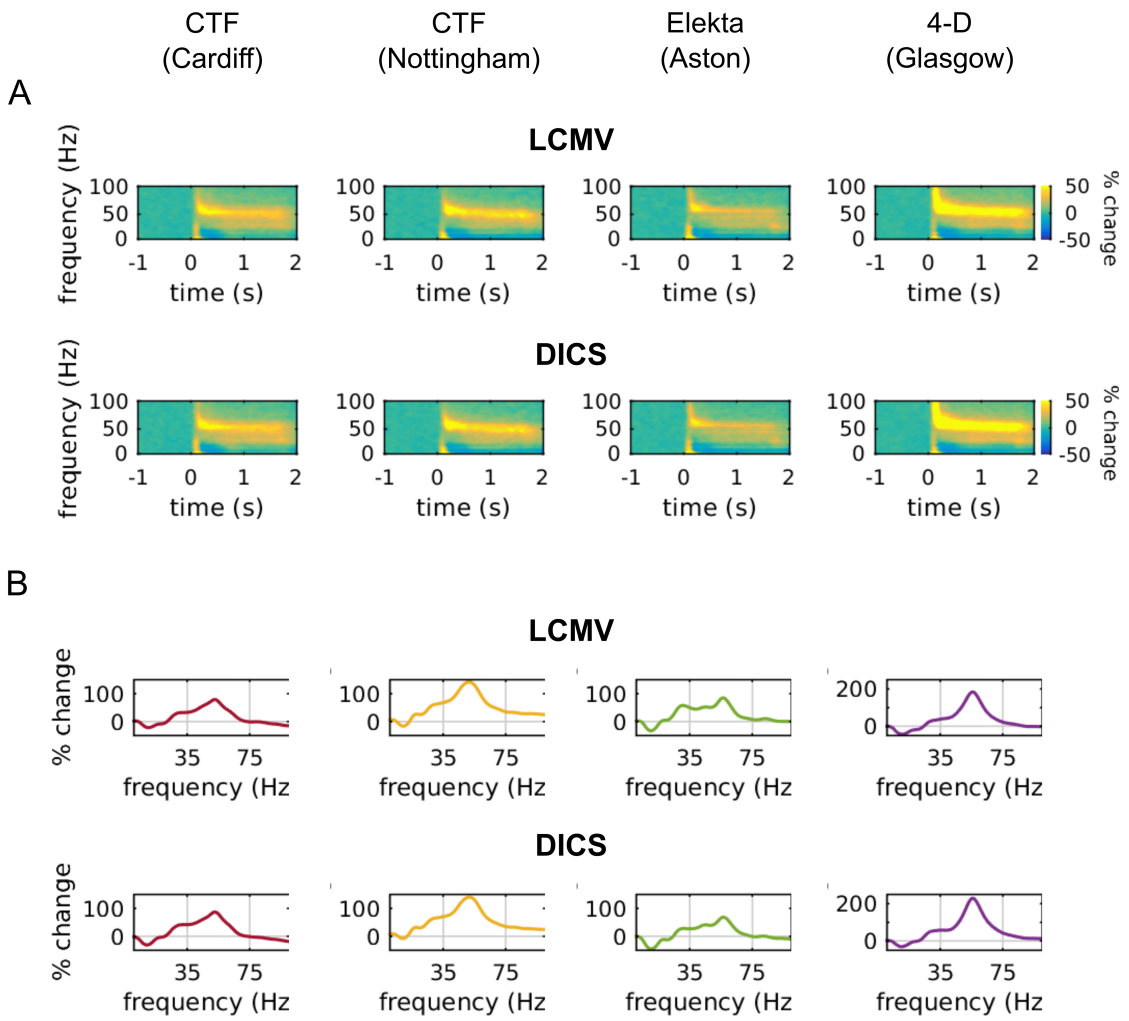

Figure 5.3. Group-level virtual sensor time-frequency and spectral analysis.

A) Time-frequency representation of the virtual sensors reconstructed in visual cortex, calculated as percentage change from baseline (-1–0 s) and averaged over participants, separately for each site. The virtual sensor time-series were reconstructed using beamformer weights calculated with the LCMV (top four panels) and DICS (bottom four panels) algorithm. **B)** Power spectra, calculated as percentage change of stimulus (0.3–1.5 s) from baseline (-1.2–0 s) and averaged over participants, separately for each site and separately for LCMV and DICS virtual sensors. Note the different y-axis amplitude scale of the Glasgow data.

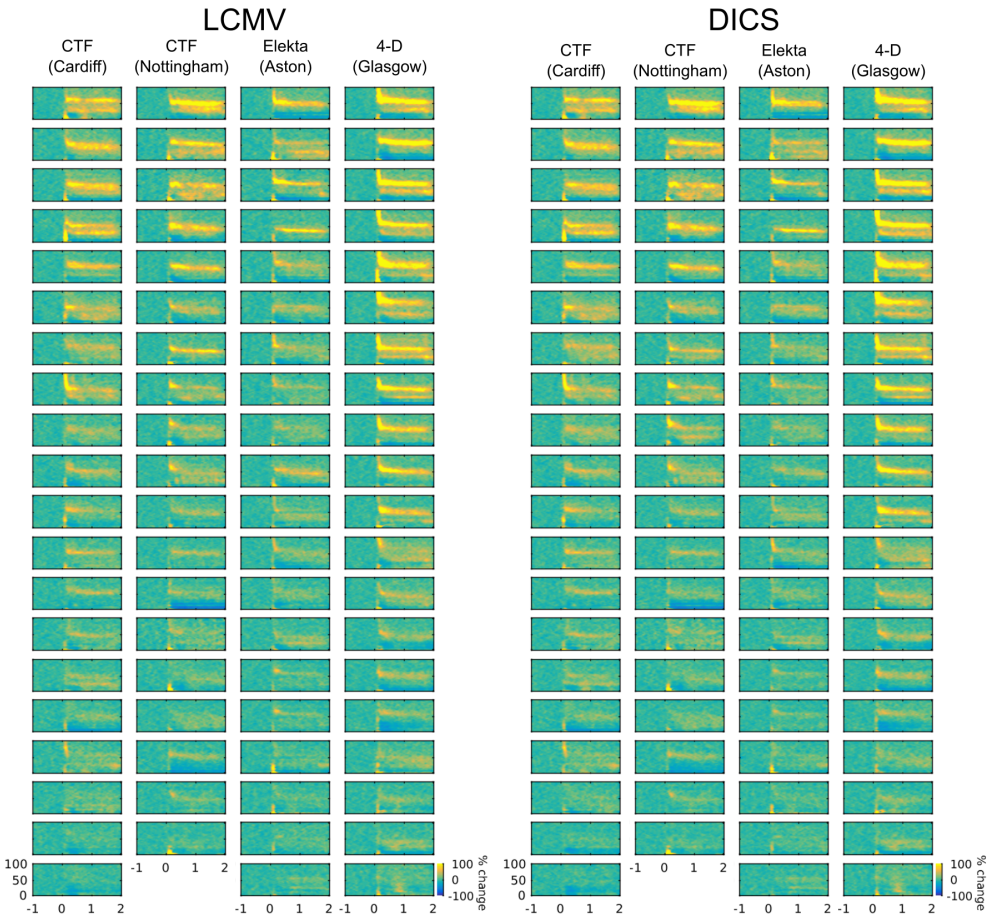

Figure 5.4. Individual time-frequency plots of the LCMV and DICS virtual sensors.

Time-frequency representations plotted individually for each participant and separately for LCMV (left) and DICS (right). For each MEG site, participants are arranged from top to bottom by their average value of percentage change in sustained gamma power (35–75 Hz; 0.3–1.5 s).

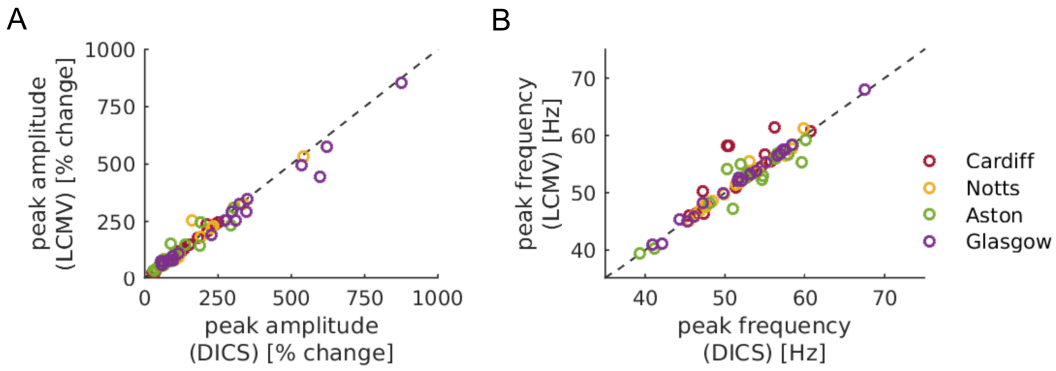

Figure 5.5. Comparison of peak amplitude and peak frequency between beamformers.

A) Scatter plot illustrating the positive linear relationship between the peak amplitude estimates obtained from the LCMV and DICS virtual sensor reconstructions. Participants from different sites are coded with different colours. **B)** The same as in A), but for the peak frequency.

5.4.3 Gamma peak amplitude and peak frequency across sites

To test for differences in the visual gamma data collected at different MEG centres and with different MEG systems, we first compared the gamma peak amplitude and peak frequency parameters across sites. The distributions of these two peak parameters are illustrated in Table 5.2, Figure 5.6 and Figure 5.7, separately for LCMV and DICS.

Table 5.2. Gamma peak amplitude and peak frequency parameters at each site (mean ± SD).

	LCMV		DICS	
MEG system	**Amplitude (% change)**	**Frequency (Hz)**	**Amplitude (% change)**	**Frequency (Hz)**
CTF (Cardiff)	118 ± 70	53 ± 5	118 ± 68	52 ± 4
CTF (Nottingham)	140 ± 125	52 ± 5	138 ± 125	51 ± 5
Elekta (Aston)	102 ± 78	53 ± 6	98 ± 82	53 ± 6
4-D (Glasgow)	250 ± 212	52 ± 7	272 ± 230	52 ± 7

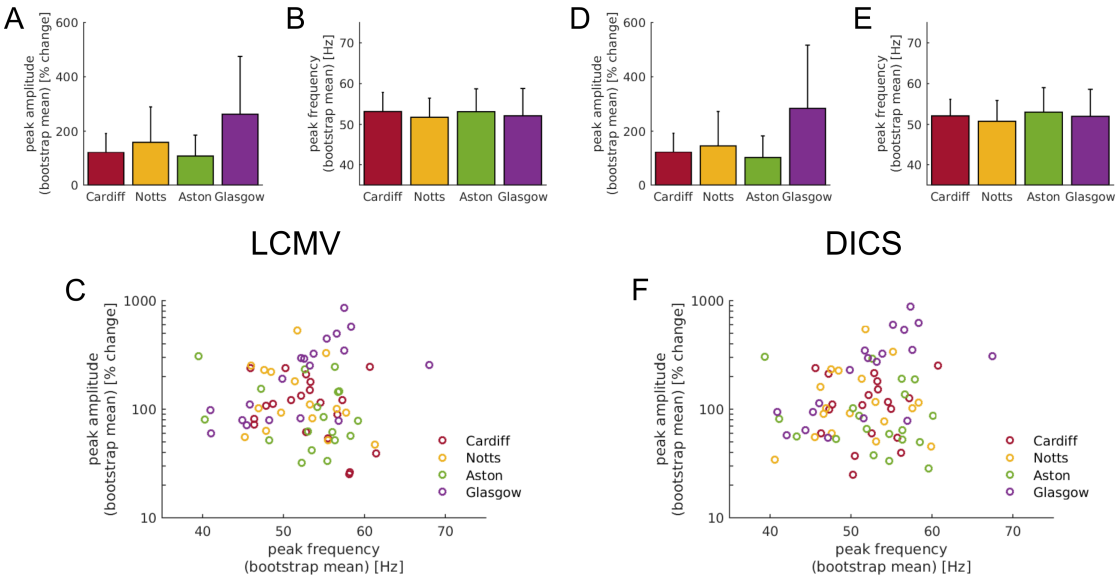

Figure 5.6. Distribution of the gamma peak amplitude and peak frequency across sites.

A) and **B)** Bar charts of the gamma peak amplitude and peak frequency, respectively. The error bars represent 1 SD. **C)** Scatter plot of the individual peak amplitude and peak frequency values across sites. Note that the amplitude values are plotted on a logarithmic scale. **D)**, **E)** and **F)** The same as in A), B) and C), but for DICS instead of LCMV.

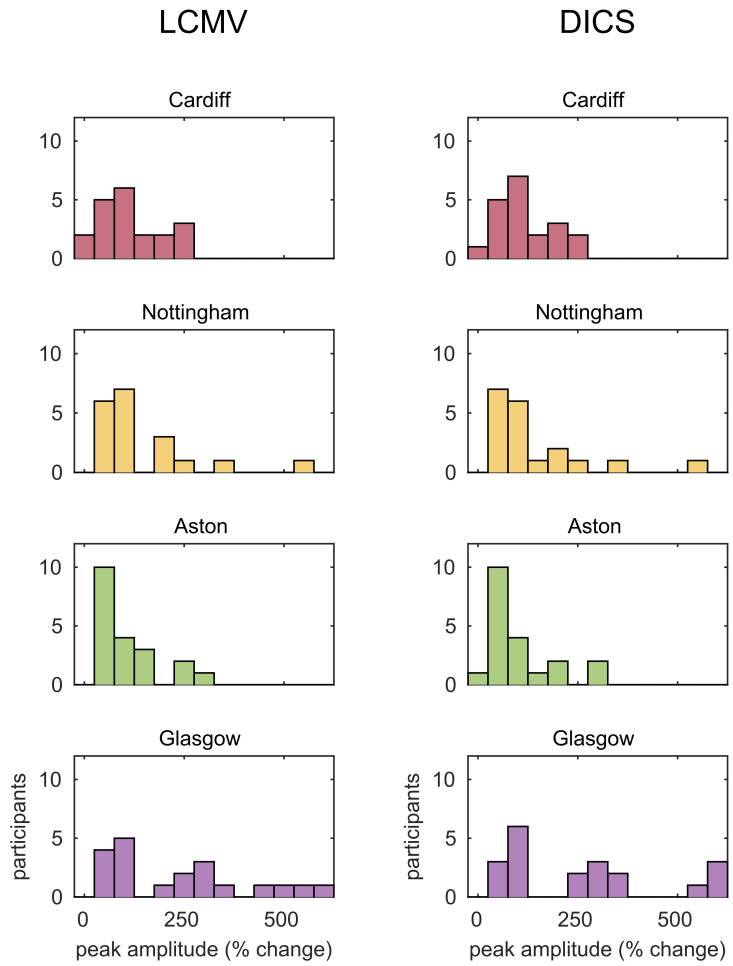

Figure 5.7. Distribution of gamma amplitude across participants, for each site.

In each plot, the histogram bars illustrate the distribution of the gamma peak amplitude (in percentage change from baseline) across participants, separately for each site and for LCMV (left column) and DICS (right column) beamformers.

To test for a statistical difference in gamma amplitude among sites, we used a one-way between-subject ANOVA with factor 'MEG site' (four levels: Cardiff, Nottingham, Aston and Glasgow). The analysis was repeated separately for the estimates of peak amplitude derived with the LCMV and DICS beamformers. The results revealed a significant effect of MEG site on peak amplitude, both for LCMV ($F(3,39.6) = 2.93$, $p = 0.045$; reporting Welch's test as homogeneity could not be assumed, Levene's test $p < 0.05$) and DICS ($F(3,39.4) = 3.38$, $p = 0.027$; Welch's test).

For LCMV, Games-Howell post-hoc tests revealed a significantly higher amplitude for Glasgow compared to Aston ($p = 0.034$) and a trend towards a significant difference between Glasgow and Cardiff ($p = 0.063$). The difference was not significant between Glasgow and Nottingham ($p = 0.22$). For DICS, Games-Howell post-hoc tests revealed

significant differences between Glasgow and Aston (p = 0.020) and between Glasgow and Cardiff (p = 0.042), but not between Glasgow and Nottingham (p = 0.13).

The same ANOVA analysis approach used to test gamma amplitude was used also to test the effect of 'MEG site' on the gamma peak frequency. This resulted in no significant difference in peak frequency among sites, neither with LCMV (F(3,75) = 1.08, p = 0.36), nor with DICS (F(3,75) = 1.15, p = 0.34).

5.4.4 Data quality across sites

The peak frequency reliability estimates (par. 5.3.11) were used to compare the quality of the data collected at different MEG sites. As illustrated in Figure 5.8, the data appeared to be of comparable quality across sites. On average, the percentage of iterations within ±0.6 Hz was higher for Glasgow (LCMV, 63±24%; DICS, 64±25%) compared to Cardiff (LCMV, 57±25%; DICS, 56±25%), Nottingham (LCMV, 56±24%; DICS, 56±25%) and Aston (LCMV, 58±26%; DICS, 56±25%). However, a one-way between-subject ANOVA with factor 'MEG site' resulted in no significant differences among sites (LCMV, F(3,75) = 0.27, p = 0.85; DICS, F(3,75) = 0.57, p = 0.64).

Next, as the Glasgow data showed both significantly higher gamma amplitude values and a tendency for more reliable peak frequency estimates, the relationship between these two parameters was tested using Pearson's r. For this purpose, the data were pooled across all four sites, for a total of 79 pairs of observations. As illustrated in Figure 5.8, the percentage of iterations within ±0.6 Hz was positively correlated with the gamma peak amplitude, both with LCMV (r = 0.57, p < 0.001) and with DICS (r = 0.58, p < 0.001).

Since, in principle, a difference in amplitude/percentage values among sites could drive this correlation, the analysis was repeated separately for each site. As illustrated in

Table 5.3, the results revealed significant positive correlations for all sites apart from Cardiff, which only showed a positive trend. Once again, the correlation results were highly consistent between LCMV and DICS beamformers. The correspondence between the peak frequency reliability estimates obtained with the two beamformers is illustrated in Figure 5.9.

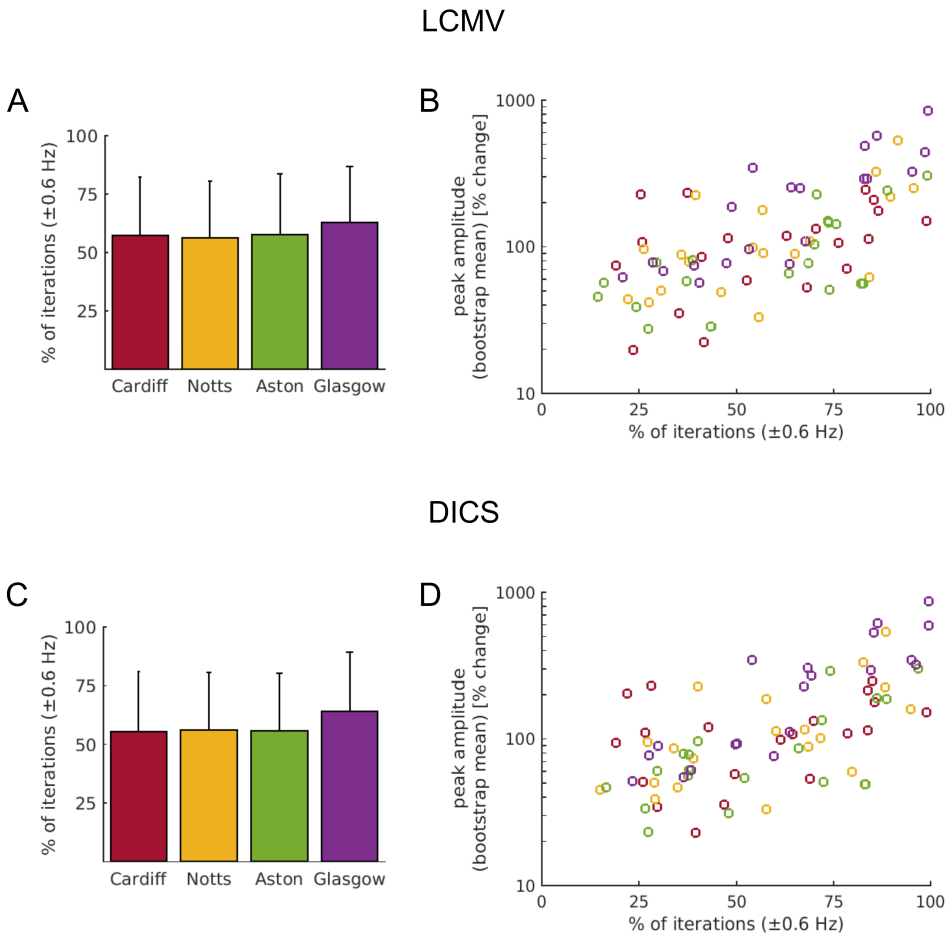

Figure 5.8. Data quality comparison across sites.

A) Bar chart illustrating the mean percentage of iterations falling within ±0.6 Hz around the bootstrap distribution mode, separately for the four MEG systems. The error bars represent 1 SD. **B)** Scatter plot illustrating the positive linear relationship between the gamma peak amplitude and the peak frequency reliability estimates. Note that the amplitude values are plotted on a logarithmic scale. Participants are colour-coded according to the colours of the bars in A). **C)** and **D)** The same as in A) and B), but for DICS instead of LCMV.

Table 5.3. Correlations between percentage of iterations (±0.6 Hz) and peak amplitude.

	LCMV		DICS	
MEG system	***r***	***p***	***r***	***p***
CTF (Cardiff)	0.32	0.17	0.32	0.17
CTF (Nottingham)	0.64	0.003	0.56	0.01
Elekta (Aston)	0.64	0.002	0.63	0.003
4-D (Glasgow)	0.79	$< 10^{-5}$	0.81	$< 10^{-5}$

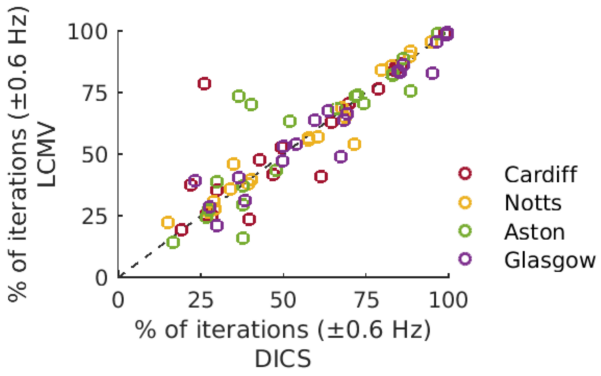

Figure 5.9. Comparison of peak frequency reliability between beamformers

Scatter plot illustrating the positive linear relationship between the gamma peak frequency reliability estimates obtained from the virtual sensors reconstructed with the LCMV and DICS beamformers. The different colours represent participants from different sites.

5.5 Discussion

In this study, we used the QC approach developed in the first experimental chapter of this thesis (Chapter 2) to analyse MEG data that were collected as part of a multi-site study known as the 'UK MEG Partnership'. We pooled data from four different MEG laboratories (Cardiff, Nottingham, Aston and Glasgow) and three different MEG systems (CTF, Elekta and 4-D), with the aim to test the comparability of visual gamma data collected at different sites and with different systems. For this purpose, we performed across-site comparisons of classic oscillatory parameters such as the gamma peak amplitude and peak frequency and used our novel approach to control data quality by estimating the reliability of the gamma peak frequency (Magazzini et al., 2016).

The data from the three different MEG systems were processed keeping between-platform discrepancies to a minimum and bringing the different data formats to a common ground. To achieve this, we designed a common analysis pipeline in Fieldtrip, which applied the same forward and inverse solutions to the three different sensor-level data formats and returned source-level processed data directly comparable across sites. This approach was particularly beneficial to overcoming the limitations of combining three different types of sensors, i.e. axial gradiometers in CTF, planar gradiometers in Elekta and magnetometers in Elekta and 4-D, which also differ in their layout configuration relative to the scalp. Ultimately, therefore, the aim was to test whether multi-site datasets can be pooled simply by adopting common analysis pipelines that bring results to a common, comparable data format.

5.5.1 Across-site comparison

One of the main findings of this study is the higher amplitude of visual gamma oscillations recorded with the 4-D MEG system at Glasgow. The ANOVA analysis showed a significant effect of the main factor 'MEG site' on the gamma peak

amplitude, estimated by spectral analysis of the virtual sensor time-series. This effect was remarkably visible also in the time-frequency spectrograms, both averaged (Figure 5.3A) and individually for each participant (Figure 5.4). The post-hoc comparisons revealed that gamma amplitude with the 4-D system differed significantly from the Elekta system at Aston and the CTF system at Cardiff (for DICS only; par. 5.4.3), but not from the CTF system at Nottingham. This latter result, however, may be due to the high variability observed for both the Nottingham and the Glasgow data (cf. Table 5.2).

Rather than reflecting differences in the properties of the neuronal response of participants recruited at Glasgow, we argue that the higher amplitude of the Glasgow data might be related to differences between 4-D and the other MEG systems. The sensor array of the 4-D MEG system is made of magnetometers, which have a different sensitivity profile compared to both the axial gradiometers of CTF and the planar gradiometers of Elekta. Magnetometers are more sensitive to distant sources, which makes them more vulnerable to noise, compared to gradiometers. This property could though result in higher SNR, when appropriate noise-suppression techniques are used. The higher sensitivity of magnetometers, however, should also be accounted for, at least partly, by the leadfield. As such, testing for differences in the absolute amplitude of the current sources, in nAm rather than in percentage signal change, would clarify whether the observed results are driven by lower levels of noise or higher amplitude signals.

One way to test the hypothesis of a different sensitivity profile between magnetometers and other types of sensors would be to analyse the Elekta data twice, using once magnetometers and once gradiometers only, rather than combining the two sensor types as we did in this study. Alternatively, another approach would be to measure visual gamma oscillations in a smaller sample, recording from the same participants with each of the three MEG systems and testing for differences in gamma amplitude in a within-

subject design. In addition to this interpretation, it is also possible that the higher gamma amplitude values of the 4-D system are a spurious result of the low sample size used in this study, i.e. only twenty participants from each site. After a visual comparison of the participants' amplitude distribution at each site, illustrated in Figure 5.7, it appears that only a small proportion of participants from Glasgow show markedly higher amplitude values, compared to the other sites. It is thus possible that this small number of participants biased the Glasgow sample towards the higher end of the population, which will become visible also for the other sites, once their samples are extended. If this was the case, then we would expect to find no difference in gamma amplitude among sites, once all eighty participants from each site are included in the analysis.

As reported in Chapter 2 for the visual gamma data of the 100 Brains study, the gamma peak amplitude was positively correlated with the estimates of peak frequency reliability, calculated as the percentage of iterations falling within a window of width 1.2 Hz around the distribution mode (par. 5.3.11). Despite this relationship between gamma amplitude and data quality, however, the reliability estimates were only marginally higher for the Glasgow data and did not differ significantly among the four sites (Figure 5.8A and Figure 5.8C). Similarly, the gamma peak frequency was also highly comparable among sites (Figure 5.6B and Figure 5.6D), suggesting that the peak frequency of visual gamma oscillations might be a better candidate measures for repeated measures or multi-site studies, compared to the gamma peak amplitude (see also Muthukumaraswamy et al., 2010; Tan et al., 2016). Additionally, this result suggests that the information provided by our QC approach is complimentary to that indexed merely by the response amplitude, particularly for the purpose of assessing or comparing gamma peak frequency measures. Finally, we noted previously that the estimates of gamma amplitude obtained with the periodogram method differed, in

absolute but not relative terms, from those extracted by averaging over the time dimension of the time-frequency spectrograms (see Chapter 2). As such, the amplitude results outlined above should be interpreted with caution until they are replicated with more conventional analysis approaches.

Another difference that we observed in the comparison among the four MEG sites is the source topography of the CTF data collected at Nottingham (Figure 5.2). One hypothesis is that the widespread activation pattern of the Nottingham data might be caused by imperfect co-registration of the head shape digitised with the Polhemus to the head surface extracted from the participant's MRI. The main consequence of such a computational error is that the leadfield would be calculated incorrectly. This, in turn, would be expected to result in lower amplitude values, which, however, have not been observed for the Nottingham data. On this note, it seems interesting also that the 'manual' approach to MEG/MRI co-registration implemented at Cardiff performed, on average, as accurately as the (semi-)automatic algorithms used for the other sites. Although head movement was not formally assessed in this work, follow-up studies will have the opportunity to assess the impact of head motion and position on the accuracy of the source estimates, for example by calculating the Euclidian distance between the peak voxel and V1/V2.

Finally, another remarkable result was the absence of a negative impact on the quality of the Glasgow data that could have been caused by the lack of visual inspection procedures aimed at identifying and excluding bad trials, which were instead adopted by every other MEG site. It is possible that visual gamma oscillations recorded with MEG are relatively insensitive to the influence of ocular activity (e.g., eye blinks) and robust against the noise introduced by low levels of muscular activity (for a review, see Muthukumaraswamy, 2013). In either case, our QC approach offers a tool to test the

effect of these factors, as well as of different analysis approaches, on the reliability of the gamma peak frequency. Importantly, once the whole multi-site sample will become available, these analyses can be repeated with higher statistical power. For this purpose, a fundamental aspect that will need to be considered is the establishment of fully standardised pipelines that minimise the differences between sites at each and every processing steps. For example, MEG/MRI co-registration could be performed with the same surface-matching algorithm at each site, ICA routines could be used to pre-process and clean the data consistently across MEG systems, and so on. Once again, the impact of alternative choices at each analysis step can in principle be evaluated using our QC method, or by developing similar approaches aimed at evaluating dependent variables other than the gamma peak frequency.

5.5.2 Between-beamformer comparison

With respect to the source analysis, one secondary aim of this work was to compare the results obtained with two different beamformer algorithms. Our comparison between LCMV and DICS revealed no remarkable differences between the two beamformers. This is not surprising considering that the two algorithms reflect the same methodological approach in two different domains, i.e. in time and in frequency, respectively. The LCMV and DICS analyses produced highly comparable source topographies (Figure 5.2) and the virtual sensor reconstructions resulted in very similar time-frequency maps (Figure 5.3A). The peak amplitude and peak frequency parameters were highly correlated between the two beamformers (Figure 5.5) and so were the estimates of peak frequency reliability (Figure 5.9).

Although sporadic individual variations could be observed, these were most likely caused by minor methodological differences between the two approaches. For example, differences in the peak parameters estimates could have arisen from the selection of

different peak voxels for virtual sensor reconstruction or from different processing parameters prior to computation of the beamformer weights, namely bandpass-filtering the time-series (for the covariance matrix with LCMV) or performing multi-taper frequency analysis (for the CSD matrix with DICS). Most importantly, however, this analysis demonstrated the applicability of our QC approach to the comparison of different data analysis approaches. By expanding the sample to the full multi-site dataset, the comparison could be extended not only to alternative beamformer algorithms, such as SAM (Robinson and Vrba, 1999), but also to different source localization approaches, such as MNE.

5.5.3 Considerations on the visual paradigm design

We had multiple reasons for choosing the visual gamma paradigm over other tasks of the MEG Partnership to perform this multi-site comparison. First, the paradigm allows the characterisation of basic and robust sensory-motor responses and was thus included as part of the MEG protocol at every partner site. Second, the visual gamma response was considered an ideal test bed because it offers relatively clear benchmarks such as its spatial localization (Fries et al., 2008a; Hoogenboom et al., 2006; Muthukumaraswamy et al., 2010) and parameter distribution (see Chapter 2).

The criteria adopted for the design of the visual gamma paradigm in the UK MEG Partnership study were in part based on previous experimental work (Muthukumaraswamy and Singh, 2013) and in part aimed at meeting the research interests of the MEG groups of all partner sites. In particular, our choice was informed by the results of Muthukumaraswamy and Singh (2013), who compared the effect of different stimulus configurations (i.e. square-wave vs. annular grating, four quadrants vs. lower left quadrant, moving vs. stationary) on the properties of the visual gamma response. In their study, on the one hand, four-quadrant moving stimuli resulted in

sustained responses with both the largest amplitudes and the most reliable gamma peak frequency estimates, compared to static single-quadrant gratings. On the other hand, however, the spatial activation patterns of the latter type of stimuli was more focal and appeared thus better suited to studies aimed at the optimisation of source-reconstruction algorithms.

5.5.4 Conclusions

To conclude, this work aimed to provide a proof of concept for combining MEG data collected at different research centres and with different MEG systems. In particular, for the first time, we demonstrated the feasibility of bringing different types of data to a standard format using common analysis pipelines, for subsequent pooling of the results. Although the results presented here are still preliminary, we note that when data are collected with different MEG systems, differences in sensor type should be considered and evaluated carefully before estimates of gamma amplitude can be combined. The gamma peak frequency, instead, appeared unaffected by the type of MEG system. Additionally, the three MEG systems evaluated here seemed to provide data of comparable quality, as far as the gamma peak frequency is concerned. Interestingly, the estimates of data quality obtained with our QC approach were complimentary to those provided, for example, simply by measuring the response amplitude. In principle, we believe that the development and adoption of QC approaches similar to the one used here could pave the way forward for the establishment of large-scale MEG databases and will facilitate the development of new multi-site collaborations.

Chapter 6.

General discussion

6.1 Rationale behind the development of a method for quality control

The aim of this thesis was to demonstrate the use of the peak frequency of visual gamma oscillations in a range of different scenarios. In Chapter 2, we first presented a novel method for estimating the gamma peak frequency and its robustness. The gamma peak frequency is, in fact, often considered a robust spectral 'signature' of the visual response recorded invasively in non-human primates (Lima et al., 2010; see also Roberts et al., 2013). This holds for oscillatory signals measured from the same cortical location (i.e. peak frequency can differ between nearby locations) in response to specific types of visual stimuli, such as gratings (Ray and Maunsell, 2015), so long as the physical properties of the stimulus are not changed (e.g., contrast, motion, size, eccentricity, etc.) and the internal state of the animal is not altered (e.g., level of sedation, attention, etc.). The gamma peak frequency is a stable measure also in humans, although the signal-to-noise ratio (SNR) of MEG is usually insufficient to characterise this parameter at the level of single trials. The repeatability of peak frequency has been demonstrated over repeated recording sessions, for up to 5 weeks, with intra-class correlation coefficients (ICCs) of ~0.9–1 (Muthukumaraswamy et al., 2010). Furthermore, estimating the peak frequency at the source level, as we did in our experiments, provides higher ICC values, compared to using sensor-level parameter estimates (Tan et al., 2016).

Together, therefore, both animal and human studies suggest that the visual gamma response can be expected to peak at the same frequency over repeated presentations of the same stimulus (although, see Brunet et al., 2014a for a contrasting result). In our view, trials that deviate significantly from the individual's gamma peak frequency, in the absence of controlled exogenous or endogenous perturbations, are likely to reflect contamination by artefacts (e.g., measurement noise, electro-myogenic activity, eye movements and changes in ocular fixation, etc.). The rationale behind our quality-

control (QC) approach was thus the following: if the oscillation frequency is highly variable within a given set of trials, the gamma peak frequency derived from the averaged trials will be noisy and potentially unreliable. Measures of variability such as the variance of the trials, though, are difficult to calculate with limited SNR. In our approach, therefore, a measure of dispersion across trials was obtained via bootstrapping.

In this procedure, the gamma peak frequency was measured over 10,000 iterations, in each of which trials were resampled with replacement. The distribution of peak frequency over bootstrap iterations thus indexed the distribution of peak frequency across the original set of trials. Bootstrapping simply offered a strategy to obtain estimates of both central tendency and variability. While the mode of the distribution indicated the oscillation frequency most prevalent in the data, the shape, or width, of the distribution indexed the variability of peak frequency, across trials. In practical terms, a reliability index was quantified by calculating the percentage of bootstrap iterations that either matched the mode of the bootstrap distribution or deviated from it, with a margin of measurement error determined by the resolution of the spectral analysis method. If an excessive proportion of iterations resulted in an estimate of peak frequency inconsistent with the bootstrap mode, i.e. if the width of the bootstrap distribution was too large, then the measured peak frequency was considered unreliable in that dataset. Alternatively, if the dataset was estimated as reliable, the gamma peak frequency was measured by averaging over the 10,000 bootstrap iterations.

The validity of the peak frequency measure calculated by averaging over bootstrap iterations was demonstrated using synthetically generated data (Magazzini et al., 2016). In this simulation study, the consistency (standard deviation) of peak frequency across trials was varied systematically, while controlling for the mean and mode of the trial

distribution. In addition, the gamma peak frequency and other parameters obtained with the QC approach were estimated in a large-sample dataset, the '100 Brains'. This allowed us to illustrate how these parameters are distributed across individuals, in real MEG data, and compare the bootstrap peak frequency with a standard measure, the 'envelope' peak frequency.

Throughout this thesis, the bootstrap mode was considered as a reference measure in the calculation of the peak frequency reliability estimates, whereas the bootstrap mean was used as an optimal measure of the gamma peak frequency. It is worth noting, though, that while mean and mode of the distribution can be expected to overlap for highly consistent oscillation frequencies across trials, the two measures are instead likely to diverge for asymmetric bootstrap distributions. This occurs, for example, when a secondary spectral peak is measured in a number of trials sufficient to produce a secondary peak also in the bootstrap distribution. It may thus appear theoretically more appropriate to use the mode of the distribution, rather than its mean, as an optimal measure of peak frequency. However, unbiased measures of the mean are guaranteed by the adoption of an additional constraint, i.e. discarding datasets in which an insufficient number of bootstrap iterations gathers in close proximity to the distribution mode. The bootstrap mean, in addition, offers the advantage of 'weighting' the frequencies by their prevalence across bootstrap samples and, therefore, across trials. The visual gamma response in fact not always reveals only one 'real' peak frequency, especially if the response amplitude is low. In real MEG recordings, the increase in spectral power often spans a relatively broad range of frequencies across the gamma spectrum. In similar circumstances, therefore, the relative contribution of different gamma frequencies would be pictured more accurately by the mean of the bootstrap distribution, not by its mode.

An alternative measure of central tendency, conceptually similar to the bootstrap distribution mean, is the centre of mass. In the centre of mass, the frequencies are weighted (multiplied) by their power, summed and divided by the total power across the frequency range of interest. This measure is particularly useful when a clear spectral peak cannot be identified and has been used to assess the gamma peak frequency both in humans (Lozano-Soldevilla et al., 2014) and animals (Brunet et al., 2014a). Other approaches consist of fitting Gaussian functions to the power spectrum (van Albada and Robinson, 2013), a method that has been used not only for gamma (Campbell et al., 2014), but also alpha oscillations (Haegens et al., 2014). One major difference between high and low oscillation frequencies is that power in the gamma range is typically calculated as a percentage change relative to a reference condition. This can reveal peaks that would otherwise be difficult to characterise, given the relatively low SNR of the MEG raw spectra and their power-law scaling (Miller et al., 2009). Alternatively, in more advanced approaches, the frequency and amplitude axes of the power spectrum can be log-transformed to remove the typical *1/f* component. As a result, the power-law curve is reshaped into a straight line ($y = -x + a$). The slope of this line can then be removed by fitting a linear regression model, allowing for the characterisation of the spectral peaks of interest (Lega et al., 2012; Manning et al., 2009).

The approaches illustrated above represent only a limited portion of the many different methods available for spectral estimation. Any time-series can be decomposed into its frequency components using the Fourier transform. In other approaches, though, the power spectrum is reconstructed by averaging over the time dimension of a time-frequency spectrogram, which can be particularly useful when the time-range of interest is not known *a priori*. In the 'envelope' method described in Chapter 2, for example, the analytic signal is computed to yield an amplitude envelope (Muthukumaraswamy et al., 2010). Once again, several methods are available also for representing a time-series in

the time-frequency domain. The data can be convolved in the time domain using Morlet's wavelets (Tallon-Baudry et al., 1997), or smoothed in the frequency domain with multi-tapering (Mitra and Pesaran, 1999). Irrespective of the approach chosen, however, our proposed QC routine can in principle be applied to any of these methods, thereby offering flexibility for its integration in the analysis pipeline of other research groups, or in open-source toolboxes such as Fieldtrip (Oostenveld et al., 2011).

6.2 Peak frequency modulations and quality control in pharmaco-MEG data

A long-standing goal of neuroscience has been that of understanding the mechanisms of normal brain function in order to restore them in pathological conditions. While human neuroimaging bears the potential for contributing to the former achievement, pharmacological intervention is likely one of the most potent approaches for clinical treatment. For these reasons, neuroimaging techniques such as functional magnetic resonance imaging (fMRI) have recently gained attention by the pharmaceutical industry as a possible tool for efficient drug discovery and development (Wise and Preston, 2010). In particular, the identification of early biomarkers of drug action can accelerate the process of drug development, while hugely reducing the associated costs. In order to bear clinical relevance, though, the indices of brain activity obtained with neuroimaging need to be robustly linked to specific mechanisms of brain function, so that disease- and drug-related changes can be reliably identified. For this purpose, the blood oxygenation level-dependent (BOLD) and cerebral blood flow (CBF) changes measured by fMRI offer an exquisitely spatially resolved approach to look at brain activity. However, the interpretation of drug-induced changes in fMRI measures can be complicated by the interplay between cerebral vasculature and neuronal activity (Muthukumaraswamy, 2014; see also Iannetti and Wise, 2007).

In the context of pharmacological studies, where a clear understanding of the nature of the measured signal is crucial (see Singh, 2012), some of the limitations of fMRI can be overcome by the use of MEG. Magnetoencephalography is sensitive to the summation of synchronous post-synaptic potentials, offering not only direct but also highly translatable measures of neuronal activity (Hall et al., 2005; Fries et al., 2008a). The evidence from pre-clinical models can thus be evaluated at early stages of clinical trials in humans, making pharmacological MEG studies a useful tool for drug development.

In Chapter 3, we proceeded to test the potential applications of the QC approach by re-analysing two previous pharmaco-MEG studies of visual gamma from our lab, one with alcohol (Campbell et al., 2014) and one with tiagabine (Muthukumaraswamy et al., 2013a). Our re-analysis of the alcohol data from Campbell et al. (2014), in particular, provided two insightful results. First, the unreliable estimates of peak frequency identified by our QC approach converged with the quality assessment reported by the authors in the original publication (Campbell et al., 2014). Second, after exclusion of four participants, the alcohol-induced reduction in gamma frequency was replicated using our bootstrap measure of peak frequency. Together, these results corroborated those of the simulation study (Chapter 2), supporting the validity of our QC approach in two ways: first, as a tool for identification of poor-quality data; second, as an optimal method for peak frequency estimation. In light of these considerations, and also of the literature described below, we were able to accept with confidence the novel results of our re-analysis of the tiagabine data from Muthukumaraswamy et al. (2013a).

In the original study, tiagabine was found to have a null effect on visual gamma oscillations, a surprising result that contrasted with the authors' initial predictions (Muthukumaraswamy et al., 2013a). It is worth noting that their result was obtained with the adoption of the most impartial approach possible, i.e. a standard analysis pipeline applied to every participant. In our study, instead, by combining objective exclusion of poor-quality data and improved estimation of peak frequency, tiagabine was found to induce a marked reduction of the gamma peak frequency (Magazzini et al., 2016). Such a modulation of the gamma oscillatory dynamics is in line with models of the role of gamma-aminobutyric acid (GABA)-ergic transmission in generating gamma oscillations. Tiagabine is a drug with a well-known mechanism of action, which, as demonstrated by *in vivo* micro-dialysis (Fink-Jensen et al., 1992), results in increased extra-cellular (i.e. synaptic) GABA concentrations. By blocking the re-uptake of GABA

into the pre-synaptic terminal, the drug prolongs the duration of the inhibitory post-synaptic potentials (IPSPs). As predicted by both *in vitro* and *in vivo* studies (Traub et al., 1996; Whittington et al., 1995), the decrease in gamma oscillation frequency would thus result from the increase in the decay-time constant of GABAergic transmission.

Currently, the possibility of measuring the relationship between gamma oscillations and GABAergic transmission, in humans, is partly still an open debate. In a recent study (Myers et al., 2014), enhancing the synaptic levels of GABA with tiagabine did not produce an increase in the neurotransmitter concentrations measured with magnetic resonance spectroscopy (MRS). It is in fact thought that MRS can only measure total GABA concentrations, without discerning between the synaptic and intra-cellular compartments (Muthukumaraswamy, 2014). This limitation of MRS may have contributed also to the notorious discrepancy between two studies in which MRS and MEG were used to test the relationship between GABA concentrations and gamma oscillation frequency (Cousijn et al., 2014; Muthukumaraswamy et al., 2009). Recently, however, the positive correlation between GABA and gamma frequency first reported by Muthukumaraswamy et al. (2009), which Cousijn et al. (2014) failed to replicate, has received support using alternative approaches. In a combined MEG and positron-emission tomography (PET) study, for example, the density of $GABA_A$ receptors in primary visual cortex correlated positively with the frequency and negatively with the amplitude of visual gamma oscillations (Kujala et al., 2015). Furthermore, various pharmacological agents have now been demonstrated to modulate the amplitude and/or frequency of visual gamma (Campbell et al., 2014; Lozano-Soldevilla et al., 2014; Muthukumaraswamy et al., 2016; Saxena et al., 2013; Shaw et al., 2015), including the recently published results of tiagabine (Magazzini et al., 2016). Multiple lines of research thus converge to support the role of GABAergic inhibition, and its balance with the glutamatergic system, in shaping the human gamma oscillatory dynamics.

At present, the pharmaco-MEG approach (Muthukumaraswamy, 2014) appears by far the most promising translational tool for studying the generative mechanisms of gamma oscillations in humans. In Chapter 3, however, we have demonstrated the importance of adopting appropriate QC routines to guarantee the robustness of the results. It is thus worth considering what factors may have contributed to determining the quality of the visual gamma data in the two re-analysed datasets. In the tiagabine dataset, the gamma peak frequency was estimated as poorly reliable in a remarkably large proportion of the recorded sessions, i.e. ~25%, compared to ~8% in the alcohol dataset. A number of factors that could have driven this disparity in overall data quality, including methodological differences between the two studies, are discussed below.

In each of the two measurement days (placebo and drug), participants of the tiagabine study were tested once before drug/placebo ingestion and three times after, for a total of eight recording sessions per participants. In the alcohol study, instead, only four sessions were recorded per participant, i.e. once before and once after alcohol/placebo consumption. Any time-varying drug effects were thus more likely to be manifested in the tiagabine data, which consisted of three times as many post-drug sessions. In fact, despite the relatively short duration of each MEG session (~10 min), drug-induced spectral changes on such short time scales have been demonstrated with the $GABA_A$ modulator diazepam (Hall et al., 2010). The repetition of the visual gamma protocol multiple times after drug administration would thus increase the likelihood of 'capturing' such rapid changes within a given recording session. One hypothetical possibility is that the effectiveness of tiagabine in blocking the GABA reuptake increased or decreased during the course of the visual gamma paradigm. As a consequence, the gamma oscillation frequency would have shifted, from trial to trial, towards lower or higher frequencies, respectively. In such a case, therefore, the high

variability of peak frequency across trials would have resulted in a poor estimates of peak frequency reliability.

The scenario hypothesised above, however, cannot fully account for the differences in data quality observed between the two studies. If only the first two sessions are considered, one before and one at 1 hour after tiagabine/placebo administration, unreliable peak frequency estimates are still observed in 10 out of 60 sessions (~17%), i.e. in twice as many sessions as in the alcohol study. One major difference between the two dataset is intrinsically related to the type of drug used, not only for their different pharmacodynamics, but also for the ability of participants to tolerate their effects. Typically, a healthy individual would be expected to comply with the demands of an experimental task more easily after consumption of alcohol, whose effects would probably be predictable and thus expected, than after taking a potent sedative such as tiagabine (see Hamandi et al., 2014). The level of participants' compliance can in fact determine the quality of an MEG session in many ways. For example, the levels of high-frequency noise in the recording can depend on the amount of movement and muscular tension (Muthukumaraswamy, 2013). Alternatively, inadequate or unstable ocular fixation could result, indirectly, in a change of stimulus eccentricity, a physical property that is known to affect the peak frequency of visual gamma oscillations (van Pelt and Fries, 2013).

In relation to the parameters of visual stimulation and their influence on the visual gamma response, the tiagabine and alcohol studies differed also by two properties of the visual stimulus. First, while the grating used in the alcohol study was presented centrally, in the tiagabine study it covered only the lower left portion of the visual field. Second, the grating of the tiagabine study stimulated a larger portion of the peripheral visual field (up to 8° horizontally), compared to the alcohol study (up to 4°

horizontally). In a recent study in monkey V1, the visual gamma response was recorded simultaneously at cortical locations representing different eccentricities of the retinotopic space (Lima et al., 2010). Between central (~3°) and peripheral (~10°) locations, the oscillations showed marked differences, decreasing in frequency with increasing eccentricity of the receptive field. This indicates that visual stimuli spanning large portions of the visual field can induce oscillatory responses at different gamma frequencies. The presence of multiple oscillation frequencies can be particularly problematic in the case of MEG, where the data are likely to reflect a spatially summated response. As discussed above (par. 6.1), the presence of multiple peaks in the power spectrum can complicate the estimation of a single, reliable gamma peak. The larger portion of peripheral visual field stimulated in the tiagabine study may thus have introduced a greater prevalence of secondary spectral peaks, resulting in a higher ratio of datasets with unreliable estimates of peak frequency.

Overall, numerous parameters related to the stimulus, the study design or the participants can theoretically produce drastic changes in the quality of the data recorded. In the future, studies providing an empirical demonstration of how these factors can impact the robustness of the gamma oscillatory parameters will contribute to establishing 'gold standard' rules for both the collection and the analysis of visual gamma data. In combination with the adoption of appropriate QC routines, such as our proposed approach, this will help to demonstrate the potential of MEG in identifying reliable biomarkers of drug action. The robustness of such biomarkers will attract the interest of pharmaceutical companies in investing in MEG research, thereby increasing the likelihood of successful drug discovery. In turn, the development of new effective pharmacological compounds will contribute to advancing our understanding of the neuronal mechanisms that support brain functions and their impairment in diseases such as epilepsy, autism and schizophrenia (Lewis et al., 2005; Uhlhaas and Singer, 2006).

6.3 Peak frequency and amplitude modulations by attention

In the first two experimental chapters of this thesis (Chapters 2 and 3), we concluded that the use of optimal measures and appropriate QC approaches can occasionally be necessary to reveal the effects of an experimental manipulation on the oscillatory parameters of interest. In addition, a comparison of the QC results in different studies sparked a number of speculative observations on the determinants of data quality in visual gamma datasets recorded with MEG (par. 6.2). In Chapter 4, one of the methodological aspects that was incorporated in our experimental design concerned the identification of the physical properties of the stimulus that were more likely to provide robust estimates of peak frequency. Although far from being exhaustive, the instructions available from the literature on the topic were sufficiently detailed for making an informed decision on such parameters.

In our study on gamma and attention (Chapter 4), the main research question that we wanted to address was related to a recent theoretical proposal on the possible functional role of shifts in oscillation frequency under different task demands. Specifically, by increasing their oscillation frequency, a group of synchronised neurons in primary visual cortex is thought to gain an advantage over competing neuronal groups (Fries, 2015). In brief, this would allow the faster oscillating neurons to enhance their impact on a group of neurons that oscillate coherently in a downstream area. In contrast, input to the same downstream neurons converging from the slower oscillating neurons would arrive at less excitable phases of the oscillation cycle and would thus be less effective. Such a modulation of the gamma oscillation frequency has been hypothesised to serve as a mechanism for attentional selection of visual representations, and is compatible with recent evidence from a study in monkeys (Bosman et al., 2012).

In our study, however, we found no evidence for an increase in the peak frequency of visual gamma oscillations in early visual cortex. However, as we found some partial evidence for a shift of the centre of mass towards higher frequencies, our results should probably be considered inconclusive. Despite this, by implementing some of the methodological considerations outlined above, we obtained visual gamma data of the highest quality, compared to all other experimental chapters of this thesis. As illustrated in Chapter 4, unreliable estimates of the gamma peak frequency were observed in only 2 out of 36 datasets. In addition, the modulation of gamma amplitude in both early (V1/V2) and late (V4) visual areas was consistent with recent theories that hypothesise a possible role for gamma-band synchronisation in propagating feed-forward signals across the visual cortical hierarchy (Michalareas et al., 2016; van Kerkoerle et al., 2014).

Although beyond the scope of this thesis, future analyses of this dataset of visual gamma with spatial attention will try to elucidate the temporal and spectral dynamics of inter-areal communication between V1/V2 and V4. In particular, this could be achieved by correlating the trial-by-trial amplitude fluctuations between the two regions, or by computing the cross-correlogram of the amplitude envelopes. Additionally, our data suggested that alpha oscillations were also significantly modulated by attention, in V1. In the abovementioned framework of feed-forward and feed-back effects, alpha oscillations could reflect the top-down influence of higher-order region controlling the oscillatory dynamics of lower areas, potentially via cross-frequency coupling mechanisms (Jensen et al., 2014).

6.4 Concluding remarks and future work

In the last experimental chapter of this thesis (Chapter 5), the QC approach was applied to a large multi-site dataset from the UK MEG Partnership. This study bears the greatest potential for extension of the preliminary work presented here, as the sample will eventually be expanded to 80 participants at each site, for a total of 640 individual visual gamma datasets. The larger sample will also allow to clarify the reasons behind the apparent difference in gamma amplitude between the data collected with the magnetometer system at Glasgow (4-D Neuroimaging) and the other MEG systems (CTF and Elekta Neuromag). In addition, it will allow to explore the inter-individual differences in the gamma oscillatory parameters and their relationship with other measures of cortical activity, brain structure, behaviour and even genetics.

The establishment of a shared MEG data repository will encourage new collaborations and facilitate large-scale, possibly multi-site, clinical studies, or pharmacological studies on smaller scales. The database will in fact provide normative distributions of basic sensory neurophysiological parameters in a healthy population, against which specific clinical groups or drug-induced modulations can be compared. It will also offer new opportunities for testing novel hypothesis with the necessary statistical power and for comparing newly developed analytical tools with existing, well-established methods. In principle, it could also serve as a testbed for the validation of recently developed technologies, such as optically-pumped magnetometers (OPMs). This type of sensors may soon kick-start a new branch of research within the field of non-invasive electrophysiology, offering higher portability and versatility at relatively low maintenance costs (Knappe et al., 2014). In a recent study, simulated whole-head OPM systems resulted in greater sensitivity, spatial resolution and reconstruction accuracy, compared to traditional SQUID-based systems (Boto et al., 2016). If such systems were to be made commercially available to the research community, they would certainly

benefit from a comparative analysis with real data from three of the most popular MEG systems currently in use.

Finally, a number of possible methodological developments can be considered also for our QC approach. For example, the method can be applied to sensor-level data, for objective and data-driven selection of the sensors for analysis. The QC metrics in the spectral domain could be compared and combined with other QC measures, e.g., in the spatial domain, to achieve a multi-dimensional representation of data quality. In the current implementation, the peak frequency reliability estimates obtained via bootstrapping indexed the consistency of peak frequency across trials. If the peak frequency within a given set of trials was estimated as too variable, the dataset was marked as of poor quality and then discarded. One potential development for future QC approaches would consist of algorithms that attempt to 'rescue' poor-quality datasets, moving away from the rejection of entire sets of trials and towards the exclusion of individual trials only. This could be achieved by tracking the bootstrap iterations that deviate most from the distribution mode and working backwards to identify which trials were included, more than others, in the resampling of those iterations.

In summary, the work presented in this thesis has contributed to our understanding of the biological basis of the human gamma peak frequency (Chapter 3), by proposing a novel QC approach for optimal estimation of this oscillatory parameter (Chapter 2). The results of the study of visual gamma with spatial attention (Chapter 4) provided new evidence of the possible functional role of these oscillations in the human visual system. The multi-site comparative analysis (Chapter 5) served as a proof-of-concept for the development of new collaborations and the establishment of large-scale MEG data repositories. We believe that this represents the future of MEG research and will allow to advance our understanding of human brain function in both health and disease.

References

Adjamian, P., Barnes, G.R., Hillebrand, A., Holliday, I.E., Singh, K.D., Furlong, P.L., Harrington, E., Barclay, C.W., Route, P.J.G., 2004a. Co-registration of magnetoencephalography with magnetic resonance imaging using bite-bar-based fiducials and surface-matching. Clin Neurophysiol 115, 691–698. doi:10.1016/j.clinph.2003.10.023

Adjamian, P., Holliday, I.E., Barnes, G.R., Hillebrand, A., Hadjipapas, A., Singh, K.D., 2004b. Induced visual illusions and gamma oscillations in human primary visual cortex. Eur. J. Neurosci. 20, 587–592. doi:10.1111/j.1460-9568.2004.03495.x

Adrian, E.D., 1942. Olfactory reactions in the brain of the hedgehog. J. Physiol. (Lond.) 100, 459–473.

Attal, Y., Bhattacharjee, M., Yelnik, J., Cottereau, B., Lefèvre, J., Okada, Y., Bardinet, E., Chupin, M., Baillet, S., 2007. Modeling and detecting deep brain activity with MEG & EEG. Conf Proc IEEE Eng Med Biol Soc 2007, 4937–4940. doi:10.1109/IEMBS.2007.4353448

Baillet, S., Mosher, J.C., Leahy, R.M., 2001. Electromagnetic brain mapping. IEEE Signal Processing Magazine 18, 14–30. doi:10.1109/79.962275

Barnes, G.R., Hillebrand, A., 2003. Statistical flattening of MEG beamformer images. Hum Brain Mapp 18, 1–12. doi:10.1002/hbm.10072

Bartels, A., Zeki, S., 2000. The architecture of the colour centre in the human visual brain: new results and a review. Eur. J. Neurosci. 12, 172–193.

Barth, D.S., 1991. Empirical comparison of the MEG and EEG: animal models of the direct cortical response and epileptiform activity in neocortex. Brain Topogr 4, 85–93.

Bartos, M., Vida, I., Jonas, P., 2007. Synaptic mechanisms of synchronized gamma oscillations in inhibitory interneuron networks. Nat. Rev. Neurosci. 8, 45–56. doi:10.1038/nrn2044

Bastos, A.M., Vezoli, J., Bosman, C.A., Schoffelen, J.-M., Oostenveld, R., Dowdall, J.R., De Weerd, P., Kennedy, H., Fries, P., 2015a. Visual areas exert feedforward and feedback influences through distinct frequency channels. Neuron 85, 390–401. doi:10.1016/j.neuron.2014.12.018

Bastos, A.M., Vezoli, J., Fries, P., 2015b. Communication through coherence with inter-areal delays. Curr. Opin. Neurobiol. 31, 173–180. doi:10.1016/j.conb.2014.11.001

Bauer, M., Kluge, C., Bach, D., Bradbury, D., Heinze, H.J., Dolan, R.J., Driver, J., 2012. Cholinergic enhancement of visual attention and neural oscillations in the human brain. Curr. Biol. 22, 397–402. doi:10.1016/j.cub.2012.01.022

Bauer, M., Stenner, M.-P., Friston, K.J., Dolan, R.J., 2014. Attentional modulation of alpha/beta and gamma oscillations reflect functionally distinct processes. J. Neurosci. 34, 16117–16125. doi:10.1523/JNEUROSCI.3474-13.2014

Bear, M.F., Connors, B.W., Paradiso, M.A., 2007. Neuroscience: exploring the brain, 3rd ed. ed. Lippincott Williams & Wilkins, Philadelphia, PA.

Berens, P., Keliris, G.A., Ecker, A.S., Logothetis, N.K., Tolias, A.S., 2008. Feature selectivity of the gamma-band of the local field potential in primate primary visual cortex. Front Neurosci 2, 199–207. doi:10.3389/neuro.01.037.2008

Berger, H., 1929. Über das Elektrenkephalogramm des Menschen. Archiv für Psychiatrie und Nervenkrankheiten 87, 527–570. doi:10.1007/BF01797193

Besl, P.J., McKay, H.D., 1992. A method for registration of 3-D shapes. IEEE Transactions on Pattern Analysis and Machine Intelligence 14, 239–256. doi:10.1109/34.121791

Bichot, N.P., Rossi, A.F., Desimone, R., 2005. Parallel and serial neural mechanisms for visual search in macaque area V4. Science 308, 529–534. doi:10.1126/science.1109676

Bloomfield, P., 2000. Fourier analysis of time series: an introduction, 2nd ed, Wiley series in probability and statistics. Applied probability and statistics section. Wiley, New York.

Borden, L.A., Murali Dhar, T.G., Smith, K.E., Weinshank, R.L., Branchek, T.A., Gluchowski, C., 1994. Tiagabine, SK&F 89976-A, CI-966, and NNC-711 are selective for the cloned GABA transporter GAT-1. Eur. J. Pharmacol. 269, 219–224.

Bosman, C.A., Lansink, C.S., Pennartz, C.M.A., 2014. Functions of gamma-band synchronization in cognition: from single circuits to functional diversity across cortical and subcortical systems. European Journal of Neuroscience 39, 1982–1999. doi:10.1111/ejn.12606

Bosman, C.A., Schoffelen, J.-M., Brunet, N., Oostenveld, R., Bastos, A.M., Womelsdorf, T., Rubehn, B., Stieglitz, T., De Weerd, P., Fries, P., 2012. Attentional stimulus selection through selective synchronization between monkey visual areas. Neuron 75, 875–888. doi:10.1016/j.neuron.2012.06.037

Boto, E., Bowtell, R., Krüger, P., Fromhold, T.M., Morris, P.G., Meyer, S.S., Barnes, G.R., Brookes, M.J., 2016. On the Potential of a New Generation of Magnetometers for MEG: A Beamformer Simulation Study. PLoS ONE 11, e0157655. doi:10.1371/journal.pone.0157655

Bouyer, J.J., Montaron, M.F., Rougeul, A., 1981. Fast fronto-parietal rhythms during combined focused attentive behaviour and immobility in cat: cortical and thalamic localizations. Electroencephalogr Clin Neurophysiol 51, 244–252.

Bouyer, J.J., Montaron, M.F., Vahnée, J.M., Albert, M.P., Rougeul, A., 1987. Anatomical localization of cortical beta rhythms in cat. Neuroscience 22, 863–869.

Bragin, A., Jandó, G., Nádasdy, Z., Hetke, J., Wise, K., Buzsáki, G., 1995. Gamma (40-100 Hz) oscillation in the hippocampus of the behaving rat. J. Neurosci. 15, 47–60.

Brahme, A., 2014. Comprehensive biomedical physics.

Brealy, J.A., 2015. The Relationship Between Variation in Genes, GABA, Structure and Gamma Oscillations in the Visual and Auditory System of Healthy Individuals and Psychiatric Disorder (Doctoral dissertation). Cardiff University.

Brookes, M.J., Vrba, J., Robinson, S.E., Stevenson, C.M., Peters, A.M., Barnes, G.R., Hillebrand, A., Morris, P.G., 2008. Optimising experimental design for MEG beamformer imaging. Neuroimage 39, 1788–1802. doi:10.1016/j.neuroimage.2007.09.050

Brunel, N., Wang, X.-J., 2003. What determines the frequency of fast network oscillations with irregular neural discharges? I. Synaptic dynamics and excitation-inhibition balance. J. Neurophysiol. 90, 415–430. doi:10.1152/jn.01095.2002

Brunet, N.M., Bosman, C.A., Vinck, M., Roberts, M., Oostenveld, R., Desimone, R., De Weerd, P., Fries, P., 2014a. Stimulus repetition modulates gamma-band synchronization in primate visual cortex. Proceedings of the National Academy of Sciences 111, 3626–3631. doi:10.1073/pnas.1309714111

Brunet, N.M., Vinck, M., Bosman, C.A., Singer, W., Fries, P., 2014b. Gamma or no gamma, that is the question. Trends Cogn. Sci. (Regul. Ed.) 18, 507–509. doi:10.1016/j.tics.2014.08.006

Bruns, A., 2004. Fourier-, Hilbert- and wavelet-based signal analysis: are they really different approaches? J. Neurosci. Methods 137, 321–332. doi:10.1016/j.jneumeth.2004.03.002

Buffalo, E.A., Fries, P., Landman, R., Buschman, T.J., Desimone, R., 2011. Laminar differences in gamma and alpha coherence in the ventral stream. Proc. Natl. Acad. Sci. U.S.A. 108, 11262–11267. doi:10.1073/pnas.1011284108

Buzsáki, G., Anastassiou, C.A., Koch, C., 2012. The origin of extracellular fields and currents--EEG, ECoG, LFP and spikes. Nat. Rev. Neurosci. 13, 407–420. doi:10.1038/nrn3241

Buzsáki, G., Wang, X.-J., 2012. Mechanisms of gamma oscillations. Annu. Rev. Neurosci. 35, 203–225. doi:10.1146/annurev-neuro-062111-150444

Campbell, A.E., Sumner, P., Singh, K.D., Muthukumaraswamy, S.D., 2014. Acute Effects of Alcohol on Stimulus-Induced Gamma Oscillations in Human Primary Visual and Motor Cortices. Neuropsychopharmacology 39, 2104–2113. doi:10.1038/npp.2014.58

Cannon, J., McCarthy, M.M., Lee, S., Lee, J., Börgers, C., Whittington, M.A., Kopell, N., 2014. Neurosystems: brain rhythms and cognitive processing. Eur. J. Neurosci. 39, 705–719. doi:10.1111/ejn.12453

Cardin, J.A., Carlén, M., Meletis, K., Knoblich, U., Zhang, F., Deisseroth, K., Tsai, L.-H., Moore, C.I., 2009. Driving fast-spiking cells induces gamma rhythm and controls sensory responses. Nature 459, 663–667. doi:10.1038/nature08002

Carl, C., Açık, A., König, P., Engel, A.K., Hipp, J.F., 2012. The saccadic spike artifact in MEG. Neuroimage 59, 1657–1667. doi:10.1016/j.neuroimage.2011.09.020

Castelo-Branco, M., Neuenschwander, S., Singer, W., 1998. Synchronization of visual responses between the cortex, lateral geniculate nucleus, and retina in the anesthetized cat. J. Neurosci. 18, 6395–6410.

Chalk, M., Herrero, J.L., Gieselmann, M.A., Delicato, L.S., Gotthardt, S., Thiele, A., 2010. Attention reduces stimulus-driven gamma frequency oscillations and spike field coherence in V1. Neuron 66, 114–125. doi:10.1016/j.neuron.2010.03.013

Chapman, R.M., Ilmoniemi, R.J., Barbanera, S., Romani, G.L., 1984. Selective localization of alpha brain activity with neuromagnetic measurements. Electroencephalogr Clin Neurophysiol 58, 569–572.

Chatrian, G.E., Bickford, R.G., Uihlein, A., 1960. Depth electrographic study of a fast rhythm evoked from the human calcarine region by steady illumination. Electroencephalogr Clin Neurophysiol 12, 167–176.

Cohen, D., 1972. Magnetoencephalography: detection of the brain's electrical activity with a superconducting magnetometer. Science 175, 664–666.

Cohen, D., 1968. Magnetoencephalography: evidence of magnetic fields produced by alpha-rhythm currents. Science 161, 784–786.

Colclough, G.L., Brookes, M.J., Smith, S.M., Woolrich, M.W., 2015. A symmetric multivariate leakage correction for MEG connectomes. Neuroimage 117, 439–448. doi:10.1016/j.neuroimage.2015.03.071

Conti, F., Minelli, A., Melone, M., 2004. GABA transporters in the mammalian cerebral cortex: localization, development and pathological implications. Brain Res. Brain Res. Rev. 45, 196–212. doi:10.1016/j.brainresrev.2004.03.003

Cousijn, H., Haegens, S., Wallis, G., Near, J., Stokes, M.G., Harrison, P.J., Nobre, A.C., 2014. Resting GABA and glutamate concentrations do not predict visual gamma frequency or amplitude. Proc. Natl. Acad. Sci. 111, 9301–9306. doi:10.1073/pnas.1321072111

Dalal, S.S., Baillet, S., Adam, C., Ducorps, A., Schwartz, D., Jerbi, K., Bertrand, O., Garnero, L., Martinerie, J., Lachaux, J.-P., 2009. Simultaneous MEG and intracranial EEG recordings during attentive reading. Neuroimage 45, 1289–1304. doi:10.1016/j.neuroimage.2009.01.017

Dalby, N.O., 2000. GABA-level increasing and anticonvulsant effects of three different GABA uptake inhibitors. Neuropharmacology 39, 2399–2407.

Del Gratta, C., Pizzella, V., Tecchio, F., Romani, G.L., 2001. Magnetoencephalography - a noninvasive brain imaging method with 1 ms time resolution. Reports on Progress in Physics 64, 1759–1814. doi:10.1088/0034-4885/64/12/204

Delorme, A., Makeig, S., 2004. EEGLAB: an open source toolbox for analysis of single-trial EEG dynamics including independent component analysis. J. Neurosci. Methods 134, 9–21. doi:10.1016/j.jneumeth.2003.10.009

Desimone, R., Duncan, J., 1995. Neural Mechanisms of Selective Visual Attention. Annual Review of Neuroscience 18, 193–222. doi:10.1146/annurev.ne.18.030195.001205

Dickinson, A., Bruyns-Haylett, M., Jones, M., Milne, E., 2015. Increased peak gamma frequency in individuals with higher levels of autistic traits. Eur. J. Neurosci. 41, 1095–1101. doi:10.1111/ejn.12881

Dimigen, O., Sommer, W., Hohlfeld, A., Jacobs, A.M., Kliegl, R., 2011. Coregistration of eye movements and EEG in natural reading: analyses and review. J Exp Psychol Gen 140, 552–572. doi:10.1037/a0023885

Donner, T.H., Siegel, M., 2011. A framework for local cortical oscillation patterns. Trends Cogn. Sci. (Regul. Ed.) 15, 191–199. doi:10.1016/j.tics.2011.03.007

Douglas, R.J., Martin, K.A.C., 2004. Neuronal circuits of the neocortex. Annu. Rev. Neurosci. 27, 419–451. doi:10.1146/annurev.neuro.27.070203.144152

Edden, R.A.E., Muthukumaraswamy, S.D., Freeman, T.C.A., Singh, K.D., 2009. Orientation discrimination performance is predicted by GABA concentration and gamma oscillation frequency in human primary visual cortex. J. Neurosci. 29, 15721–15726. doi:10.1523/JNEUROSCI.4426-09.2009

Eickhoff, S., Nichols, T.E., Van Horn, J.D., Turner, J.A., 2016. Sharing the wealth: Neuroimaging data repositories. Neuroimage 124, 1065–1068. doi:10.1016/j.neuroimage.2015.10.079

Eickhoff, S.B., Stephan, K.E., Mohlberg, H., Grefkes, C., Fink, G.R., Amunts, K., Zilles, K., 2005. A new SPM toolbox for combining probabilistic cytoarchitectonic maps and functional imaging data. Neuroimage 25, 1325–1335. doi:10.1016/j.neuroimage.2004.12.034

Engel, A.K., Fries, P., Singer, W., 2001. Dynamic predictions: oscillations and synchrony in top-down processing. Nat. Rev. Neurosci. 2, 704–716. doi:10.1038/35094565

Faulkner, H.J., Traub, R.D., Whittington, M.A., 1998. Disruption of synchronous gamma oscillations in the rat hippocampal slice: a common mechanism of anaesthetic drug action. Br. J. Pharmacol. 125, 483–492. doi:10.1038/sj.bjp.0702113

Fink-Jensen, A., Suzdak, P.D., Swedberg, M.D., Judge, M.E., Hansen, L., Nielsen, P.G., 1992. The gamma-aminobutyric acid (GABA) uptake inhibitor, tiagabine, increases extracellular brain levels of GABA in awake rats. Eur. J. Pharmacol. 220, 197–201.

Fisahn, A., Pike, F.G., Buhl, E.H., Paulsen, O., 1998. Cholinergic induction of network oscillations at 40 Hz in the hippocampus in vitro. Nature 394, 186–189. doi:10.1038/28179

Freeman, W.J., 1975. Mass action in the nervous system: examination of the neurophysiological basis of adaptive behavior through the EEG. Academic Press, New York.
Freeman, W.J., van Dijk, B.W., 1987. Spatial patterns of visual cortical fast EEG during conditioned reflex in a rhesus monkey. Brain Res. 422, 267–276.
Friedman-Hill, S., Maldonado, P.E., Gray, C.M., 2000. Dynamics of striate cortical activity in the alert macaque: I. Incidence and stimulus-dependence of gamma-band neuronal oscillations. Cereb. Cortex 10, 1105–1116.
Frien, A., Eckhorn, R., Bauer, R., Woelbern, T., Gabriel, A., 2000. Fast oscillations display sharper orientation tuning than slower components of the same recordings in striate cortex of the awake monkey. Eur. J. Neurosci. 12, 1453–1465.
Fries, P., 2015. Rhythms for Cognition: Communication through Coherence. Neuron 88, 220–235. doi:10.1016/j.neuron.2015.09.034
Fries, P., 2009. Neuronal gamma-band synchronization as a fundamental process in cortical computation. Annu. Rev. Neurosci. 32, 209–224. doi:10.1146/annurev.neuro.051508.135603
Fries, P., 2005. A mechanism for cognitive dynamics: neuronal communication through neuronal coherence. Trends Cogn. Sci. (Regul. Ed.) 9, 474–480. doi:10.1016/j.tics.2005.08.011
Fries, P., Reynolds, J.H., Rorie, A.E., Desimone, R., 2001. Modulation of oscillatory neuronal synchronization by selective visual attention. Science 291, 1560–1563. doi:10.1126/science.291.5508.1560
Fries, P., Scheeringa, R., Oostenveld, R., 2008a. Finding gamma. Neuron 58, 303–305. doi:10.1016/j.neuron.2008.04.020
Fries, P., Womelsdorf, T., Oostenveld, R., Desimone, R., 2008b. The effects of visual stimulation and selective visual attention on rhythmic neuronal synchronization in macaque area V4. J. Neurosci. 28, 4823–4835. doi:10.1523/JNEUROSCI.4499-07.2008
Fry, A., Mullinger, K.J., O'Neill, G.C., Barratt, E.L., Morris, P.G., Bauer, M., Folland, J.P., Brookes, M.J., 2016. Modulation of post-movement beta rebound by contraction force and rate of force development: Modulation of PMBR by force & RFD. Human Brain Mapping 37, 2493–2511. doi:10.1002/hbm.23189
Gaetz, W., Roberts, T.P.L., Singh, K.D., Muthukumaraswamy, S.D., 2012. Functional and structural correlates of the aging brain: Relating visual cortex (V1) gamma band responses to age-related structural change. Human Brain Mapping 33, 2035–2046. doi:10.1002/hbm.21339
Galambos, R., 1992. A comparison of certain gamma band (40–Hz) brain rhythms in cat and man, in: Induced Rhythms in the Brain. Birkhäuser, Boston, pp. 201–216.
Gieselmann, M.A., Thiele, A., 2008. Comparison of spatial integration and surround suppression characteristics in spiking activity and the local field potential in macaque V1. European Journal of Neuroscience 28, 447–459. doi:10.1111/j.1460-9568.2008.06358.x
Goldberg, D.P., Williams, P., 1988. The User's Guide to the General Health Questionnaire.
Goncharova, I.I., McFarland, D.J., Vaughan, T.M., Wolpaw, J.R., 2003. EMG contamination of EEG: spectral and topographical characteristics. Clin Neurophysiol 114, 1580–1593.
Gonzalez-Burgos, G., Lewis, D.A., 2012. NMDA receptor hypofunction, parvalbumin-positive neurons, and cortical gamma oscillations in schizophrenia. Schizophr Bull 38, 950–957. doi:10.1093/schbul/sbs010

Gonzalez-Burgos, G., Lewis, D.A., 2008. GABA Neurons and the Mechanisms of Network Oscillations: Implications for Understanding Cortical Dysfunction in Schizophrenia. Schizophrenia Bulletin 34, 944–961. doi:10.1093/schbul/sbn070

Gorgolewski, K.J., Poldrack, R.A., 2016. A Practical Guide for Improving Transparency and Reproducibility in Neuroimaging Research. PLoS Biol. 14, e1002506. doi:10.1371/journal.pbio.1002506

Grant, K.A., Lovinger, D.M., 1995. Cellular and behavioral neurobiology of alcohol: receptor-mediated neuronal processes. Clin. Neurosci. 3, 155–164.

Gray, C.M., Engel, A.K., König, P., Singer, W., 1990. Stimulus-Dependent Neuronal Oscillations in Cat Visual Cortex: Receptive Field Properties and Feature Dependence. Eur. J. Neurosci. 2, 607–619.

Gray, C.M., König, P., Engel, A.K., Singer, W., 1989. Oscillatory responses in cat visual cortex exhibit inter-columnar synchronization which reflects global stimulus properties. Nature 338, 334–337. doi:10.1038/338334a0

Gray, C.M., Singer, W., 1989. Stimulus-specific neuronal oscillations in orientation columns of cat visual cortex. Proc. Natl. Acad. Sci. U.S.A. 86, 1698–1702.

Gray, C.M., Skinner, J.E., 1988. Centrifugal regulation of neuronal activity in the olfactory bulb of the waking rabbit as revealed by reversible cryogenic blockade. Exp Brain Res 69, 378–386.

Gray, C.M., Viana Di Prisco, G., 1997. Stimulus-dependent neuronal oscillations and local synchronization in striate cortex of the alert cat. J. Neurosci. 17, 3239–3253.

Gregoriou, G.G., Gotts, S.J., Zhou, H., Desimone, R., 2009. High-frequency, long-range coupling between prefrontal and visual cortex during attention. Science 324, 1207–1210. doi:10.1126/science.1171402

Gregoriou, G.G., Paneri, S., Sapountzis, P., 2015. Oscillatory synchrony as a mechanism of attentional processing. Brain Research 1626, 165–182. doi:10.1016/j.brainres.2015.02.004

Gross, J., Baillet, S., Barnes, G.R., Henson, R.N., Hillebrand, A., Jensen, O., Jerbi, K., Litvak, V., Maess, B., Oostenveld, R., Parkkonen, L., Taylor, J.R., van Wassenhove, V., Wibral, M., Schoffelen, J.-M., 2013. Good practice for conducting and reporting MEG research. Neuroimage 65, 349–363. doi:10.1016/j.neuroimage.2012.10.001

Gross, J., Kujala, J., Hämäläinen, M., Timmermann, L., Schnitzler, A., Salmelin, R., 2001. Dynamic imaging of coherent sources: studying neural interactions in the human brain. Proceedings of the National Academy of Sciences 98, 694–699.

Grothe, I., Neitzel, S.D., Mandon, S., Kreiter, A.K., 2012. Switching neuronal inputs by differential modulations of gamma-band phase-coherence. J. Neurosci. 32, 16172–16180. doi:10.1523/JNEUROSCI.0890-12.2012

Gruber, T., Müller, M.M., Keil, A., Elbert, T., 1999. Selective visual-spatial attention alters induced gamma band responses in the human EEG. Clin Neurophysiol 110, 2074–2085.

Hadjipapas, A., Adjamian, P., Swettenham, J.B., Holliday, I.E., Barnes, G.R., 2007. Stimuli of varying spatial scale induce gamma activity with distinct temporal characteristics in human visual cortex. NeuroImage 35, 518–530. doi:10.1016/j.neuroimage.2007.01.002

Hadjipapas, A., Lowet, E., Roberts, M.J., Peter, A., De Weerd, P., 2015. Parametric variation of gamma frequency and power with luminance contrast: A comparative study of human MEG and monkey LFP and spike responses. Neuroimage 112, 327–340. doi:10.1016/j.neuroimage.2015.02.062

Haegens, S., Barczak, A., Musacchia, G., Lipton, M.L., Mehta, A.D., Lakatos, P., Schroeder, C.E., 2015. Laminar Profile and Physiology of the Rhythm in

Primary Visual, Auditory, and Somatosensory Regions of Neocortex. Journal of Neuroscience 35, 14341–14352. doi:10.1523/JNEUROSCI.0600-15.2015

Haegens, S., Cousijn, H., Wallis, G., Harrison, P.J., Nobre, A.C., 2014. Inter- and intra-individual variability in alpha peak frequency. NeuroImage 92, 46–55. doi:10.1016/j.neuroimage.2014.01.049

Hall, S.D., Barnes, G.R., Furlong, P.L., Seri, S., Hillebrand, A., 2010. Neuronal network pharmacodynamics of GABAergic modulation in the human cortex determined using pharmaco-magnetoencephalography. Hum Brain Mapp 31, 581–594. doi:10.1002/hbm.20889

Hall, S.D., Holliday, I.E., Hillebrand, A., Singh, K.D., Furlong, P.L., Hadjipapas, A., Barnes, G.R., 2005. The missing link: analogous human and primate cortical gamma oscillations. Neuroimage 26, 13–17. doi:10.1016/j.neuroimage.2005.01.009

Hämäläinen, M., Hari, R., Ilmoniemi, R.J., Knuutila, J., Lounasmaa, O.V., 1993. Magnetoencephalography—theory, instrumentation, and applications to noninvasive studies of the working human brain. Reviews of Modern Physics 65, 413–497. doi:10.1103/RevModPhys.65.413

Hämäläinen, M.S., Ilmoniemi, R.J., 1994. Interpreting magnetic fields of the brain: minimum norm estimates. Med Biol Eng Comput 32, 35–42.

Hämäläinen, M.S., Sarvas, J., 1989. Realistic conductivity geometry model of the human head for interpretation of neuromagnetic data. IEEE Trans Biomed Eng 36, 165–171. doi:10.1109/10.16463

Hamandi, K., Myers, J., Muthukumaraswamy, S., 2014. Tiagabine-induced stupor - more evidence for an encephalopathy. Epilepsy Behav 31, 196–197. doi:10.1016/j.yebeh.2013.12.027

Hari, R., Salmelin, R., 2012. Magnetoencephalography: From SQUIDs to neuroscience. Neuroimage 20th anniversary special edition. Neuroimage 61, 386–396. doi:10.1016/j.neuroimage.2011.11.074

Henrie, J.A., Shapley, R., 2005. LFP power spectra in V1 cortex: the graded effect of stimulus contrast. J. Neurophysiol. 94, 479–490. doi:10.1152/jn.00919.2004

Herrick, R., Horton, W., Olsen, T., McKay, M., Archie, K.A., Marcus, D.S., 2016. XNAT Central: Open sourcing imaging research data. Neuroimage 124, 1093–1096. doi:10.1016/j.neuroimage.2015.06.076

Herrmann, C.S., Munk, M.H.J., Engel, A.K., 2004. Cognitive functions of gamma-band activity: memory match and utilization. Trends Cogn. Sci. (Regul. Ed.) 8, 347–355. doi:10.1016/j.tics.2004.06.006

Hillebrand, A., Barnes, G.R., 2002. A quantitative assessment of the sensitivity of whole-head MEG to activity in the adult human cortex. Neuroimage 16, 638–650.

Hillebrand, A., Singh, K.D., Holliday, I.E., Furlong, P.L., Barnes, G.R., 2005. A new approach to neuroimaging with magnetoencephalography. Hum Brain Mapp 25, 199–211. doi:10.1002/hbm.20102

Hipp, J.F., Siegel, M., 2013. Dissociating neuronal gamma-band activity from cranial and ocular muscle activity in EEG. Front Hum Neurosci 7, 338. doi:10.3389/fnhum.2013.00338

Hodge, M.R., Horton, W., Brown, T., Herrick, R., Olsen, T., Hileman, M.E., McKay, M., Archie, K.A., Cler, E., Harms, M.P., Burgess, G.C., Glasser, M.F., Elam, J.S., Curtiss, S.W., Barch, D.M., Oostenveld, R., Larson-Prior, L.J., Ugurbil, K., Van Essen, D.C., Marcus, D.S., 2016. ConnectomeDB--Sharing human brain connectivity data. Neuroimage 124, 1102–1107. doi:10.1016/j.neuroimage.2015.04.046

Hoogenboom, N., Schoffelen, J.-M., Oostenveld, R., Fries, P., 2010. Visually induced gamma-band activity predicts speed of change detection in humans. Neuroimage 51, 1162–1167. doi:10.1016/j.neuroimage.2010.03.041

Hoogenboom, N., Schoffelen, J.-M., Oostenveld, R., Parkes, L.M., Fries, P., 2006. Localizing human visual gamma-band activity in frequency, time and space. Neuroimage 29, 764–773. doi:10.1016/j.neuroimage.2005.08.043

Huang, M.X., Mosher, J.C., Leahy, R.M., 1999. A sensor-weighted overlapping-sphere head model and exhaustive head model comparison for MEG. Phys Med Biol 44, 423–440.

Iannetti, G.D., Wise, R.G., 2007. BOLD functional MRI in disease and pharmacological studies: room for improvement? Magn Reson Imaging 25, 978–988. doi:10.1016/j.mri.2007.03.018

Jenkinson, M., Smith, S., 2001. A global optimisation method for robust affine registration of brain images. Med Image Anal 5, 143–156.

Jensen, O., Gips, B., Bergmann, T.O., Bonnefond, M., 2014. Temporal coding organized by coupled alpha and gamma oscillations prioritize visual processing. Trends in Neurosciences 37, 357–369. doi:10.1016/j.tins.2014.04.001

Jensen, O., Goel, P., Kopell, N., Pohja, M., Hari, R., Ermentrout, B., 2005. On the human sensorimotor-cortex beta rhythm: sources and modeling. Neuroimage 26, 347–355. doi:10.1016/j.neuroimage.2005.02.008

Jensen, O., Kaiser, J., Lachaux, J.-P., 2007. Human gamma-frequency oscillations associated with attention and memory. Trends Neurosci. 30, 317–324. doi:10.1016/j.tins.2007.05.001

Jia, X., Smith, M.A., Kohn, A., 2011. Stimulus selectivity and spatial coherence of gamma components of the local field potential. J. Neurosci. 31, 9390–9403. doi:10.1523/JNEUROSCI.0645-11.2011

Jia, X., Xing, D., Kohn, A., 2013. No consistent relationship between gamma power and peak frequency in macaque primary visual cortex. J. Neurosci. 33, 17–25. doi:10.1523/JNEUROSCI.1687-12.2013

Juergens, E., Guettler, A., Eckhorn, R., 1999. Visual stimulation elicits locked and induced gamma oscillations in monkey intracortical- and EEG-potentials, but not in human EEG. Experimental Brain Research 129, 247–259. doi:10.1007/s002210050895

Kähkönen, S., 2006. Magnetoencephalography (MEG): a non-invasive tool for studying cortical effects in psychopharmacology. Int. J. Neuropsychopharmacol. 9, 367–372. doi:10.1017/S1461145705005894

Kahlbrock, N., Butz, M., May, E.S., Brenner, M., Kircheis, G., Häussinger, D., Schnitzler, A., 2012a. Lowered frequency and impaired modulation of gamma band oscillations in a bimodal attention task are associated with reduced critical flicker frequency. Neuroimage 61, 216–227. doi:10.1016/j.neuroimage.2012.02.063

Kahlbrock, N., Butz, M., May, E.S., Schnitzler, A., 2012b. Sustained gamma band synchronization in early visual areas reflects the level of selective attention. Neuroimage 59, 673–681. doi:10.1016/j.neuroimage.2011.07.017

Kandel, E.R., Schwartz, J.H., Jessell, T.M. (Eds.), 2000. Principles of neural science, 4th ed. ed. McGraw-Hill, Health Professions Division, New York.

Kaplan, R., Doeller, C.F., Barnes, G.R., Litvak, V., Düzel, E., Bandettini, P.A., Burgess, N., 2012. Movement-Related Theta Rhythm in Humans: Coordinating Self-Directed Hippocampal Learning. PLoS Biology 10, e1001267. doi:10.1371/journal.pbio.1001267

Kayser, C., Salazar, R.F., Konig, P., 2003. Responses to natural scenes in cat V1. J. Neurophysiol. 90, 1910–1920. doi:10.1152/jn.00195.2003

Kleiner, M., Brainard, D., Pelli, D., Ingling, A., Murray, R., Broussard, C., 2007. What's new in Psychtoolbox-3. Perception 36, 1.

Knappe, S., Sander, T., Trahms, L., 2014. Optically-Pumped Magnetometers for MEG, in: Supek, S., Aine, C.J. (Eds.), Magnetoencephalography. Springer Berlin Heidelberg, Berlin, Heidelberg, pp. 993–999.

Koelewijn, L., Rich, A.N., Muthukumaraswamy, S.D., Singh, K.D., 2013. Spatial attention increases high-frequency gamma synchronisation in human medial visual cortex. Neuroimage 79, 295–303. doi:10.1016/j.neuroimage.2013.04.108

Kopell, N., Ermentrout, G.B., Whittington, M.A., Traub, R.D., 2000. Gamma rhythms and beta rhythms have different synchronization properties. Proceedings of the National Academy of Sciences 97, 1867–1872. doi:10.1073/pnas.97.4.1867

Kujala, J., Jung, J., Bouvard, S., Lecaignard, F., Lothe, A., Bouet, R., Ciumas, C., Ryvlin, P., Jerbi, K., 2015. Gamma oscillations in V1 are correlated with GABAA receptor density: A multi-modal MEG and Flumazenil-PET study. Scientific Reports 5, 16347. doi:10.1038/srep16347

Lancaster, J.L., Tordesillas-Gutiérrez, D., Martinez, M., Salinas, F., Evans, A., Zilles, K., Mazziotta, J.C., Fox, P.T., 2007. Bias between MNI and Talairach coordinates analyzed using the ICBM-152 brain template. Hum Brain Mapp 28, 1194–1205. doi:10.1002/hbm.20345

Larson-Prior, L.J., Oostenveld, R., Della Penna, S., Michalareas, G., Prior, F., Babajani-Feremi, A., Schoffelen, J.-M., Marzetti, L., de Pasquale, F., Di Pompeo, F., Stout, J., Woolrich, M., Luo, Q., Bucholz, R., Fries, P., Pizzella, V., Romani, G.L., Corbetta, M., Snyder, A.Z., WU-Minn HCP Consortium, 2013. Adding dynamics to the Human Connectome Project with MEG. Neuroimage 80, 190–201. doi:10.1016/j.neuroimage.2013.05.056

Leach, J.P., Brodie, M.J., 1998. Tiagabine. The Lancet 351, 203–207. doi:10.1016/S0140-6736(97)05035-6

Le Van Quyen, M., Bragin, A., 2007. Analysis of dynamic brain oscillations: methodological advances. Trends in Neurosciences 30, 365–373. doi:10.1016/j.tins.2007.05.006

Le Van Quyen, M., Foucher, J., Lachaux, J., Rodriguez, E., Lutz, A., Martinerie, J., Varela, F.J., 2001. Comparison of Hilbert transform and wavelet methods for the analysis of neuronal synchrony. J. Neurosci. Methods 111, 83–98.

Lega, B.C., Jacobs, J., Kahana, M., 2012. Human hippocampal theta oscillations and the formation of episodic memories. Hippocampus 22, 748–761. doi:10.1002/hipo.20937

Lewis, D.A., Hashimoto, T., Volk, D.W., 2005. Cortical inhibitory neurons and schizophrenia. Nature Reviews Neuroscience 6, 312–324. doi:10.1038/nrn1648

Lima, B., Singer, W., Chen, N.-H., Neuenschwander, S., 2010. Synchronization dynamics in response to plaid stimuli in monkey V1. Cereb. Cortex 20, 1556–1573. doi:10.1093/cercor/bhp218

Lopes da Silva, F.H., 2010. Electrophysiological Basis of MEG Signals, in: Hansen, P., Kringelbach, M., Salmelin, R. (Eds.), MEG: An Introduction to Methods. Oxford University Press, pp. 1–23.

Lopes da Silva, F.H., van Rotterdam, A., Storm van Leeuwen, W., Tielen, A.M., 1970. Dynamic characteristics of visual evoked potentials in the dog. II. Beta frequency selectivity in evoked potentials and background activity. Electroencephalogr Clin Neurophysiol 29, 260–268.

Lozano-Soldevilla, D., ter Huurne, N., Cools, R., Jensen, O., 2014. GABAergic modulation of visual gamma and alpha oscillations and its consequences for working memory performance. Curr. Biol. 24, 2878–2887. doi:10.1016/j.cub.2014.10.017

Lü, Z.L., Williamson, S.J., 1991. Spatial extent of coherent sensory-evoked cortical activity. Exp Brain Res 84, 411–416.
Magazzini, L., Muthukumaraswamy, S.D., Campbell, A.E., Hamandi, K., Lingford-Hughes, A., Myers, J.F.M., Nutt, D.J., Sumner, P., Wilson, S.J., Singh, K.D., 2016. Significant reductions in human visual gamma frequency by the gaba reuptake inhibitor tiagabine revealed by robust peak frequency estimation. Hum Brain Mapp. doi:10.1002/hbm.23283
Maier, A., Adams, G.K., Aura, C., Leopold, D.A., 2010. Distinct superficial and deep laminar domains of activity in the visual cortex during rest and stimulation. Front Syst Neurosci 4. doi:10.3389/fnsys.2010.00031
Maier, A., Aura, C.J., Leopold, D.A., 2011. Infragranular sources of sustained local field potential responses in macaque primary visual cortex. J. Neurosci. 31, 1971–1980. doi:10.1523/JNEUROSCI.5300-09.2011
Mäkelä, J.P., Hari, R., 1987. Evidence for cortical origin of the 40 Hz auditory evoked response in man. Electroencephalogr Clin Neurophysiol 66, 539–546.
Manning, J.R., Jacobs, J., Fried, I., Kahana, M.J., 2009. Broadband Shifts in Local Field Potential Power Spectra Are Correlated with Single-Neuron Spiking in Humans. Journal of Neuroscience 29, 13613–13620. doi:10.1523/JNEUROSCI.2041-09.2009
Maris, E., Oostenveld, R., 2007. Nonparametric statistical testing of EEG- and MEG-data. J. Neurosci. Methods 164, 177–190. doi:10.1016/j.jneumeth.2007.03.024
Markram, H., Toledo-Rodriguez, M., Wang, Y., Gupta, A., Silberberg, G., Wu, C., 2004. Interneurons of the neocortical inhibitory system. Nat. Rev. Neurosci. 5, 793–807. doi:10.1038/nrn1519
Marshall, T.R., Bergmann, T.O., Jensen, O., 2015a. Frontoparietal Structural Connectivity Mediates the Top-Down Control of Neuronal Synchronization Associated with Selective Attention. PLoS Biol. 13, e1002272. doi:10.1371/journal.pbio.1002272
Marshall, T.R., O'Shea, J., Jensen, O., Bergmann, T.O., 2015b. Frontal eye fields control attentional modulation of alpha and gamma oscillations in contralateral occipitoparietal cortex. J. Neurosci. 35, 1638–1647. doi:10.1523/JNEUROSCI.3116-14.2015
Mason, K.M., Ebersole, S.M., Fujiwara, H., Lowe, J.P., Bowyer, S.M., 2013. What you need to know to become a MEG technologist. Neurodiagn J 53, 191–206.
Michalareas, G., Vezoli, J., van Pelt, S., Schoffelen, J.-M., Kennedy, H., Fries, P., 2016. Alpha-Beta and Gamma Rhythms Subserve Feedback and Feedforward Influences among Human Visual Cortical Areas. Neuron 89, 384–397. doi:10.1016/j.neuron.2015.12.018
Milham, M.P., 2012. Open neuroscience solutions for the connectome-wide association era. Neuron 73, 214–218. doi:10.1016/j.neuron.2011.11.004
Miller, K.J., Sorensen, L.B., Ojemann, J.G., den Nijs, M., 2009. Power-law scaling in the brain surface electric potential. PLoS Comput. Biol. 5, e1000609. doi:10.1371/journal.pcbi.1000609
Milner, P.M., 1974. A model for visual shape recognition. Psychol Rev 81, 521–535.
Mitra, P.P., Pesaran, B., 1999. Analysis of dynamic brain imaging data. Biophys. J. 76, 691–708. doi:10.1016/S0006-3495(99)77236-X
Mosher, J.C., Leahy, R.M., Lewis, P.S., 1999. EEG and MEG: forward solutions for inverse methods. IEEE Trans Biomed Eng 46, 245–259.
Müller, M.M., Gruber, T., Keil, A., 2000. Modulation of induced gamma band activity in the human EEG by attention and visual information processing. Int J Psychophysiol 38, 283–299.

Murakami, S., Okada, Y., 2006. Contributions of principal neocortical neurons to magnetoencephalography and electroencephalography signals. J. Physiol. (Lond.) 575, 925–936. doi:10.1113/jphysiol.2006.105379

Murphy, J.E. (Ed.), 2011. Clinical pharmacokinetics, Fifth. ed. American Society of Health-System Pharmacists, Bethesda, Maryland.

Muthukumaraswamy, S.D., 2014. The use of magnetoencephalography in the study of psychopharmacology (pharmaco-MEG). Journal of Psychopharmacology 28, 815–829. doi:10.1177/0269881114536790

Muthukumaraswamy, S.D., 2013. High-frequency brain activity and muscle artifacts in MEG/EEG: a review and recommendations. Front Hum Neurosci 7, 138. doi:10.3389/fnhum.2013.00138

Muthukumaraswamy, S.D., Edden, R.A.E., Jones, D.K., Swettenham, J.B., Singh, K.D., 2009. Resting GABA concentration predicts peak gamma frequency and fMRI amplitude in response to visual stimulation in humans. Proc. Natl. Acad. Sci. U.S.A. 106, 8356–8361. doi:10.1073/pnas.0900728106

Muthukumaraswamy, S.D., Myers, J.F.M., Wilson, S.J., Nutt, D.J., Hamandi, K., Lingford-Hughes, A., Singh, K.D., 2013a. Elevating endogenous GABA levels with GAT-1 blockade modulates evoked but not induced responses in human visual cortex. Neuropsychopharmacology 38, 1105–1112. doi:10.1038/npp.2013.9

Muthukumaraswamy, S.D., Myers, J.F.M., Wilson, S.J., Nutt, D.J., Lingford-Hughes, A., Singh, K.D., Hamandi, K., 2013b. The effects of elevated endogenous GABA levels on movement-related network oscillations. NeuroImage 66, 36–41. doi:10.1016/j.neuroimage.2012.10.054

Muthukumaraswamy, S.D., Routley, B., Droog, W., Singh, K.D., Hamandi, K., 2016. The effects of AMPA blockade on the spectral profile of human early visual cortex recordings studied with non-invasive MEG. Cortex 81, 266–275. doi:10.1016/j.cortex.2016.03.004

Muthukumaraswamy, S.D., Singh, K.D., 2013. Visual gamma oscillations: the effects of stimulus type, visual field coverage and stimulus motion on MEG and EEG recordings. Neuroimage 69, 223–230. doi:10.1016/j.neuroimage.2012.12.038

Muthukumaraswamy, S.D., Singh, K.D., 2009. Functional decoupling of BOLD and gamma-band amplitudes in human primary visual cortex. Hum Brain Mapp 30, 2000–2007. doi:10.1002/hbm.20644

Muthukumaraswamy, S.D., Singh, K.D., Swettenham, J.B., Jones, D.K., 2010. Visual gamma oscillations and evoked responses: variability, repeatability and structural MRI correlates. Neuroimage 49, 3349–3357.

Myers, J.F.M., Evans, C.J., Kalk, N.J., Edden, R.A.E., Lingford-Hughes, A.R., 2014. Measurement of GABA using J-difference edited 1H-MRS following modulation of synaptic GABA concentration with tiagabine. Synapse 68, 355–362. doi:10.1002/syn.21747

Neuenschwander, S., Singer, W., 1996. Long-range synchronization of oscillatory light responses in the cat retina and lateral geniculate nucleus. Nature 379, 728–732. doi:10.1038/379728a0

Niso, G., Rogers, C., Moreau, J.T., Chen, L.-Y., Madjar, C., Das, S., Bock, E., Tadel, F., Evans, A.C., Jolicoeur, P., Baillet, S., 2016. OMEGA: The Open MEG Archive. Neuroimage 124, 1182–1187. doi:10.1016/j.neuroimage.2015.04.028

Nolte, G., 2003. The magnetic lead field theorem in the quasi-static approximation and its use for magnetoencephalography forward calculation in realistic volume conductors. Physics in medicine and biology 48, 3637.

Nunez, P.L., Srinivasan, R., 2010. Scale and frequency chauvinism in brain dynamics: too much emphasis on γ band oscillations. Brain Struct Funct 215, 67–71. doi:10.1007/s00429-010-0277-6

O'Donnell, R.D., Berkhout, J., Adey, W.R., 1974. Contamination of scalp EEG spectrum during contraction of cranio-facial muscles. Electroencephalogr Clin Neurophysiol 37, 145–151.

Oke, O.O., Magony, A., Anver, H., Ward, P.D., Jiruska, P., Jefferys, J.G.R., Vreugdenhil, M., 2010. High-frequency gamma oscillations coexist with low-frequency gamma oscillations in the rat visual cortex in vitro. Eur. J. Neurosci. 31, 1435–1445. doi:10.1111/j.1460-9568.2010.07171.x

Oldfield, R.C., 1971. The assessment and analysis of handedness: the Edinburgh inventory. Neuropsychologia 9, 97–113.

Oostenveld, R., Fries, P., Maris, E., Schoffelen, J.-M., 2011. FieldTrip: Open source software for advanced analysis of MEG, EEG, and invasive electrophysiological data. Comput Intell Neurosci 2011, 156869. doi:10.1155/2011/156869

Orekhova, E.V., Butorina, A.V., Sysoeva, O.V., Prokofyev, A.O., Nikolaeva, A.Y., Stroganova, T.A., 2015. Frequency of gamma oscillations in humans is modulated by velocity of visual motion. Journal of Neurophysiology 114, 244–255. doi:10.1152/jn.00232.2015

Perry, G., 2015. The effects of cross-orientation masking on the visual gamma response in humans. European Journal of Neuroscience 41, 1484–1495. doi:10.1111/ejn.12900

Perry, G., Adjamian, P., Thai, N.J., Holliday, I.E., Hillebrand, A., Barnes, G.R., 2011. Retinotopic mapping of the primary visual cortex - a challenge for MEG imaging of the human cortex. Eur. J. Neurosci. 34, 652–661. doi:10.1111/j.1460-9568.2011.07777.x

Perry, G., Brindley, L.M., Muthukumaraswamy, S.D., Singh, K.D., Hamandi, K., 2014. Evidence for increased visual gamma responses in photosensitive epilepsy. Epilepsy Res. 108, 1076–1086. doi:10.1016/j.eplepsyres.2014.04.012

Perry, G., Hamandi, K., Brindley, L.M., Muthukumaraswamy, S.D., Singh, K.D., 2013. The properties of induced gamma oscillations in human visual cortex show individual variability in their dependence on stimulus size. NeuroImage 68, 83–92. doi:10.1016/j.neuroimage.2012.11.043

Perry, G., Randle, J.M., Koelewijn, L., Routley, B.C., Singh, K.D., 2015. Linear Tuning of Gamma Amplitude and Frequency to Luminance Contrast: Evidence from a Continuous Mapping Paradigm. PLoS ONE 10, e0124798. doi:10.1371/journal.pone.0124798

Pesaran, B., Pezaris, J.S., Sahani, M., Mitra, P.P., Andersen, R.A., 2002. Temporal structure in neuronal activity during working memory in macaque parietal cortex. Nat. Neurosci. 5, 805–811. doi:10.1038/nn890

Phillips, K.G., Uhlhaas, P.J., 2015. Neural oscillations as a translational tool in schizophrenia research: Rationale, paradigms and challenges. Journal of Psychopharmacology 29, 155–168. doi:10.1177/0269881114562093

Poldrack, R.A., Gorgolewski, K.J., 2015. OpenfMRI: Open sharing of task fMRI data. Neuroimage. doi:10.1016/j.neuroimage.2015.05.073

Poldrack, R.A., Gorgolewski, K.J., 2014. Making big data open: data sharing in neuroimaging. Nat. Neurosci. 17, 1510–1517. doi:10.1038/nn.3818

Poline, J.-B., Breeze, J.L., Ghosh, S., Gorgolewski, K., Halchenko, Y.O., Hanke, M., Haselgrove, C., Helmer, K.G., Keator, D.B., Marcus, D.S., Poldrack, R.A., Schwartz, Y., Ashburner, J., Kennedy, D.N., 2012. Data sharing in neuroimaging research. Front Neuroinform 6, 9. doi:10.3389/fninf.2012.00009

Popescu, A.T., Popa, D., Paré, D., 2009. Coherent gamma oscillations couple the amygdala and striatum during learning. Nat. Neurosci. 12, 801–807. doi:10.1038/nn.2305

Ramìrez, R., 2008. Source localization. Scholarpedia 3, 1733. doi:10.4249/scholarpedia.1733

Ray, S., Maunsell, J.H.R., 2015. Do gamma oscillations play a role in cerebral cortex? Trends in Cognitive Sciences 19, 78–85. doi:10.1016/j.tics.2014.12.002

Ray, S., Maunsell, J.H.R., 2011. Different origins of gamma rhythm and high-gamma activity in macaque visual cortex. PLoS Biol. 9, e1000610. doi:10.1371/journal.pbio.1000610

Ray, S., Maunsell, J.H.R., 2010. Differences in gamma frequencies across visual cortex restrict their possible use in computation. Neuron 67, 885–896. doi:10.1016/j.neuron.2010.08.004

Reynolds, J.H., Chelazzi, L., 2004. Attentional modulation of visual processing. Annual Review of Neuroscience 27, 611–647. doi:10.1146/annurev.neuro.26.041002.131039

Ribary, U., Ioannides, A.A., Singh, K.D., Hasson, R., Bolton, J.P., Lado, F., Mogilner, A., Llinás, R., 1991. Magnetic field tomography of coherent thalamocortical 40-Hz oscillations in humans. Proc. Natl. Acad. Sci. U.S.A. 88, 11037–11041.

Roberto, M., Madamba, S.G., Moore, S.D., Tallent, M.K., Siggins, G.R., 2003. Ethanol increases GABAergic transmission at both pre- and postsynaptic sites in rat central amygdala neurons. Proceedings of the National Academy of Sciences 100, 2053–2058. doi:10.1073/pnas.0437926100

Roberts, M.J., Lowet, E., Brunet, N.M., Ter Wal, M., Tiesinga, P., Fries, P., De Weerd, P., 2013. Robust gamma coherence between macaque V1 and V2 by dynamic frequency matching. Neuron 78, 523–536. doi:10.1016/j.neuron.2013.03.003

Robinson, S., Vrba, J., 1999. Functional neuroimaging by synthetic aperture manetometry (SAM), in: Recent Advances in Biomagnetism. Tohoku University Press: Sendai, pp. 302–305.

Robson, S.E., Muthukumarawswamy, S.D., John Evans, C., Shaw, A., Brealy, J., Davis, B., McNamara, G., Perry, G., Singh, K.D., 2015. Structural and neurochemical correlates of individual differences in gamma frequency oscillations in human visual cortex. Journal of Anatomy 227, 409–417. doi:10.1111/joa.12339

Roepstorff, A., Lambert, J.D., 1994. Factors contributing to the decay of the stimulus-evoked IPSC in rat hippocampal CA1 neurons. J. Neurophysiol. 72, 2911–2926.

Rougeul, A., Bouyer, J.J., Dedet, L., Debray, O., 1979. Fast somato-parietal rhythms during combined focal attention and immobility in baboon and squirrel monkey. Electroencephalogr Clin Neurophysiol 46, 310–319.

Saxena, N., Muthukumaraswamy, S.D., Diukova, A., Singh, K., Hall, J., Wise, R., 2013. Enhanced Stimulus-Induced Gamma Activity in Humans during Propofol-Induced Sedation. PLoS ONE 8, e57685. doi:10.1371/journal.pone.0057685

Scheeringa, R., Koopmans, P.J., van Mourik, T., Jensen, O., Norris, D.G., 2016. The relationship between oscillatory EEG activity and the laminar-specific BOLD signal. Proc. Natl. Acad. Sci. U.S.A. 113, 6761–6766. doi:10.1073/pnas.1522577113

Schwarzkopf, D.S., Robertson, D.J., Song, C., Barnes, G.R., Rees, G., 2012. The Frequency of Visually Induced Gamma-Band Oscillations Depends on the Size of Early Human Visual Cortex. Journal of Neuroscience 32, 1507–1512. doi:10.1523/JNEUROSCI.4771-11.2012

Sedley, W., Cunningham, M.O., 2013. Do cortical gamma oscillations promote or suppress perception? An under-asked question with an over-assumed answer. Frontiers in Human Neuroscience 7. doi:10.3389/fnhum.2013.00595

Sekihara, K., Nagarajan, S.S., Poeppel, D., Marantz, A., 2002. Performance of an MEG adaptive-beamformer technique in the presence of correlated neural activities: effects on signal intensity and time-course estimates. IEEE Trans Biomed Eng 49, 1534–1546.

Shaw, A.D., Saxena, N., E. Jackson, L., Hall, J.E., Singh, K.D., Muthukumaraswamy, S.D., 2015. Ketamine amplifies induced gamma frequency oscillations in the human cerebral cortex. European Neuropsychopharmacology 25, 1136–1146. doi:10.1016/j.euroneuro.2015.04.012

Siegel, M., Donner, T.H., Oostenveld, R., Fries, P., Engel, A.K., 2008. Neuronal synchronization along the dorsal visual pathway reflects the focus of spatial attention. Neuron 60, 709–719. doi:10.1016/j.neuron.2008.09.010

Sik, A., Penttonen, M., Ylinen, A., Buzsáki, G., 1995. Hippocampal CA1 interneurons: an in vivo intracellular labeling study. J. Neurosci. 15, 6651–6665.

Singer, W., 2007. Binding by synchrony. Scholarpedia 2, 1657. doi:10.4249/scholarpedia.1657

Singer, W., 1999. Neuronal synchrony: a versatile code for the definition of relations? Neuron 24, 49–65, 111–125.

Singer, W., 1993. Synchronization of cortical activity and its putative role in information processing and learning. Annu. Rev. Physiol. 55, 349–374. doi:10.1146/annurev.ph.55.030193.002025

Singer, W., Gray, C.M., 1995. Visual feature integration and the temporal correlation hypothesis. Annu. Rev. Neurosci. 18, 555–586. doi:10.1146/annurev.ne.18.030195.003011

Singh, K.D., 2012. Which "neural activity" do you mean? fMRI, MEG, oscillations and neurotransmitters. Neuroimage 62, 1121–1130. doi:10.1016/j.neuroimage.2012.01.028

Singh, K.D., 2006. Magnetoencephalography, in: Methods in Mind. MIT Press, Cambridge, USA, pp. 291–326.

Smith, S.M., 2002. Fast robust automated brain extraction. Hum Brain Mapp 17, 143–155. doi:10.1002/hbm.10062

Snel, S., Jansen, J.A., Mengel, H.B., Richens, A., Larsen, S., 1997. The Pharmacokinetics of Tiagabine in Healthy Elderly Volunteers and Elderly Patients with Epilepsy. The Journal of Clinical Pharmacology 37, 1015–1020. doi:10.1002/j.1552-4604.1997.tb04282.x

Sohal, V.S., Zhang, F., Yizhar, O., Deisseroth, K., 2009. Parvalbumin neurons and gamma rhythms enhance cortical circuit performance. Nature 459, 698–702. doi:10.1038/nature07991

Spaak, E., Bonnefond, M., Maier, A., Leopold, D.A., Jensen, O., 2012. Layer-specific entrainment of γ-band neural activity by the α rhythm in monkey visual cortex. Curr. Biol. 22, 2313–2318. doi:10.1016/j.cub.2012.10.020

Stroganova, T.A., Butorina, A.V., Sysoeva, O.V., Prokofyev, A.O., Nikolaeva, A.Y., Tsetlin, M.M., Orekhova, E.V., 2015. Altered modulation of gamma oscillation frequency by speed of visual motion in children with autism spectrum disorders. Journal of Neurodevelopmental Disorders 7. doi:10.1186/s11689-015-9121-x

Swettenham, J.B., Muthukumaraswamy, S.D., Singh, K.D., 2009. Spectral Properties of Induced and Evoked Gamma Oscillations in Human Early Visual Cortex to Moving and Stationary Stimuli. Journal of Neurophysiology 102, 1241–1253. doi:10.1152/jn.91044.2008

Tallon-Baudry, null, Bertrand, null, 1999. Oscillatory gamma activity in humans and its role in object representation. Trends Cogn. Sci. (Regul. Ed.) 3, 151–162.

Tallon-Baudry, C., Bertrand, O., Delpuech, C., Permier, J., 1997. Oscillatory gamma-band (30-70 Hz) activity induced by a visual search task in humans. J. Neurosci. 17, 722–734.

Tallon-Baudry, C., Bertrand, O., Delpuech, C., Pernier, J., 1996. Stimulus specificity of phase-locked and non-phase-locked 40 Hz visual responses in human. J. Neurosci. 16, 4240–4249.

Tan, H.-R.M., Gross, J., Uhlhaas, P.J., 2016. MEG sensor and source measures of visually induced gamma-band oscillations are highly reliable. Neuroimage 137, 34–44. doi:10.1016/j.neuroimage.2016.05.006

Taulu, S., Simola, J., 2006. Spatiotemporal signal space separation method for rejecting nearby interference in MEG measurements. Phys Med Biol 51, 1759–1768. doi:10.1088/0031-9155/51/7/008

Taylor, K., Mandon, S., Freiwald, W.A., Kreiter, A.K., 2005. Coherent oscillatory activity in monkey area v4 predicts successful allocation of attention. Cereb. Cortex 15, 1424–1437. doi:10.1093/cercor/bhi023

Thompson, S.M., Gähwiler, B.H., 1992. Effects of the GABA uptake inhibitor tiagabine on inhibitory synaptic potentials in rat hippocampal slice cultures. J. Neurophysiol. 67, 1698–1701.

Tiesinga, P., Sejnowski, T.J., 2009. Cortical enlightenment: are attentional gamma oscillations driven by ING or PING? Neuron 63, 727–732. doi:10.1016/j.neuron.2009.09.009

Traub, R.D., Whittington, M.A., Colling, S.B., Buzsáki, G., Jefferys, J.G., 1996. Analysis of gamma rhythms in the rat hippocampus in vitro and in vivo. J. Physiol. (Lond.) 493 (Pt 2), 471–484.

Troebinger, L., López, J.D., Lutti, A., Bestmann, S., Barnes, G., 2014. Discrimination of cortical laminae using MEG. Neuroimage 102 Pt 2, 885–893. doi:10.1016/j.neuroimage.2014.07.015

Tzourio-Mazoyer, N., Landeau, B., Papathanassiou, D., Crivello, F., Etard, O., Delcroix, N., Mazoyer, B., Joliot, M., 2002. Automated anatomical labeling of activations in SPM using a macroscopic anatomical parcellation of the MNI MRI single-subject brain. Neuroimage 15, 273–289. doi:10.1006/nimg.2001.0978

Uhlhaas, P.J., Singer, W., 2006. Neural Synchrony in Brain Disorders: Relevance for Cognitive Dysfunctions and Pathophysiology. Neuron 52, 155–168. doi:10.1016/j.neuron.2006.09.020

van Albada, S.J., Robinson, P.A., 2013. Relationships between Electroencephalographic Spectral Peaks Across Frequency Bands. Frontiers in Human Neuroscience 7. doi:10.3389/fnhum.2013.00056

Van Essen, D.C., Smith, S.M., Barch, D.M., Behrens, T.E.J., Yacoub, E., Ugurbil, K., WU-Minn HCP Consortium, 2013. The WU-Minn Human Connectome Project: an overview. Neuroimage 80, 62–79. doi:10.1016/j.neuroimage.2013.05.041

van Kerkoerle, T., Self, M.W., Dagnino, B., Gariel-Mathis, M.-A., Poort, J., van der Togt, C., Roelfsema, P.R., 2014. Alpha and gamma oscillations characterize feedback and feedforward processing in monkey visual cortex. Proc. Natl. Acad. Sci. U.S.A. 111, 14332–14341. doi:10.1073/pnas.1402773111

van Pelt, S., Boomsma, D.I., Fries, P., 2012. Magnetoencephalography in Twins Reveals a Strong Genetic Determination of the Peak Frequency of Visually Induced Gamma-Band Synchronization. Journal of Neuroscience 32, 3388–3392. doi:10.1523/JNEUROSCI.5592-11.2012

van Pelt, S., Fries, P., 2013. Visual stimulus eccentricity affects human gamma peak frequency. Neuroimage 78, 439–447. doi:10.1016/j.neuroimage.2013.04.040

Van Veen, B.D., Buckley, K.M., 1988. Beamforming: a versatile approach to spatial filtering. IEEE ASSP Magazine 5, 4–24. doi:10.1109/53.665

Van Veen, B.D., van Drongelen, W., Yuchtman, M., Suzuki, A., 1997. Localization of brain electrical activity via linearly constrained minimum variance spatial filtering. IEEE Trans Biomed Eng 44, 867–880. doi:10.1109/10.623056

van Vugt, M.K., Sederberg, P.B., Kahana, M.J., 2007. Comparison of spectral analysis methods for characterizing brain oscillations. J. Neurosci. Methods 162, 49–63. doi:10.1016/j.jneumeth.2006.12.004

Varela, F., Lachaux, J.P., Rodriguez, E., Martinerie, J., 2001. The brainweb: phase synchronization and large-scale integration. Nat. Rev. Neurosci. 2, 229–239. doi:10.1038/35067550

Viana Di Prisco, G., Freeman, W.J., 1985. Odor-related bulbar EEG spatial pattern analysis during appetitive conditioning in rabbits. Behav. Neurosci. 99, 964–978.

Vrba, J., Robinson, S.E., 2001. Signal processing in magnetoencephalography. Methods 25, 249–271. doi:10.1006/meth.2001.1238

Vrba, J., Taulu, S., Nenonen, J., Ahonen, A., 2010. Signal space separation beamformer. Brain Topogr 23, 128–133. doi:10.1007/s10548-009-0120-7

Walker, L., Chang, L.-C., Nayak, A., Irfanoglu, M.O., Botteron, K.N., McCracken, J., McKinstry, R.C., Rivkin, M.J., Wang, D.-J., Rumsey, J., Pierpaoli, C., Brain Development Cooperative Group, 2016. The diffusion tensor imaging (DTI) component of the NIH MRI study of normal brain development (PedsDTI). Neuroimage 124, 1125–1130. doi:10.1016/j.neuroimage.2015.05.083

Wang, X.-J., 2010. Neurophysiological and computational principles of cortical rhythms in cognition. Physiol. Rev. 90, 1195–1268. doi:10.1152/physrev.00035.2008

Weiner, J.L., Valenzuela, C.F., 2006. Ethanol modulation of GABAergic transmission: The view from the slice. Pharmacology & Therapeutics 111, 533–554. doi:10.1016/j.pharmthera.2005.11.002

Whitham, E.M., Lewis, T., Pope, K.J., Fitzgibbon, S.P., Clark, C.R., Loveless, S., DeLosAngeles, D., Wallace, A.K., Broberg, M., Willoughby, J.O., 2008. Thinking activates EMG in scalp electrical recordings. Clin Neurophysiol 119, 1166–1175. doi:10.1016/j.clinph.2008.01.024

Whittington, M.A., Cunningham, M.O., LeBeau, F.E.N., Racca, C., Traub, R.D., 2011. Multiple origins of the cortical γ rhythm. Dev Neurobiol 71, 92–106. doi:10.1002/dneu.20814

Whittington, M.A., Jefferys, J.G., Traub, R.D., 1996. Effects of intravenous anaesthetic agents on fast inhibitory oscillations in the rat hippocampus in vitro. Br. J. Pharmacol. 118, 1977–1986.

Whittington, M.A., Traub, R.D., Jefferys, J.G., 1995. Synchronized oscillations in interneuron networks driven by metabotropic glutamate receptor activation. Nature 373, 612–615. doi:10.1038/373612a0

Whittington, M.A., Traub, R.D., Kopell, N., Ermentrout, B., Buhl, E.H., 2000. Inhibition-based rhythms: experimental and mathematical observations on network dynamics. Int J Psychophysiol 38, 315–336.

Wieczorek, K., 2015. Investigating the relationship between microsaccades and oscillations in the human visual cortex (Doctoral dissertation). Cardiff University.

Williamson, S.J., Kaufman, L., 1990. Theory of neuroelectric and neuromagnetic fields, in: Auditory Evoked Magnetic Fields and Electric Potentials. Karger, Basel, pp. 1–39.

Wise, R.G., Preston, C., 2010. What is the value of human FMRI in CNS drug development? Drug Discov. Today 15, 973–980. doi:10.1016/j.drudis.2010.08.016

Womelsdorf, T., Fries, P., Mitra, P.P., Desimone, R., 2006. Gamma-band synchronization in visual cortex predicts speed of change detection. Nature 439, 733–736. doi:10.1038/nature04258

Xing, D., Shen, Y., Burns, S., Yeh, C.-I., Shapley, R., Li, W., 2012a. Stochastic generation of gamma-band activity in primary visual cortex of awake and anesthetized monkeys. J. Neurosci. 32, 13873–13880a. doi:10.1523/JNEUROSCI.5644-11.2012

Xing, D., Yeh, C.-I., Burns, S., Shapley, R.M., 2012b. Laminar analysis of visually evoked activity in the primary visual cortex. Proc. Natl. Acad. Sci. U.S.A. 109, 13871–13876. doi:10.1073/pnas.1201478109

Yuval-Greenberg, S., Tomer, O., Keren, A.S., Nelken, I., Deouell, L.Y., 2008. Transient induced gamma-band response in EEG as a manifestation of miniature saccades. Neuron 58, 429–441. doi:10.1016/j.neuron.2008.03.027

Zimmerman, J.E., 1970. Design and Operation of Stable rf-Biased Superconducting Point-Contact Quantum Devices, and a Note on the Properties of Perfectly Clean Metal Contacts. Journal of Applied Physics 41, 1572. doi:10.1063/1.1659074